UNIVERSITÄT ZU LÜBECK

From the Institute of Neurobiology

of the University of Lübeck

Director: Prof. Dr. Henrik Oster

"Metabolic and immune effects of *Bmal1* deletion in neutrophils"

Dissertation

for Fulfillment of Requirements

for the Doctoral Degree

of the University of Lübeck

from the Department of Natural Sciences

Submitted by

Brinja Leinweber

from Braunschweig, Germany

Lübeck, 2022

First referee: Prof. Dr. Henrik Oster

Second referee: Prof. Dr. Henriette Kirchner

Date of oral examination: March 30, 2022

Approved for printing. Lübeck, March 31, 2022

Declaration

Herewith, I confirm that I have written the present PhD thesis independently and with no other sources and aids than quoted.

Lübeck, January 2022
Brinja Leinweber

“In the universe,
there are things that are known,
and things that are unknown,
and in between,
there are doors.”
William Blake

Table of Contents

Abbreviations

ADGRE1	Adhesion G protein-coupled receptor E1 (F4/80)
AGRP	Agouti-related peptide
ANOVA	Analysis of variance
ANT2	Adenine nucleotide translocase 2
AMPK	Adenosine monophosphate-activated protein kinase
APC	Allophycocyanin
ARC	Arcuate nucleus
bHLH	Basic helix-loop-helix
BMAL1	Brain and muscle arnt-like 1
BSA	Bovine serum albumin
BV421	Brilliant violet 421
cAMP	Cyclic adenosine monophosphate
CART	Cocaine- and amphetamine-regulated transcript
CCG	Clock-controlled gene
CD	Cluster of differentiation
cDNA	Complementary deoxyribonucleic acid
CHRONO	Computationally highlighted repressor of the network oscillator
CK	Casein kinase
CLOCK	Circadian locomotor output cycles kaput
CREB	Cyclic adenosine monophosphate response element-binding protein
CRP	C-reactive protein
CRY	Cryptochrome
CXCL	(C-X-C) motif ligand
CXCR	C-X-C chemokine receptor
DAMPs	Danger-associated molecular patterns
DBP	D-site of albumin promoter binding protein
DD	Dark-dark (constant darkness)
DEC	Differentiated embryo chondrocyte
DIO	Diet-induced obesity
DNA	Deoxyribonucleic acid

E4BP4	E4 promoter-binding protein 4
E-box	Enhancer Box
ECM	Extracellular matrix
EDTA	Ethylenediaminetetraacetic acid
EEF1α	Eukaryotic elongation factor 1 α
e.g.	*exempli gratia* (Latin), for example
et al.	*et alia* (Latin), and others
eWAT	Epididymal white adipose tissue
FACS	Fluorescence activated cell sorting
FBXL3	F-box/leucine-rich repeat protein 3
FCGR	Fcγ receptor
FELASA	Federation of European Laboratory Animal Science Associations
FITC	Fluorescein
GABA	γ-Aminobutyric acid
GRA	Granulocytes
GSK3β	Glycogen synthase kinase 3β
HFD	High-fat diet
HIF-1α	Hypoxia-inducible factor 1α
ICAM	Intercelluar adhesion molecule
i.e.	*id est* (Latin), that is
IFN-γ	Interferon-γ
IL	Interleukin
ILC	Innate lymphoid cell
ipRGC	Intrinsically photosensitive retinal ganglion cell
ITGAX	Integrin subunit α X (CD11c)
ITGM	Integrin subunit α M (CD11b)
JNK	c-Jun N-terminal kinase
KLF2	Krüppel-like factor 2
LD	Light-dark (12h:12h)
LFA-1	Lymphocyte function-associated antigen 1
LH	Luteinizing hormone
LPS	Lipopolysaccharide

LTB4	Leukotriene B4
Ly6G	Lymphocyte antigen 6 complex locus 6GD
LYM	Lymphocytes
MAC-1	Macrophage receptor 1
MCP-1	Monocyte chemoattractant protein 1
MMR	Macrophage mannose receptor (CD206)
MON	Monocytes
MPO	Myeloperoxidase
NADPH	Nicotinamide adenine dinucleotide phosphate
NE	Neutrophil elastase
NET	Neutrophil extracellular trap
Neutrophil-BKO	*Bmal1* knockout in neutrophils
NF-κB	Nuclear factor κB
NLRP3	Nod-like receptor 3
NPAS2	Neuronal PAS domain protein 2
NPY	Neuropeptide Y
OPN4	Melanopsin
PAS	Per-Arnt-Sim
PBS	Phosphate-buffered saline
PCR	Polymerase chain reaction
PE	Phycoerythrin
PER	Period
PerCP/Cy5.5	Peridinin chlorophyll protein-Cyanine5.5
PLT	Platelets
POMC	Pro-opiomelanocortin
PSGL-1	P-selectin glycoprotein ligand-1
PTPRC	Protein tyrosine phosphatase, receptor type, C (CD45)
qPCR	Quantitative real-time polymerase chain reaction
RBC	Red blood cell
RER	Respiratory exchange ratio
REV-ERBα/β	Reverse-erythroblastosis virus α/β
RNA	Ribonucleic Acid

ROR	Retinoic acid receptor-related orphan receptor
ROS	Reactive oxygen species
SAT	Subcutaneous adipose tissue
SCF	SKP, Cullin, F-box containing complex
SCN	Suprachiasmatic Nuclei/Nucleus
scWAT	Subcutaneous white adipose tissue
SEMs	Standard errors of the mean
SFAs	Saturated free fatty acids
SKP	S-phase kinase-associated protein
SVCs	Stromal vascular cells
T2DM	Type 2 diabetes mellitus
TNF-α	Tumor necrosis factor α
TLR	Toll-like receptor
TSH	Thyroid-stimulating hormone
TTFL	Transcriptional-translational feedback loop
VAT	Visceral adipose tissue
VCO_2	Carbon dioxide production
VO_2	Oxygen consumption
WAT	White adipose tissue
WBCs	White blood cells
WHO	World Health Organization
ZT	*Zeitgeber* Time

Summary

The daily light-dark cycle drives circadian rhythms of, *e.g.*, sleep and wakefulness or eating and fasting. Modern lifestyle with artificial light, constant availability of food and shift work often causes circadian disruption. This disruption is a risk factor for obesity and metabolic disease, global health problems of increasing incidence.

Due to chronic low-grade inflammation in adipose tissue and other metabolic organs, so-called metaflammation, obesity often goes along with impaired insulin sensitivity, thereby leading to insulin resistance and type 2 diabetes mellitus. The underlying mechanisms are studied in mice that receive high-fat diet (HFD), a paradigm that mimics large aspects of human obesity. Metaflammation is mainly driven by macrophages. These cells are recruited to adipose tissue early after onset of HFD feeding and acquire proinflammatory properties. Similarly, neutrophils are recruited into adipose tissue at early stages. While the role of macrophages is intensely studied, the contribution of neutrophils to metaflammation is less well understood. In particular, a functional circadian clock in macrophages is characterized to be protective, but the role of the neutrophil circadian clock remains unclear. It was the aim of this thesis to investigate the influence of the neutrophil circadian clock on body weight regulation and metaflammation under HFD feeding. It was hypothesized that absence of the circadian clock in neutrophils would aggravate body weight gain and metabolic state due to higher neutrophil infiltration into adipose tissue.

To investigate this, I established a mouse model in which the clock gene Brain and muscle arnt-like 1 (*Bmal1*) is ablated specifically in neutrophils (Neutrophil-BKO mice). Contrary to the original hypothesis, Neutrophil-BKO animals displayed lower body weight and decreased adiposity when they were exposed to HFD. This phenotype was accompanied by improved glucose tolerance and insulin sensitivity, demonstrating an improved metabolic state of these mice under HFD feeding. Moreover, numbers and circadian rhythms of neutrophils in adipose tissue were not influenced by the circadian clock in neutrophils, indicating that BMAL1 in neutrophils influences the outcome of HFD feeding *via* other mechanisms. While locomotor activity and energy expenditure were unaffected, food intake of Neutrophil-BKO mice was reduced. Furthermore, macrophages in epididymal white adipose tissue showed a phenotypic switch towards more anti-inflammatory cells that could reduce metaflammation. These two factors might contribute to the improved metabolic resilience of Neutrophil-BKO mice.

The model generated in this thesis provides a targeted intervention which improves obesity, glucose tolerance, and insulin sensitivity under HFD feeding in mice. Translating this model to the human situation can be a promising approach to develop new therapeutic options for the treatment of obesity.

Zusammenfassung

Der täglich wiederkehrende Licht-Dunkel-Zyklus steuert zirkadiane Rhythmen, die zum Beispiel rhythmische Schlaf- und Essenszeiten regeln. Ein moderner Lebensstil mit künstlichem Licht, Schichtarbeit und permanenter Verfügbarkeit von Nahrungsmitteln führt häufig zur Störung von zirkadianen Rhythmen, was wiederum Übergewicht und metabolische Erkrankungen begünstigt. Diese nehmen in ihrer Prävalenz global stark zu und stellen inzwischen ein großes Gesundheitsproblem dar.

Durch eine chronische niedrigschwellige Entzündung im Fettgewebe und anderen metabolischen Organen, die sogenannte Metaflammation, führt Übergewicht zu Komplikationen wie einer gestörten Insulinsensitivität, was zu Insulinresistenz und Typ 2 Diabetes Mellitus führt. In Mäusen werden die zugrunde liegenden Mechanismen erforscht, indem die Tiere mit Hochfettdiät (HFD) gefüttert werden. Dieses Modell spiegelt die Situation von übergewichtigen Menschen gut wider. Metaflammation geht hauptsächlich auf Makrophagen zurück, die schon früh nach Beginn einer HFD-Fütterung ins Fettgewebe einwandern und proinflammatorisch transformieren. Gleichzeitig werden auch Neutrophile ins Fettgewebe rekrutiert. Während die Rolle von Makrophagen intensiv erforscht wurde, ist die Beteiligung von Neutrophilen an der Metaflammation bisher weniger gut verstanden. In Mäusen wurde gezeigt, dass ein Ausschalten der zirkadianen Uhr in Makrophagen die Metaflammation verstärkt. Die Rolle der zirkadianen Uhr in Neutrophilen ist hingegen noch unklar. Ziel dieser Arbeit war es, den Einfluss der zirkadianen Uhr in Neutrophilen auf Körpergewicht und Metabolismus bei HFD-Fütterung zu untersuchen und gleichzeitig zu klären, wie sich die zirkadiane Uhr in Neutrophilen auf die Einwanderung von Neutrophilen und Makrophagen ins Fettgewebe auswirkt. Es wurde vermutet, dass ein Ausschalten der zirkadianen Uhr in Neutrophilen die Zahl der Neutrophilen im Fettgewebe erhöht und damit Auswirkungen auf Körpergewicht und Metabolismus verschlechtert.

Um dies zu untersuchen, habe ich ein Mausmodell entwickelt, in dem das Uhrengen Brain and muscle arnt-like 1 (*Bmal1*) spezifisch in Neutrophilen ausgeschaltet ist (Neutrophil-BKO-Mäuse). Entgegen der ursprünglichen Hypothese zeigten diese Tiere unter HFD-Fütterung eine geringere Körpergewichts-zunahme und geringere Fettmasse. Gleichzeitig zeigten sie eine erhöhte Glukose-Toleranz und verbesserte Insulin-Sensitivität, was den insgesamt begünstigten metabolischen Status bei HFD-Fütterung unterstreicht. Weiterhin hatte die zirkadiane Uhr in Neutrophilen keine Auswirkung auf die Zahlen oder die Rhythmen von Neutrophilen im Fettgewebe. Dem beobachteten Phänotyp müssen daher andere Mechanismen zugrunde liegen. Die Bewegungs-Aktivität und der Grundumsatz waren in Neutrophil-BKO-Mäusen nicht verändert, aber die Tiere zeigten eine verringerte Futteraufnahme. Außerdem ließ sich eine Veränderung der Eigenschaften von Makrophagen im epididymalen weißen Fettgewebe hin zu mehr anti-inflammatorischen Zellen nachweisen. Diese können Metaflammation verringern. So wurden zwei Faktoren identifiziert, die zu einer verbesserten Widerstandskraft von

Neutrophil-BKO-Mäusen gegen die negativen metabolischen Auswirkungen von HFD beitragen könnten.

Das Mausmodell, das hier entwickelt wurde, ermöglicht eine gezielte Intervention, die Übergewicht, Glukosetoleranz und Insulinsensitivität bei HFD-Fütterung verbessert. Es kann daher ein vielversprechender Ansatz sein, dieses Modell in die Klinik zu übertragen, um neue Therapie-möglichkeiten für Übergewicht zu entwickeln.

1. Introduction

The earth's rotation causes an environment that is characterized by regular changes of light-dark and temperature conditions. Organisms across different phyla harbor circadian clocks that enable them to anticipate these changes by regulating, for example, their sleep-wake cycle, their body temperature, or their mealtimes. The word circadian is composed of the two Latin words *circa* (about) and *dies* (day), indicating that circadian rhythms have a periodicity of approximately 24 hours (Creux and Harmer, 2019; Johnson et al., 1996; Patke et al., 2020).

Circadian clocks are present in almost every cell of a mammalian organism. As such, they influence, for example, immune function, stress regulation, hormonal responses, metabolism, or neuronal circuits. In mice, at least 40 % of transcripts show rhythmic expression in at least one tissue (Zhang et al., 2014).

The circadian clock is tightly connected to energy metabolism (Gopalakrishnan and Kannan, 2020) and to metabolic pathologies such as obesity (Engin, 2017). Obesity is a health problem of growing prevalence that is difficult to treat so date (WHO, 2021). Research on circadian clocks in this context might generate new therapeutic strategies.

In this thesis, I investigated how the circadian clock gene brain and muscle arnt-like 1 (*Bmal1*) in neutrophil granulocytes (hereinafter called neutrophils) influences body weight and metabolic outcome in a mouse model of diet-induced obesity (DIO).

1.1. The circadian clock

Circadian rhythms are characterized by three fundamental properties. They are self-sustained, entrainable and temperature compensated. Self-sustained rhythms are independent of external stimuli. They persist even in the absence of external time cues. The concept of entrainment describes the ability of external factors such as light or temperature to stably shift circadian rhythms. This allows adaptation to the environment, *e.g.,* after travels across time zones. Lastly, unlike most biochemical reactions, the period (determined by the speed of reactions) is stable over a wide range of temperatures (Buhr and Takahashi, 2013).

Circadian clocks are assumed to provide an evolutionary advantage. This might explain why circadian clocks can be found in all kingdoms of life – for example, plants, bacteria, insects, fish, and mammals. The circadian clocks of all these species share common principles. For studies that might have relevance for the human situation, the mouse is a very common model organism, because the structure of the circadian clock is conserved in all mammals. From now on, the term circadian clock refers to the mammalian circadian clock, which was studied in this project.

1.1.1. The molecular circadian clock

The circadian clock is present in nearly every cell of a mammalian organism. It is constituted of a transcriptional-translational feedback loop (TTFL) that generates rhythmic expression of clock genes and of clock-controlled genes (CCGs). In addition, several interlocking feedback loops stabilize and fine-tune circadian rhythms (**Figure 1**). Genes that are present within the core TTFL are necessary to sustain circadian rhythms within a cell. They are called core clock genes. In contrast, additional clock genes of interlocking feedback loops have modulatory function, but they are not required for the generation of circadian rhythms. In addition, rhythmic output genes without influence on parameters of the circadian clock are called CCGs.

Within the core TTFL, two basic helix-loop-helix/Per-Arnt-Sim (bHLH/PAS) transcription factors heterodimerize *via* their PAS domains. Mostly, the heterodimer is comprised of BMAL1, also called ARNTL or MOP3, and of circadian locomotor output cycles kaput (CLOCK). The heterodimer binds to enhancer box (E-Box, DNA element containing a CACGTG sequence) elements in target genes and activates transcription (Bunger et al., 2000; Gekakis et al., 1998; Hao et al., 1997; Hogenesch et al., 1998).

The timing of transcriptional activation mediated by the BMAL1:CLOCK heterodimer needs to be coordinated in order to generate rhythms (Sato et al., 2006). This is achieved *via* feedback repression by period (PER 1-3) and cryptochrome (CRY 1/2) proteins. *Per* and *Cry* genes harbor E-box elements in their promoter regions so that their transcription is activated by BMAL1:CLOCK. With delay, large complexes of PER and CRY proteins assemble in the cytoplasm and translocate back to the nucleus to inhibit BMAL1:CLOCK-mediated transcription (Aryal et al., 2017; Kume et al., 1999; Buhr and Takahashi, 2013). Mechanistically, it is assumed that CRY proteins block BMAL1:CLOCK-mediated transcription, whereas PER and CRY proteins together promote dissociation of BMAL1:CLOCK from the promoter (Ye et al., 2014). In case of CRY proteins, this mechanism is further specified in that binding of CRY proteins to BMAL1 inhibits phosphorylation of BMAL1, thereby favoring a transcriptionally inactive form (Dardente et al., 2007; Xu et al., 2015). Displacement of BMAL1:CLOCK from the promoter by a PER-CRY complex is thought to be associated with recruitment of casein kinase (CK) 1δ that phosphorylates CLOCK (Cao et al., 2021).

CK1δ also plays an important role in re-initiation of the transcriptional cycle. For a new cycle to start, repression mediated by CRY and PER proteins needs to be terminated. To this end, CK1δ associates with PER1 and PER2, which are destabilized (Camacho et al., 2001). Similarly, CK1ε phosphorylates PER proteins, priming them for proteasomal degradation (Keesler et al., 2000; Meng et al., 2008). A gain-of-function mutation in CK1ε was the first mutation that was described to affect the circadian system in mammals. The so called *tau* mutation accelerates the circadian clock, leading to short rest-activity

periods of 20 h under constant darkness conditions in homozygous animals, whereas heterozygous animals show a period of 22 h (Ralph and Menaker, 1988).

Proteasomal degradation of the CRY proteins is mediated by the S-phase kinase-associated protein (SKP), Cullin, F-box containing (SCF) ubiquitin ligase complex that harbors the F-box/leucine-rich repeat protein 3 (FBXL3) (Busino et al., 2007). In addition, glycogen synthase kinase 3β (GSK3β) and adenosine monophosphate-activated protein kinase (AMPK) are involved in degradation of CRY proteins (Harada et al., 2005; Lamia et al., 2009).

In summary, the core TTFL of the circadian clock consists of BMAL1 and CLOCK, which form heterodimers that activate transcription of *Pers* and *Crys*. Their protein products repress BMAL1:CLOCK-mediated transcription, forming a negative feedback loop. Timed and delayed degradation of PERs and CRYs releases transcriptional repression so that a new cycle can start.

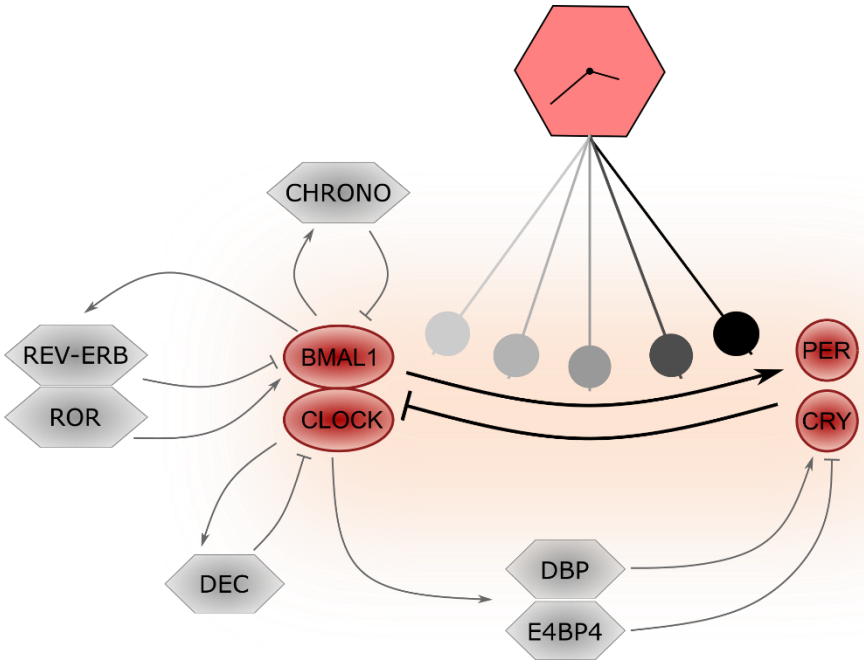

Figure 1: The mammalian molecular clock. The molecular clockwork consists of a core transcriptional-translational feedback loop (red symbols) and several additional interlocking feedback loops (grey symbols). In the core loop, BMAL1 and CLOCK activate transcription of *Per* and *Cry*. As a negative feedback mechanism, PER and CRY proteins inhibit their own transcription. Additional feedback loops stabilize and fine-tune circadian rhythms. Pointed arrows indicate activation, blunt-ended arrows indicate inhibition.

In addition to the core TTFL, there are several interlocking auxiliary loops that stabilize and fine-tune circadian rhythms. One of these auxiliary loops consists of the nuclear receptors Reverse-erythroblastosis virus α/β (REV-ERBα/β) and retinoic acid receptor-related orphan receptor α/β/γ (ROR α/β/γ). Both *Rev-Erbs* and *Rors* contain E-boxes in their promoter sequences that are activated by the CLOCK:BMAL1 heterodimer (Buhr and Takahashi, 2013). REV-ERBs and RORs compete for binding sites within the *Bmal1* promoter and inhibit or activate *Bmal1* transcription, respectively (Akashi and Takumi, 2005; Sato et al., 2004; Triqueneaux et al., 2004; Guillaumond et al., 2005). This feedback loop is classified as an auxiliary loop because the components can influence circadian oscillations, but they are not required for their generation *per se* (Liu et al., 2008). Within the loop, REV-ERBs seem to have a stronger influence on *Bmal1* oscillations than RORs. While deletion of *Rors* leads to a dampening of *Bmal1* oscillations, those rhythms are lost if *Rev-Erb*s are knocked out. However, *Per2* rhythms persist in this situation, indicating that the core clock machinery can compensate the loss. It is therefore assumed that the REV-ERB/ROR/BMAL1 loop has a major function in regulating clock output genes in addition to stabilizing core circadian rhythms (Liu et al., 2008; Preitner et al., 2002).

Differentiated embryo chondrocyte (DEC) 1 and 2 are two bHLH transcription factors that form a modulatory loop with BMAL1 and CLOCK. Transcription of *Dec* is induced by binding of BMAL1:CLOCK to E-box sequences in their promoter regions. DEC proteins inhibit BMAL1:CLOCK transactivation by direct binding to BMAL1 or by competing for E-box elements. That way, DECs influence transcription of other clock genes such as *Per1* (Honma et al., 2002; Kawamoto et al., 2004). As described for RORs and REV-ERBs, DECs are not required for generation of circadian rhythms, but they stabilize oscillations. This is shown in knockdown and knockout studies both *in vitro* and *in vivo*, where absence or overexpression of DECs influences timing and period of the circadian clock, but circadian oscillations still persist in double knockout situations (Nakashima et al., 2008; Bode et al., 2011).

Moreover, two leucine zipper transcription factors contribute to fine-tuning of the negative limb of the core TTFL. D-site of albumin promoter binding protein (*Dbp*) is a PAR leucine zipper transcription factor whose promoter region contains E-boxes that are activated by BMAL1:CLOCK. DBP binds to D-boxes in the promoters of clock genes such as *Per1* and stimulates transcription (Yamaguchi et al., 2000). In contrast, E4 promoter-binding protein 4 (E4BP4), a basic leucine zipper transcription factor that is activated by ROR, inhibits DBP-mediated transactivation at the D-box (Mitsui et al., 2001; Takeda et al., 2012). The phase-inversed oscillations of *Dbp* and *E4bp4* transcripts suggest a "repressor-antiphasic-to-activator-mechanism" of the clock modulation performed by E4BP4 and DBP (Ueda et al., 2005). Again, knockout of *E4bp4* or *Dbp* modifies circadian behavior, but does not abolish circadian rhythms, which is why these genes have modulatory function for the core TTFL (Lopez-Molina et al., 1997; Yoshitane et al., 2019).

Recent research additionally identified computationally highlighted repressor of the network oscillator (CHRONO) as a modulator of the circadian clock. The *Chrono* promoter region harbors E-box elements that are activated by BMAL1:CLOCK. It interacts with BMAL1 *in vitro* and suppresses BMAL1:CLOCK-mediated transcription. *In vivo*, *Chrono* knockout mice have a longer free-running period, but they are rhythmic, indicating that CHRONO plays a role in feedback modulation, but it is not as essential as PERs and CRYs (Anafi et al., 2014; Goriki et al., 2014).

As pointed out above, auxiliary loops fine-tune the circadian clock, but they are dispensable for generating circadian rhythms. For studying the role of the circadian clock in a certain context, it is helpful to have a model that is arrhythmic. The easiest way to achieve this *in vivo* is a single gene knockout. The core clock genes *Bmal1*, *Clock*, *Per1/2/3* and *Cry1/2* could be suitable targets in this approach. For *Cry* and *Per* genes it has been shown that single gene knockouts affect the circadian period, but circadian oscillations are retained due to compensation by the intact homologues (Bae et al., 2001; van der Horst et al., 1999; Vitaterna et al., 1994; Zheng et al., 2001). In case of *Clock*, rhythms persist when the gene is missing because neuronal PAS domain protein 2 (*Npas2*, also called *Mop4*) can functionally replace it (DeBruyne et al., 2007; Landgraf et al., 2016). Loss of *Bmal1* ablates rhythmic behavior of mice in constant darkness (Bunger et al., 2000). Therefore, the only single gene that is essential for circadian rhythms is *Bmal1*. Knockout of this gene is widely used in inducible and tissue-specific approaches to study circadian clock function.

1.1.2. Hierarchical organization of the circadian clock

To maintain rhythmic coherence between different tissues, the circadian system is organized in a hierarchical manner. A master clock in the suprachiasmatic nuclei (SCN) of the hypothalamus is at the top of this hierarchy, synchronizing subordinate peripheral and central non-SCN tissue clocks. Lesioning of the SCN in rats leads to loss of circadian locomotor activity, drinking rhythms, and corticosterone oscillations (Moore and Eichler, 1972; Stephan and Zucker, 1972). More evidence for the SCN as master pacemaker was collected from a transplantation study in hamsters. Wild type SCN-lesioned animals were transplanted with SCN tissue from *tau* hamsters and *vice versa*. Host animals show locomotor activity periods according to the donor SCN tissue (Ralph et al., 1990). These lesion studies collectively show that SCN tissue harbors a master clock that orchestrates circadian rhythms in the whole organism. In addition, a non-invasive, genetic approach was developed to ablate the SCN clock. As such, a mouse line with *Bmal1* deletion specific to the SCN was created. In this mouse line, peripheral clocks desynchronize when external time cues are missing. This emphasizes the superior role of the SCN in the circadian hierarchy and demonstrates that the SCN tissue itself is responsible for synchronization of peripheral rhythms (Husse et al., 2014).

SCN projections to hypothalamic regions that regulate endocrine systems and the autonomic nervous system represent the main routes of communication to transmit SCN signals to peripheral organs (Buijs et al., 2003). As pointed out above, the SCN controls circadian rhythms of glucocorticoid secretion *via* neuroendocrine signals that control the hypothalamus-pituitary-adrenal axis. Rhythmic glucocorticoids are potent synchronizers of peripheral clocks (Balsalobre et al., 2000). SCN projections also influence other hormonal systems targeting, for example, the gonads or the thyroid gland (Kalsbeek et al., 2006).

Influence of the SCN on the autonomous nervous system contributes to regulation of sleep and wakefulness, as well as food intake and metabolism (Buijs et al., 2001, 2003; la Fleur et al., 2000; Kreier et al., 2002). Furthermore, SCN outputs influence the balance between sympathetic and parasympathetic activity in the autonomous nervous system, thereby affecting for example rhythms in resting heart rate (Kalsbeek et al., 2006).

In addition, the SCN clock regulates body temperature and sleep rhythms (Eastman et al., 1984), which serve as synchronizing signals to downstream clocks. Lastly, release of the pineal hormone melatonin is controlled by the SCN (Kalsbeek et al., 2000; Cui et al., 2001; Perreau-Lenz et al., 2003). Several inbred mouse strains that are used for circadian studies are melatonin-deficient without major disturbances of the circadian system (Ebihara et al., 1986; Roseboom et al., 1998). However, melatonin rhythms play a role for regulating sleep rhythms and it may also influence circadian physiology of the immune system (Claustrat et al., 2005).

1.1.3. Entrainment of the circadian clock

Circadian rhythms persist without any external timing information. However, in a constant environment they cycle with an endogenous (free-running) period that is approximately, but not exactly, 24 hours. In humans, it is typically a bit longer than 24 hours (Eastman et al., 2015). In contrast, C57BL/6J mice, which are the most commonly used mouse strain for circadian studies, show a free-running period that is shorter than 24 hours in constant darkness but becomes longer under constant light conditions (Valentinuzzi et al., 1997; Sudo et al., 2003; Eckel-Mahan and Sassone-Corsi, 2015). To stay synchronous with external 24-hour days, external time cues called *Zeitgebers* (German for 'time-giver') adjust the circadian system every day.

The most potent *Zeitgeber* in the mammalian circadian clockwork is light. Information on light intensity is registered by the retina. Here, intrinsically photosensitive reginal ganglion cells (ipRGCs) containing melanopsin (OPN4) depolarize upon stimulation by light. *Opn4* knockout mice show intact entrainment to light-dark cycles but impaired phase shifting properties after light pulses. This indicates that

additional factors are involved in light entrainment (Berson et al., 2002; Hattar et al., 2002; Panda et al., 2002). In that context, it was discovered that ipRGCs receive synaptic input from rods and cones that are responsible for image-forming vision. Interestingly, when ipRGCs are completely ablated, circadian photoentrainment is no longer functional (Güler et al., 2008). This indicates that ipRGCs transmit light information from rods and cones and from their own melanopsin. ipRGCs project directly to the SCN *via* the retinohypothalamic tract (Moore and Lenn, 1972). Following light exposure, the transcription factor cyclic adenosine monophosphate (cAMP) response element-binding protein (CREB) is phosphorylated and thereby activated within minutes (Gau et al., 2002; Ginty et al., 1993). CREB binds cAMP-responsive elements within the promoter regions of *Per1* and *Per2*. That way, light stimulation ultimately results in activation of *Per1* and *Per2* transcription (Shigeyoshi et al., 1997; Travnickova-Bendova et al., 2002).

While light directly influences clock gene expression in the SCN and thereby influences the master circadian clock, there are other *Zeitgebers* that mainly affect peripheral clocks. As such, timing of food intake strongly influences the phase of the circadian clock in peripheral tissues. When food availability is restricted to the light phase, which is the inactive phase for mice, peripheral clocks respond with nearly inversed phases within a few days. Likewise, daily rhythms in energy metabolism and body temperature can be phase-inverted by rest time-restricted feeding. However, clock gene expression in the SCN remains unaffected under these conditions (Damiola et al., 2000; Satoh et al., 2006; Stokkan et al., 2001). Following up on these studies, it has been shown that different peripheral tissues vary in their phase-shifting properties when food is restricted to the light phase. Liver and white adipose tissue (WAT) show strong oscillations that are phase-inversed, while for example clock gene expression in the lung is hardly affected and kidney and heart show intermediate effects (Manella et al., 2021).

In addition to light and food, there are other potential *Zeitgebers* such as environmental or endogenous fluctuations of temperature (Barrett and Takahashi, 1995; Brown et al., 2002; Saini et al., 2012), timed exercise (Stetler et al., 2004; Wolff and Esser, 2012) or social interaction (Aschoff et al., 1971; Kuck et al., 2014). However, detailed mechanisms are incompletely understood and their relevance for the mammalian circadian system remains controversial.

In a natural environment, different *Zeitgebers* interact and cause tissue-specific responses. For example, entrainment to time-restricted daytime feeding is accelerated in mice that cannot produce glucocorticoids, pointing at an interplay between SCN-controlled glucocorticoid signaling and food-derived entrainment (Le Minh et al., 2001). Moreover, conflicting *Zeitgeber* signals in a study with 28-hour light periodicity and 24-hour food periodicity revealed that periods of SCN and peripheral tissue clocks, locomotor activity, and hormonal rhythms differentially align between 24 and 28 hours.

This demonstrates the interaction of the *Zeitgebers* light and food and their differential contribution to entrain tissue rhythms (Heyde and Oster, 2019).

Interestingly, most of the studies on food entrainment use rest time-restricted feeding protocols that provide food for 12 hours per day. However, when natural food intake rhythms with high intake during the night and lower intake during the day are phase-inverted using automated feeders, clock gene expression in peripheral tissues shifts only very moderately. This indicates that the entrainment signal derived by feeding needs to be very pronounced in order to provoke a clear phase-shifting response (Xie et al., 2020).

In summary, light signals are perceived by the retina and transmitted to the SCN. Here, they directly influence clock gene expression in the master pacemaker of the circadian clock network. Light is therefore the most potent *Zeitgeber* for circadian clocks. Further *Zeitgebers*, as for example timing of food intake and environmental temperature, additionally contribute to entrain our internal clock system to the external surrounding.

1.2. Interaction between circadian clocks and metabolism

Major metabolic organs like liver, pancreas, and adipose tissue harbor circadian clocks. Multiple transcripts involved in nutrient processing are expressed in a circadian fashion. The circadian clock in the SCN regulates meal timing and food intake, which in turn have a huge impact on the rhythmicity of peripheral organs. These facts demonstrate the tight interactions between the circadian clock and metabolic systems on several levels. Consequently, disruptions of the circadian system negatively influence metabolism and *vice versa* (Coomans et al., 2013; Marcheva et al., 2013).

1.2.1. Metabolic consequences of clock disruption

The circadian clock has evolved in conditions of regular environmental changes that reliably occur every day. In our modern world, we are confronted with an environment that is more and more instable. In 2015, almost 20 % of all employees in Europe were involved in shift work and this number is increasing. Shift work is associated with a disruption of sleep and eating patterns. Meals shift to times that are later during the day and meal frequency increases (Lowden et al., 2010; Nea et al., 2015). This, in combination with other factors, has adverse consequences for metabolic health. Regular night shift work is associated with a higher incidence of chronic diseases such as cardiovascular disorders, obesity, and type 2 diabetes mellitus (T2DM) (Kecklund and Axelsson, 2016; Torquati et al., 2018;

Vetter et al., 2018; Wang et al., 2011). This is also recapitulated in animal models. Chronic phase shifts that mimic shift work in mice lead to adipocyte hypertrophy and increased adipose tissue inflammation. In addition, insulin signaling is impaired, which is an early event in the development of T2DM (Xiong et al., 2021). In female mice, the effect is less pronounced, as insulin sensitivity seems to be increased in shift work conditions. Still, rhythms of glucose tolerance are altered. This suggests metabolic alterations under shift work conditions (Zhong et al., 2019). Interestingly, restriction of food access to the normal active phase largely reduces adverse metabolic effects in a shift work model in rats. Animals are protected from body weight gain, indicating a beneficial effect of regular food intake at natural times (Salgado-Delgado et al., 2010).

In addition to external factors that cause circadian desynchrony, genetic manipulations of clock genes affect the circadian clock or even completely disrupt circadian rhythms. As part of the positive limb of the core TTFL, loss of function of *Bmal1* or *Clock* affect metabolism. A mutation that deletes Exon 19 of *Clock* causes long-period and destabilized rhythms in constant darkness. In addition, it leads to increased food intake and obesity in mice (Turek et al., 2005). Likewise, loss of *Bmal1* interferes with lipid metabolism. Mice display an elevated respiratory quotient, indicating that lipids are less frequently used as source of energy. In addition, circulating fatty acids are increased and ectopic fat depots are observed (Shimba et al., 2011). Additionally, liver-specific deletion of *Bmal1* interferes with glucose metabolism (Lamia et al., 2008) and intact *Bmal1* is necessary for proper adaption of pancreatic beta cells to high-fat diet (HFD) feeding (Rakshit et al., 2016). When *Bmal1* is knocked out in murine adipocytes, food intake rhythms are shifted towards the light phase. This leads to increased body weight (Paschos et al., 2012). Interestingly, deletion of *Rev-Erbα* in mouse adipocytes also causes increased body weight gain under HFD feeding, but without development of the accompanying inflammation (Hunter et al., 2021). Conversely, deletion of *Bmal1* in the intestine protects mice against obesity when they receive HFD (Yu et al., 2021).

Metabolic phenotypes are also observed when *Cry* and *Per* are manipulated, even though the mutants are not always behaviorally arrhythmic due to functional redundancies. Deletion of *Per2* ablates diurnal feeding rhythms and thereby aggravates obesity when animals are exposed to HFD (Yang et al., 2009). Similarly, *Per3* knockout makes mice more vulnerable to obesity upon HFD feeding. Interestingly, this effect is also observed in *Per1/2/3* triple-deficient mice as well as in *Cry1/2* double-deficient mice (Barclay et al., 2013; Dallmann and Weaver, 2010).

All these studies strongly suggest a genetic association between clock genes and metabolic phenotypes in animal models. These findings are extrapolated to the human situation in studies showing genetic association between variants of *BMAL1* and prevalence of T2DM (Woon et al., 2007). Moreover, another study revealed associations between a *PER3* variant and extreme obesity and a single

nucleotide polymorphism of *CLOCK* is linked to metabolic syndrome (Azevedo et al., 2021; Shin and Lee, 2021). Metabolic syndrome is defined by presence of at least three of the following symptoms: abdominal obesity, atherogenic dyslipidemia, hypertension, insulin resistance, low-grade systemic inflammation, and prothrombotic state. Metabolic syndrome is a strong risk factor for cardiovascular disease and for T2DM (Grundy et al., 2004).

In summary, disturbance of the circadian clockwork by shift work or genetic manipulations promotes metabolic disorders such as obesity and T2DM in mice and humans.

1.2.2. Effects of (diet-induced) obesity on circadian clocks

Due to reciprocal connections between circadian clocks and metabolism, metabolic alterations affect circadian rhythms. I will focus on the effects of overweight and obesity on circadian clocks since those represent the most relevant metabolic imbalance in patients. According to the World Health Organization (WHO), overweight and obesity are defined as a body mass index above 25 or 30, respectively. Their prevalence is constantly increasing worldwide and in most parts of the world there are more people dying from the consequences of being overweight than from starvation (WHO, 2021).

This already demonstrates that overweight and obesity, hereinafter collectively called obesity, are more than an excess of energy that is stored as fat. Obesity goes along with several comorbidities, *e.g.,* arthritis, depression, cancer, cardiovascular disease or T2DM (Lawrence and Kopelman, 2004). To explore the underlying mechanisms leading to these comorbidities, the consequences of obesity for the circadian system have been well-studied.

A common animal model of obesity is DIO. In this model, animals are fed an obesogenic diet, for example HFD. This model largely reflects the human situation of obesity as animals develop increased body weight, elevated blood glucose and leptin levels, and impaired insulin sensitivity (Li et al., 2008). Using a DIO model in rabbits, it was shown that HFD feeding ablates diurnal rhythms of blood pressure and heart rate (Carroll et al., 2005). Another study performed in rats proved that HFD intake abolishes endocrine rhythms. Twenty-four-hour patterns of plasma thyroid-stimulating hormone (TSH), luteinizing hormone (LH), and testosterone are abolished and daily corticosterone rhythms are blunted (Cano et al., 2008). In mice, HFD consumption impairs photic entrainment of the circadian clock and obstructs adaptation of behavioral and body temperature rhythms to 6-h phase shifts (Mendoza et al., 2008). On the molecular level, clock gene expression rhythms are disrupted in hypothalamus, liver, and adipose tissue when mice consume HFD. Additionally, locomotor activity rhythms are altered. Furthermore, the liver clock is phase advanced upon HFD feeding and food intake rhythms are dampened. Mice on regular chow have a clear peak of food intake during the dark phase. This rhythm

is severely dampened with a higher degree of food intake during the light phase when mice consume HFD. Elevated food intake during the light phase is compensated by lower food intake during the dark phase (Kohsaka et al., 2007; Pendergast et al., 2013). While food intake rhythms are dampened, daily rhythms of respiratory quotient, reflecting energy metabolism, are lost after a few days of HFD feeding (Satoh et al., 2006). Altogether, it can be stated that HFD consumption alters the function of the mammalian circadian clock.

Interestingly, there are sex-specific effects in the way that HFD feeding influences the circadian clock. In female mice, HFD affects eating behavior and locomotor activity only when mice are ovariectomized. This suggests some degree of protection by ovarian hormones that can also be observed in humans: female obesity increases after menopause when estrogen levels decrease (Palmisano et al., 2017).

The knowledge of interactions between obesity and the circadian clock is used in therapeutic approaches. Stabilization of the circadian system has become a potential therapeutic target to treat obesity. Several studies have shown that restriction of HFD access to the normal active phase (dark phase) can significantly improve the outcome of DIO. Time-restricted feeding during the dark phase confers protection against obesity and hyperinsulinemia and stabilizes clock gene expression in the liver. These effects are not related to caloric restriction, since total caloric intake is not different between groups of restricted or *ad libitum* access to food (Arble et al., 2009; Hatori et al., 2012).

Translating these findings to the human situation, a clear connection was shown between late timing of meals and obesity. An observational study investigated how meal timing affects weight loss therapy. Patients that consumed their main meal comparably early were more successful with weight loss therapy. This effect was independent of total energy intake, estimated energy expenditure, and dietary composition (Garaulet et al., 2013). An additional study found that participants who consume more than a third of their food in the evening are more likely to be overweight or obese, even though effects were not significant (Wang et al., 2014a). This result is supported by another study addressing meal timing and obesity: food intake restricted to the evening is associated with body weight increase and with blood parameters that are indicative of decreased glucose tolerance. In contrast, food consumption during morning times protects against these effects (Singh et al., 2020). These studies demonstrate that timing of meals has a significant effect on metabolic health in the human system.

1.3. Metaflammation

As described above, obesity is more than just an excess of energy that is stored in fat depots. It is rather the basis for several comorbidities, among them insulin resistance, metabolic syndrome, and T2DM, which are major burdens of public health systems. The progression from obesity to insulin resistance or T2DM is caused by the activation of inflammatory cascades in adipose tissue that ultimately result in chronic low-grade inflammation. These inflammatory signals spread *via* the circulation to other organs including liver, muscle, pancreas, and brain and contribute to impaired insulin signaling (Gregor and Hotamisligil, 2011; Zatterale et al., 2019). Processes involved in this chronic inflammatory state are described by the term metaflammation.

The inflammatory state in metaflammation is characterized by increased levels of the inflammatory markers tumor necrosis factor α (TNF-α), interleukin (IL)-6 and C-reactive protein (CRP) in both humans (Dandona et al., 1998; Hotamisligil et al., 1995; Kern et al., 2001; Phosat et al., 2017) and rodents (Hotamisligil et al., 1993; Kim et al., 2013; Xi et al., 2011).

Proinflammatory signals activate c-Jun N-terminal kinases (JNKs) and the nuclear factor κB (NF-κB) pathway, which further promote the secretion of proinflammatory cytokines and chemotactic mediators so that monocytes are attracted and differentiate into proinflammatory macrophages. These events collectively contribute to impaired insulin signaling (Blüher et al., 2009; Hotamisligil et al., 1993; Jiao et al., 2011; Nakatani et al., 2004; Shoelson et al., 2003).

1.3.1. Onset of metaflammation

In the context of obesity, WAT is confronted with dysregulation of fatty acid homeostasis, increased adipocyte size, adipocyte death, local hypoxia, mitochondrial dysfunction, and changes in extracellular matrix (ECM) composition. All these factors are potentially involved in the initiation of the inflammatory response in WAT. They serve as danger-associated molecular patterns (DAMPs) that activate the immune system, even though precise mechanisms are often unknown (Zatterale et al., 2019).

Obesity goes along with elevated levels of saturated free fatty acids (SFAs) in plasma (Hellmann et al., 2013). SFAs are either directly derived from the diet (Snodgrass et al., 2013) or they are generated by breakdown of triglycerides in adipose tissue and liver (Wang et al., 2020). SFAs are detected by toll-like receptor (TLR) 4 in adipocytes and macrophages. Activation of TLR4 stimulates proinflammatory signaling and cytokine expression (Shi et al., 2006) (**Figure 2**). Palmitate, a common SFA, additionally activates TLR2 on human monocytes and stimulates secretion of the proinflammatory cytokine IL-1β

(Snodgrass et al., 2013). Interestingly, an acute lipid infusion in mice is sufficient to reduce insulin sensitivity in muscle. This effect is blunted in *Tlr4* knockout mice. These mice further display a reduction of adipose tissue inflammation triggered by SFAs (Shi et al., 2006).

Next to TLR signaling, the nod-like receptor protein3 (NLRP3) inflammasome is activated by DAMPs in obesity and promotes inflammation. An increase of intracellular ceramides activates NLRP3, leading to active caspase 1. Caspase 1 cleaves and thereby activates the proinflammatory cytokines IL-1β and IL-18 (Vandanmagsar et al., 2011). However, the relevance of NLRP3 activation in the context of metaflammation is controversial. While one study reports that *Nlrp3* knockout mice are protected from DIO (Stienstra et al., 2011), another publication did not find beneficial effects of *Nlrp3* knockout (Ringling et al., 2016).

Hypoxia and cellular hypertrophy are additional factors that contribute to immune activation in obesity (**Figure 2**). In humans, large and small adipocytes show different gene expression patterns. Certain immune-related genes are strongly upregulated in large cells, indicating immune activation in hypertrophic adipose tissue (Jernås et al., 2006). Furthermore, necrosis-like cell death is induced if expansion capacities of adipocytes are exceeded. Dying and dead adipocytes attract and activate proinflammatory macrophages (Cinti et al., 2005).

Rapid tissue expansion causes local hypoxia since angiogenesis cannot be stimulated fast enough to meet increased oxygen demands (Sun et al., 2011). In mouse models of DIO, hypoxia is associated with an upregulation of inflammatory genes (Ye et al., 2007). Overexpression of the main mediator of the hypoxic response, hypoxia-inducible factor 1α (HIF-1α), increases adipose tissue inflammation in mice (Halberg et al., 2009). In contrast to clear data in animal models, results of human studies are ambiguous. Therefore, the influence of hypoxia in human adipose tissue remains uncertain (Goossens et al., 2011; Hodson et al., 2013; Kabon et al., 2004; Pasarica et al., 2009).

While hypoxia activates inflammatory signaling, mitochondrial dysfunction further increases oxygen demands of the tissue and promotes hypoxia signaling. Mitochondrial dysfunction is induced by SFAs that increase the activity of mitochondrial adenine nucleotide translocase 2 (ANT2). ANT2 promotes uncoupled respiration so that oxygen utilization is less efficient. This state stimulates HIF-1α-mediated inflammation (Lee et al., 2014). Consequently, knockdown of *Ant2* in mice alleviates obesity-associated hypoxia in adipose tissue and improves insulin sensitivity (Seo et al., 2019).

Lastly, adipose tissue of obese animals and humans undergoes changes in ECM composition. The tissue is more fibrotic and there is a positive correlation between the degree of fibrosis and insulin resistance (Lawler et al., 2016; Lin et al., 2016). Moreover, it was shown *in vitro* that high density of ECM proteins

activates NF-κB signaling and thereby increases secretion of monocyte chemoattractant protein 1 (MCP-1), a key molecule to recruit macrophages.

In summary, there is a plethora of factors that contribute to the initiation of metaflammation, and it remains unclear which factors are first and/or most important. However, it is likely that effects of SFAs and adipocyte hypertrophy are early events since they have a direct connection to meal composition and food intake.

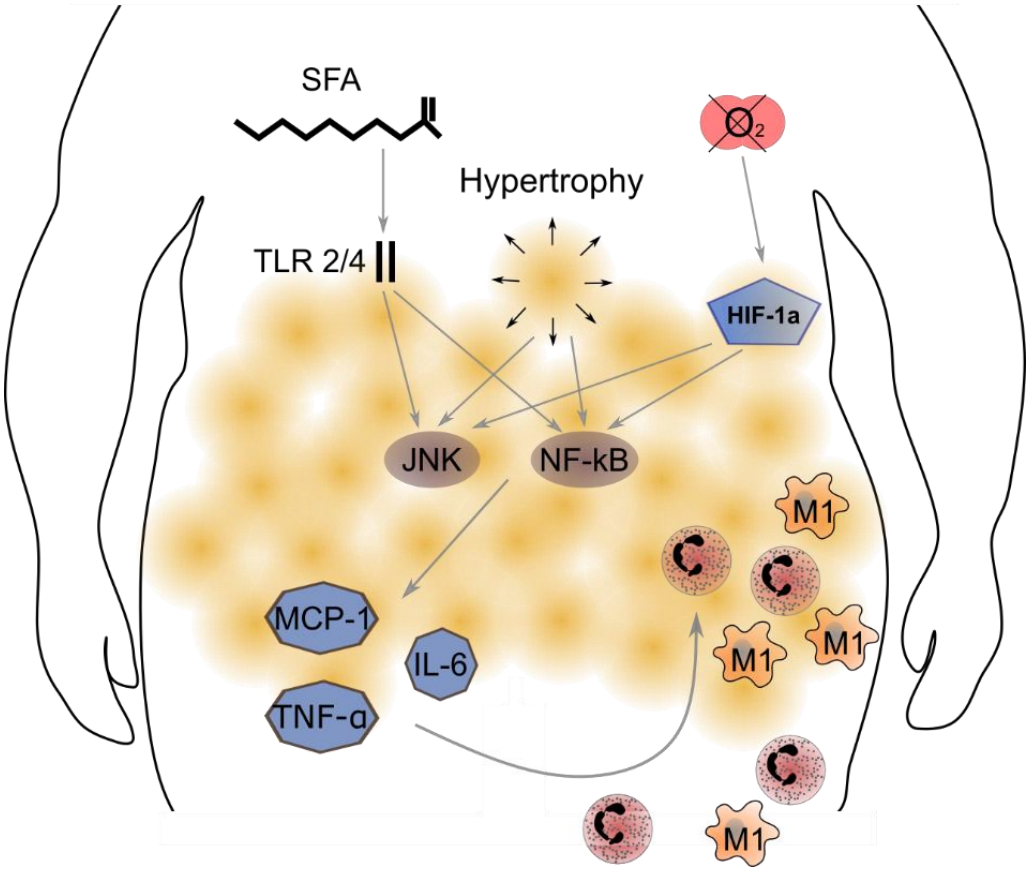

Figure 2: Initiation of adipose tissue inflammation in obesity. JNK and NF-kB are activated by SFAs binding to TLR2/4, by adipocyte hypertrophy, and by hypoxia. Activation of these proinflammatory pathways stimulates secretion of cytokines like MCP-1, IL-6, and TNF-α. These cytokines attract neutrophils and proinflammatory M1-like macrophages.

1.3.2. Cellular players of metaflammation in adipose tissue

Multiple different immune cells infiltrate adipose tissue during metaflammation. Cells of both the adaptive and the innate immune system are represented and contribute to inflammation. The most abundant immune cell type in inflamed obese adipose tissue are macrophages. In normal conditions, macrophages constitute 5-10 % of all stromal vascular cells (SVCs) in adipose tissue. In obese adipose tissue, this number rises quickly (already three days after onset of HFD feeding) and strongly (up to

40 %) (Lee and Olefsky, 2021). The rise in macrophage counts is derived from increased migration of monocytes into adipose tissue, largely mediated by the chemokines MCP-1 and leukotriene B4 (LTB4) (Li et al., 2015; Oh et al., 2012). Additionally, macrophages are retained in adipose tissue (Ramkhelawon et al., 2014). Furthermore, macrophage proliferation contributes to higher cell counts, in particular during early days of HFD feeding (Zheng et al., 2016).

In parallel to the increase in number, adipose tissue macrophages change their phenotype. In a lean state, resident macrophages possess anti-inflammatory properties. As such, they are classified M2-like or "alternatively activated" macrophages. In contrast, when animals are obese, macrophages acquire a proinflammatory M1-like or "classically activated" phenotype. In that case they express proinflammatory genes and therefore fuel metaflammation (Lumeng et al., 2007a). Proinflammatory macrophages are considered to be the main source of TNF-α, which is a potent driver of insulin resistance (Hotamisligil et al., 1993). M1-like macrophages form unique clusters around dead adipocytes that are detectable as so-called crown-like structures. Macrophages in crown-like structures are associated with high expression of TNF-α (Cinti et al., 2005; Lee and Lee, 2014). Of note, the differentiation between M1-like and M2-like macrophages is based on *in vitro* stimulation experiments. *In vivo*, the macrophage cell population is more diverse and single cells can have intermediate states (Li et al., 2019; Mills et al., 2000).

Inflammatory activation of macrophages occurs *via* TLR4 signaling, which is initiated by SFAs. *Tlr4* knockout leads to a shift of macrophage polarization towards the M2-like phenotype (Holland et al., 2011; Orr et al., 2012). However, the overall effect of *Tlr4* knockout on adipose tissue inflammation and insulin resistance is debated (Orr et al., 2012; Saberi et al., 2009; Tao et al., 2017).

Monocyte activation is prevented by Krüppel-like factor 2 (KLF2), but this myeloid factor is decreased in DIO. KLF2 inhibits NK-κB activation and thereby reduces expression of proinflammatory cytokines. *Klf2* knockout mice develop more severe obesity when they are fed a HFD, accompanied by increased metaflammation (Das et al., 2006; Sweet et al., 2020).

In addition to macrophages, there are several other innate immune cells that contribute to the inflammatory reactions during metaflammation. However, their role is less well-studied, and their function is often referred to an influence on macrophage polarization.

Natural killer cells are increased in DIO and they directly increase macrophage numbers and adipose tissue inflammation (Lee et al., 2016). Similarly, group1 innate lymphoid cells (ILCs) are present in adipose tissue and proliferate in DIO. They secrete interferon-γ (IFN-γ), which is necessary and sufficient to induce M1-like macrophage polarization (O'Sullivan et al., 2016). In addition, HFD feeding

attracts dendritic cells to adipose tissue and promotes macrophage infiltration (Stefanovic-Racic et al., 2012).

In contrast, cells that would promote the M2-like phenotype of macrophages are decreased in DIO. Group2 ILCs produce IL-5 and IL-13, which serve to retain eosinophils in adipose tissue (Molofsky et al., 2013). Obesity is associated with a decrease in group2 ILCs in mice and humans (Brestoff et al., 2015). Consequently, eosinophils are decreased as well. Since eosinophils are the main source of IL-4 in adipose tissue and this factor stimulates M2-like macrophages, reduced eosinophil numbers result in higher degree of proinflammatory macrophages (Wu et al., 2011a).

Neutrophils have a special role in this context since they might contribute to metaflammation independent of macrophages. Neutrophil numbers in adipose tissue increase already 3 days after onset of HFD feeding (Elgazar-Carmon et al., 2008). While neutrophil presence was described to be transient in this publication, a later study reports permanent elevation of these cells (Talukdar et al., 2012).

Neutrophil infiltration into adipose tissue of human obese subjects is stimulated by the chemokine (C-X-C) motif ligand (CXCL) 2 that is produced by adipose tissue. CXCL2 mediates neutrophil adhesion to endothelial cells, a first step in the infiltration process (Rouault et al., 2013). *In vitro*, it could be demonstrated that also macrophages attract neutrophils when they are stimulated with the SFA palmitate (Tam et al., 2020).

Reversely, neutrophils are involved in the recruitment of macrophages during inflammatory reactions. In addition, secretion of neutrophil elastase (NE), a neutrophil-derived protease, directly induces insulin resistance in the liver (Talukdar et al., 2012). Another protein that is secreted by neutrophils, myeloperoxidase (MPO), was reported to be associated with insulin resistance in DIO, but the article was retracted due to questionable Western blot images (Wang et al., 2014b). Nevertheless, MPO inhibition positively influences microvascular insulin sensitivity in DIO rats (Chai et al., 2019).

Besides innate immune cells, effector cells of adaptive immunity are present in adipose tissue and shape the inflammatory response during DIO. As such, cluster of differentiation (CD)8 positive T cells are increased in adipose tissue during HFD feeding and regulatory T cells are decreased. These changes are associated with increased macrophage numbers (Nishimura et al., 2009). Similarly, B2 lymphocytes are increased in obese adipose tissue. B2 lymphocytes represent the classic adaptive B cells, responsible for production of high-affinity antibodies (Laule et al., 2019; Lin et al., 2020). However, B cell-deficient mice develop only moderate insulin resistance in DIO (Ying et al., 2017). While these studies clearly show that B cells and T cells are involved in metaflammation, they seem to have an

inferior role compared to ILCs. When mice lack all lymphocytes (B cells, T cells, and ILCs), they are protected from DIO, but restoration of ILCs is sufficient to abolish this effect (Sasaki et al., 2019).

In summary, numerous cell types representing both the innate and adaptive immune system are involved in metaflammation. Macrophages are the best-studied cell type with very pronounced effects on metabolic outcome and the effects of many other cell types converge in their influence on macrophage function. Neutrophils might have an independent effect *via* secreted proteins such as NE and MPO.

1.3.3. Differences between visceral and subcutaneous adipose tissue

Most of the inflammatory processes described above are studied in visceral adipose tissue (VAT). However, fat is also stored in subcutaneous adipose tissue (SAT). Both types of fat depots differ in their inflammatory, endocrine, and metabolic properties. It is therefore not surprising that they differentially contribute to metabolic disease in obesity.

Humans who tend to have more visceral than subcutaneous fat are more prone to develop metabolic disease. This can be attributed to several differences between the two depots. Firstly, SAT has a higher angiogenic potential than VAT. It can therefore be concluded that the exposure to hypoxia is lower in SAT and inflammatory triggers are reduced (Gealekman et al., 2011).

Secondly, mice on a HFD show tissue expansion in both SAT and VAT. However, VAT expansion occurs *via* hypertrophy, while SAT grows by hyperplasia. Given the hypertrophy-associated cellular stress that can activate inflammatory pathways, this difference makes VAT more prone to metaflammation (Joe et al., 2009).

Thirdly, γ-aminobutyric acid (GABA) signaling selectively suppresses monocyte infiltration into SAT so that macrophage number is overall lower in SAT (Hwang et al., 2019). Consequently, crown-like structures are more prevalent in VAT (Murano et al., 2008), VAT releases more proinflammatory factors (Fain et al., 2004; Fried et al., 1998), and certain immune cells such as NK cells are only increased in VAT (Lee et al., 2016).

The sensitivity to leptin and adiponectin, two major adipokine factors, is different between SAT and VAT. Leptin is secreted by adipose tissue proportional to the fat content and is an important regulator of energy homeostasis. In addition, leptin has proinflammatory effects (La Cava, 2017). In obesity, leptin levels are overall high, but SAT has a higher secretion than VAT (van Harmelen et al., 2002; Hube et al., 1996). In contrast, adiponectin has anti-inflammatory effects and reduced levels in obesity (Fang

and Judd, 2018; Wanders et al., 2013). Adiponectin receptors are lower in VAT, indicating that the beneficial anti-inflammatory effects are less pronounced in this depot (Rasmussen et al., 2006).

Lipolysis, a process that releases proinflammatory SFAs, is stimulated by catecholamines and inhibited by insulin. SAT is less sensitive to catecholamine-mediated lipolysis, but more sensitive to insulin-driven inhibition of this process (Bolinder et al., 1983; van Harmelen et al., 2002). In total, this results in a lower rate of lipolysis in SAT so that SFA-mediated stimulation of inflammation is reduced.

In general, it can be stated that SAT is less prone to metaflammation and therefore SAT-associated obesity goes along with a healthier metabolic state.

1.3.4. Neuroinflammation and consequences for regulation of food intake

In parallel to metaflammation in peripheral tissues, central areas are affected by obesity-related inflammation. Special attention has been attracted to the hypothalamus since it is involved in the regulation of food intake and energy expenditure.

The center of hypothalamic regulation of food intake is the arcuate nucleus (ARC). Here, peripheral signals that convey information on satiety (cholecystokinin, glucagon-like peptide-1, and peptide YY), adiposity (leptin and insulin), or hunger (ghrelin, hypoglycemia, vagus nerve signaling related to empty stomach) are integrated to generate an orexigenic (stimulating food intake) or an anorexigenic (inhibiting food intake) response. To this end, ARC neurons secrete either orexigenic or anorexigenic peptides. Orexigenic stimuli are neuropeptide Y (NPY) and agouti-related peptide (AGRP), their anorexigenic counterplayers are pro-opiomelanocortin (POMC) and cocaine- and amphetamine-regulated transcript (CART, gene name *Cartpt*). Together, this peptidergic system creates an output that stimulates or inhibits food intake, depending on the needs of the organism (Amin and Mercer, 2016; Valassi et al., 2008). The peptidergic system is further influenced by the adipokine adiponectin, which stimulates food intake (Kubota et al., 2007).

Like peripheral inflammation, neuroinflammation in the hypothalamus is characterized by increased expression of proinflammatory cytokines such as IL-1β, IL-6 and TNF-α and by activation of JNK and NF-κB pathways. This is mediated through activation of TLR4 by dietary fats. Proinflammatory genes are upregulated as early as 3 days after onset of HFD feeding. After seven days, expression levels normalize, probably due to neuroprotective mechanisms that compensate, but on long-term HFD feeding (after four weeks), levels are high again (De Souza et al., 2005; Milanski et al., 2009; Thaler et al., 2012). Comparable to the increase of macrophage numbers in peripheral tissues, the number of microglia is elevated in the hypothalamus. Microglia sense SFAs and get activated. Depletion of

microglia in the mediobasal hypothalamus, which includes the ARC, diminishes SFA-mediated inflammation, restores leptin signaling, and reduces food intake. This indicates that microglia are the main cellular mediators of inflammation-related damage in the hypothalamus (Thaler et al., 2012; Valdearcos et al., 2014).

Next to microglia, it was demonstrated that astrocytes are involved in hypothalamic inflammation. *In vitro*, cultured astrocytes release TNF-α and IL-6 when they are stimulated with SFAs. This effect is again mediated by TLR4 (Gupta et al., 2012). *In vivo*, astrocyte-specific blockade of NF-κB signaling improves body weight development on HFD *via* reduction of hypothalamic inflammation, reduction of food intake, and increase of energy expenditure (Douglass et al., 2017).

Inflammatory processes in the hypothalamus are associated with decreased sensitivity against the anorexigenic effects of leptin and insulin. Leptin and insulin resistance can be induced by the SFA palmitate. Consequently, food intake is dysregulated (Kleinridders et al., 2009; Posey et al., 2009). Furthermore, HFD feeding induces apoptosis of hypothalamic neurons. In this context, TLR4 has a dual role. On the one hand, it senses SFAs and activates proinflammatory pathways, on the other hand it was shown to decrease apoptotic activity, protecting neurons from death (Moraes et al., 2009).

Activation of inflammation in the brain can occur *via* humoral, neuronal, or cellular stimuli from the periphery. Humoral stimuli include SFAs, cytokines, and adipokines from the periphery that cross the blood-brain-barrier and activate inflammation (Pflieger et al., 2018a). Neuronal communication to the brain is described for the vagus nerve that transmits inflammatory signals to the brain, even though it is not entirely clear whether this route of transmission is activated in DIO (Schweighöfer et al., 2016). Lastly, it is increasingly acknowledged that peripheral immune cells are recruited to the brain and contribute to neuroinflammation in DIO. As such, peripheral immune cells labeled with green fluorescent protein are detected in the brain of mice that received HFD. Based on their surface marker expression, these cells are classified as macrophages and neutrophils (Buckman et al., 2014; Yang et al., 2019).

Collectively, SFAs, peripheral immune cells, and peripheral cytokines activate inflammatory responses in the brain. These are characterized by increased cytokine expression and proliferation as well as activation of microglia and astrocytes. Neuroinflammation causes central resistance to leptin and insulin, leading to a dysbalance of the regulation of food intake.

1.3.5. Role of the circadian clock in metaflammation

Most of the cells that are involved in metaflammation harbor circadian clocks. Published data are available for monocytes (Nguyen et al., 2013), macrophages (Keller et al., 2009), neutrophils (Ella et al., 2016), natural killer cells (Arjona and Sarkar, 2005), eosinophils (Baumann et al., 2013), dendritic cells, B cells (Silver et al., 2012), T cells (Bollinger et al., 2011; Druzd et al., 2017), and microglia (Fonken et al., 2015). For ILCs, rhythmic core clock gene expression has not been demonstrated, but these cells exhibit rhythmic functions (Nussbaum et al., 2013). Since a plethora of immune processes is under circadian control (Scheiermann et al., 2018), it is possible that the circadian clock is also involved in onset and progression of metaflammation, although there are only few studies addressing this interaction.

In general, it was found that the clock gene *Rev-Erbα* controls innate immune responses. The cytokine response to a challenge with lipopolysaccharide (LPS) is time-of-day dependent, but this effect is no longer observed in mice that lack *Rev-Erbα* in myeloid cells (monocytes, macrophages, and granulocytes). The same is observed in myeloid-specific *Bmal1* knockout mice. LPS-induced secretion of IL-6 is no longer time-of-day dependent and it is flat on a high level (Gibbs et al., 2012). Therefore, it can be concluded that lack of *Rev-Erbα* makes myeloid cells more responsive to inflammatory stimuli. A similar effect was observed for neuroinflammation in *Rev-Erbα* knockout mice. In the hippocampus, loss of *Rev-Erbα* caused an increase in proinflammatory cytokines and higher spontaneous microglial activation (Griffin et al., 1999). This result suggests that REV-ERBα controls inflammatory processes in the brain. In the context of DIO, this effect was confirmed in mice that have a combined *Rev-Erbα/β* knockout specific to non-SCN hypothalamic regions. These mice gain more weight on HFD feeding because they show higher food intake and decreased energy expenditure. Furthermore, leptin sensitivity is reduced in these mice (Adlanmerini et al., 2021). In contrast, microglia-specific knockout of *Bmal1* ameliorates DIO (Wang et al., 2021).

Mice with global *Bmal1* knockout gain more weight than controls in the initial phase of HFD feeding. Interestingly, this effect does not persist over a long period of 15 weeks. At the end of the experiment, body weight of knockout and control mice was comparable. However, the experiment might be confounded by the premature aging phenotype of global *Bmal1* knockout mice so that interpretation is difficult (Hemmeryckx et al., 2011). For an adipocyte-specific knockout of *Bmal1*, it is described that mice have a higher body weight and shifted food intake rhythms. However, the consequences for metaflammation are not known under these conditions (Paschos et al., 2012).

Among peripheral immune cells, mice with a myeloid cell-specific *Bmal1* knockout were characterized for their susceptibility to DIO and metaflammation. Mutant mice gained more weight, accompanied by decreased glucose tolerance and a higher macrophage cell count in epididymal WAT (eWAT)

(Nguyen et al., 2013). Even though the driver line that was used in this study is often referred to as monocyte/macrophage-specific, it must be considered that it also targets granulocytes (*i.e.*, eosinophils, basophils, and neutrophils). Considering the multiple interaction between myeloid cells, particularly between neutrophils and macrophages, it would be interesting to have a model that enables to distinguish the impact of different myeloid clocks in the context of metaflammation.

Taken together, the role of the circadian clock in different immune cell types or brain areas can have differential impact on the susceptibility to DIO and metaflammation. From a therapeutic perspective, it would be desirable to have a clock system that is easily accessible for manipulation and that can be modified in a beneficial way.

1.4. Neutrophils

Neutrophils are the most abundant type of white blood cells (WBCs) in humans. They are considered first responders in the defense against pathogens, and they play important roles in sterile inflammatory processes. Due to the typical lobulated nucleus of these cells they are also called polymorphonuclear leukocytes (Amulic et al., 2012; Fine et al., 2019). Neutrophils are relatively short-lived cells, yet there is an emerging field of research focusing on circadian functions of neutrophils.

1.4.1. Life cycle of neutrophils

Neutrophils develop from hematopoietic stem cells in the bone marrow in a sequential process that takes 10-14 days in humans. Hematopoietic stem cells give rise to a common granulocyte/macrophage progenitor, which further differentiates into cells that are committed to the neutrophil lineage. During maturation, cells lose their potential to proliferate. Several intermediate cells are described for the development from the granulocyte/macrophage progenitor to the mature neutrophil (Cowland and Borregaard, 1999; Hidalgo et al., 2019). In this process, cells are distinguished by their morphological properties (Dancey et al., 1976), surface marker expression (Kim et al., 2017), or by mass cytometry (Evrard et al., 2018), with each technique yielding a different nomenclature for different types of premature neutrophils.

Mature neutrophils are released into the bloodstream in a manner dependent on C-X-C chemokine receptor (CXCR) 2. At the end of their lifespan, neutrophils increase their expression of CXCR4. This factor supports homing to the bone marrow, where they are eliminated (Martin et al., 2003). In addition to the bone marrow, neutrophils can be eliminated in the liver. They also enter multiple other tissues, for example, the lungs for immunosurveillance or the spleen where they contribute to B cell

maturation (Hidalgo et al., 2019; Løvås et al., 1996). In addition, steady-state neutrophil infiltration has been described for the intestines, skin, WAT, muscle, and lymph nodes (Casanova-Acebes et al., 2018).

During acute inflammation, neutrophils are rapidly released from the bone marrow so that their numbers in blood increase. This is achieved by shortening of the maturation time and by release of premature neutrophils (Orr et al., 2007). Similarly, homing of neutrophils to the bone marrow is downregulated during inflammation, probably to increase the availability of neutrophils for action in inflammatory processes (Løvås et al., 1996).

The half-life of neutrophils in blood is debated. Reports vary from less than one day (Athens et al., 1961; Dancey et al., 1976; Dresch et al., 1971; Lahoz-Beneytez et al., 2016) to several days (Pillay et al., 2010). Even though the majority of studies reports short half-lives, many of them suffer from confounding factors that make it difficult to draw final conclusions (Hidalgo et al., 2019; Tak et al., 2013). However, it is clear that neutrophils in the blood undergo phenotypic changes that are described as neutrophil aging. When neutrophils are freshly released from the bone marrow, they express high levels of L-selectin and these levels steadily decrease as neutrophils age (Adrover et al., 2019). Simultaneously, CXCR4 levels increase and facilitate neutrophil clearance (Casanova-Acebes et al., 2013).

All in all, neutrophils are produced and eliminated in the bone marrow. The time spent in the bloodstream is controversially debated, ranging from a few hours up to several days. Under inflammatory conditions, neutrophil numbers in the blood can increase spontaneously and strongly.

1.4.2. Role of neutrophils in the innate immune system

To exert their functions in immune reactions, neutrophils extravasate from the blood to the site of inflammation. This is a cascade of several steps that include capture of the neutrophil by the endothelial wall, slow rolling along the vessel wall, adhesion strengthening, intraluminal crawling, and finally paracellular and transcellular migration as well as migration through the basement membrane (Ley et al., 2007). Capturing of neutrophils is triggered by the cytokine-mediated upregulation of P-selectins, E-selectins, and intercellular adhesion molecules (ICAMs) on the endothelial wall. These factors are recognized by P-selectin glycoprotein ligand-1 (PSGL-1) and L-selectin on the surface of neutrophils. Binding to selectins on the endothelium mediates slow rolling of the neutrophils along the vessel wall (Yago et al., 2010). During this process, binding of neutrophils to E-selectin on the endothelial wall activates a signaling cascade that stimulates expression of integrins in neutrophils. Integrins, in particular lymphocyte function-associated antigen 1 (LFA-1) and macrophage receptor 1 (MAC-1), further participate in rolling and support adhesion strengthening by binding to endothelial

ICAM-1 (Mueller et al., 2010; Simon et al., 2000). Binding of MAC-1 to ICAM-1 on the endothelial wall promotes crawling of the neutrophil. During this process, neutrophils identify preferred sites of transmigration (Phillipson et al., 2006). Transmigration is triggered by chemokines from the tissue and by shear flow of the blood (Amulic et al., 2012; Cinamon et al., 2004; Ley et al., 2007).

Already during the migratory process, neutrophil activation takes place, a process that primes neutrophils for their immune actions, such as phagocytosis, release of antimicrobial peptides and proinflammatory cytokines, generation of reactive oxygen species (ROS), and generation of neutrophil extracellular traps (NETs) (Amulic et al., 2012).

In the defense against pathogens, neutrophils are potent phagocytotic cells. Pathogens are opsonized *via* Fcγ receptors or complement receptors (Dale et al., 2008; Kim et al., 2003). Engulfed pathogens are killed by fusion of the phagosome with intracellular granules, leading to release of toxic granule content into the phagosome (Liew and Kubes, 2019).

Four different types of intracellular granules have been described that harbor different effector proteins. Primary or azurophil granules contain MPO. In addition, other proteases like cathepsin G, NE, proteinase 3 and defensins are present. Secondary or specific granules contain lactoferrin, whereas tertiary granules harbor gelatinase proteins like matrix metalloproteinase 9. In addition, secretory granules contain serum albumin and preformed cytokines. Granules are formed during development in the bone marrow development in the order they are listed here, which means that primary granules are formed at a relatively early, premature stage and secretory granules are latest. When it comes to degranulation, each type of granules has a different sensitivity so that degranulation of secretory granules is easiest to achieve and it is hardest for primary granules (Sengeløv et al., 1993; Borregaard and Cowland, 1997; Amulic et al., 2012). The different content of granules predisposes them for different functions: primary and secondary granules are involved in pathogen killing and digestion, tertiary granules help in degrading extracellular matrix during migratory processes, and secretory granules support immune activation. Of note, granule contents can also be released into the extracellular space upon granule fusion with the plasma membrane (Liew and Kubes, 2019).

An additional mechanism by which neutrophils fight pathogens is the rapid generation of ROS in a process called oxidative burst. Nicotinamide adenine dinucleotide phosphate (NADPH) oxidase is integrated into the membrane of the phagosome or the plasma membrane and catalyzes the transfer of electrons from NADPH in the cytoplasm onto oxygen in the phagosome or in the extracellular space. This reaction generates superoxide (O_2^-) (Segal, 2005). Superoxide is further converted to hydrogen peroxide, or it reacts with nitric oxide and forms peroxynitrite. MPO catalyzes the reaction from hydrogen peroxide to hypochlorous oxide (Amulic et al., 2012). Thus, a plethora of ROS is built that have strong oxidant function and contribute to the defense against pathogens.

Lastly, formation of NETs is an important weapon of neutrophils in their immune action. NETs are characterized by extracellular DNA in conjunction with histones and antimicrobial proteins such as MPO or NE that form a web-like structure. NETs entrap a large variety of microbes to neutralize and kill them (Papayannopoulos, 2018; Rada, 2019).

With this arsenal of toxic agents, neutrophil activity must be tightly controlled before it becomes detrimental to host tissue. In this context, neutrophils undergo apoptosis when they have exerted their functions and are cleared by macrophages (Amulic et al., 2012).

While all these functions of neutrophils focus on the defense against pathogens, it is widely accepted that neutrophils also play a role in sterile inflammation. This term refers to inflammatory conditions that are not triggered by invading microorganisms, but by tissue injury such as hypoxia, necrosis, or other damage, as for example in metaflammation (Chen and Nuñez, 2010). In sterile inflammation, neutrophils are also recruited to the site of inflammation (McDonald et al., 2010) and they use their full arsenal of functions, for example, secretion of proinflammatory cytokines, release of proteases, or production of NETs (Chen and Nuñez, 2010; Cui et al., 2012). Furthermore, neutrophils are involved in clearing debris after sterile inflammation *via* phagocytosis. That way they contribute to limit tissue damage (Oved et al., 2021).

Altogether, neutrophils are fast responders to inflammatory stimuli. They have a variety of effector functions to initiate and promote inflammatory responses, attract other immune cells, and contribute to the defense against pathogens. Their action must be carefully controlled, otherwise they can be dangerous to host tissue.

1.4.3. Neutrophil heterogeneity

As described above, neutrophils are very effective killer cells when it comes to pathogen defense. In this mode, they stimulate inflammatory conditions to attract further immune cells. In contrast, there are conditions where neutrophils participate in tissue repair to resolve inflammation. Due to this functional spectrum, it has been suggested that, like macrophages, neutrophils can acquire proinflammatory or anti-inflammatory phenotypes. First hints for such heterogeneity were derived from *in vitro* studies showing that neutrophils of different origins (blood or tissue) respond differently to external stimuli that are supposed to inhibit superoxide production (al-Essa et al., 1995). In a further study, a subpopulation of neutrophils was identified which is distinguished by variable immune-receptor expression (Puellmann et al., 2006). Furthermore, *in vitro* stimulation with cytokines induces a phenotypic switch in neutrophils (Chakravarti et al., 2009). In inflammatory conditions *in vivo*, neutrophils subsets were first described in the context of tumor formation, where protumorigenic

neutrophils were discriminated from antitumorigenic neutrophils (Fridlender et al., 2009). Different neutrophil subpopulations have been described in the brain after stroke, with the possibility to promote the beneficial phenotypes by activating peroxisome proliferator-activated receptor-γ (Cuartero et al., 2013). However, even though it is now widely accepted that neutrophils are heterogenous, little is known about the mechanisms behind this heterogeneity (Liew and Kubes, 2019; Ng et al., 2019).

1.4.4. Neutrophil-macrophage crosstalk

When exerting their various functions, neutrophils interact with other immune cells. A particularly close interaction was described between neutrophils and macrophages as these cells orchestrate the innate immune response (Bouchery and Harris, 2019). When an inflammatory response is induced, tissue-resident macrophages regulate neutrophil infiltration by secretion of chemokines. Interestingly, both stimulatory and inhibitory effects have been described in different conditions (Beck-Schimmer et al., 2005; De Filippo et al., 2008). When neutrophils are recruited to the tissue, macrophage-derived survival factors increase their lifespan (Takano et al., 2009). At the same time, neutrophil granule proteins are chemotactic to attract more macrophages and neutrophils to the site of inflammation. This creates a feed-forward loop that enhances inflammation (Chertov et al., 1997; Soehnlein et al., 2008). However, there are reports of macrophages preventing further neutrophil infiltration to minimize tissue damage and to break this feed-forward loop (Uderhardt et al., 2019).

Neutrophils and macrophages cooperate in resolving inflammation. Here, contact between neutrophils and macrophages can induce neutrophil apoptosis (Allenbach et al., 2006). In addition, macrophages clear apoptotic neutrophils by phagocytosis and this triggers polarization into anti-inflammatory M2-like macrophages (Fadok et al., 1998). In contrast, there are reports about macrophages that make use of phagocytosed neutrophil granules to exert antimicrobial activity against pathogens (Tan et al., 2006). In addition to neutrophil granules, NETs influence macrophages. In a recent study, it was demonstrated that certain microRNAs in NETs are able to increase TNF-α production by macrophages (Linhares-Lacerda et al., 2020).

Finally, neutrophils can influence macrophage polarization. In *Streptococcus pyogenes* infections, neutrophils co-stimulate monocytes to express proinflammatory cytokines (Påhlman et al., 2006). In contrast, neutrophil-derived IL-13 promotes M2-like polarization of macrophages in helminth infections (Chen et al., 2014). *In vitro*, LPS-stimulated increase of TNF-α in macrophages can be dampened by co-culture with neutrophils. Of note, these findings were traced back to a reduction of NF-κB signaling in macrophages (Marwick et al., 2018). In another setting, secretion of colony-

stimulating factor 1 by neutrophils was necessary to polarize macrophages into anti-inflammatory cells that mediate tolerance after organ transplantation (Braza et al., 2018).

In summary, there are multiple interactions between neutrophils and macrophages on all levels of the inflammatory response. For some stages, there are contradictory data regarding the outcome of neutrophil-macrophage cooperation. This is likely context-dependent and further research is necessary to clarify the exact mechanisms.

1.4.5. The circadian clock in neutrophils

Given the short lifespan of neutrophils in the circulation and their low expression of clock genes, it was postulated for a long time that the circadian clock in neutrophils plays a minor role, even though many neutrophil functions are rhythmic over the course of the day. In recent years, however, several studies were published that challenge this view, emphasizing a role of the neutrophil-intrinsic circadian clock (Ella et al., 2016; He et al., 2018; Adrover et al., 2019; Aroca-Crevillén et al., 2020).

In both human and rat neutrophils, functions like the distribution of young and aged cells, the capacity to produce ROS or the phagocytic potential were found to be time-of-day dependent (Ella et al., 2016; Hriscu et al., 2002; Melchart et al., 1992). Nevertheless, it was doubted that these changes are related to an intrinsic circadian clock of neutrophils. Instead, they were rather considered to be dependent on the maturation status (Ella et al., 2018).

This view was recently questioned by new studies addressing the circadian clock in neutrophils. It was demonstrated that the circadian clock regulates rhythmic expression of adhesion molecules like PSGL-1, CXCR2, and CXCR4 as well as rhythmic migration into tissues. Furthermore, neutrophil abundance in the blood shows a clear circadian oscillation, peaking at the beginning of the inactive phase (Casanova-Acebes et al., 2013; He et al., 2018).

The aging state of neutrophils changes over the course of the day. Fresh neutrophils are mainly released from the bone marrow during the dark phase, leading to a peak of fresh neutrophils in blood during the second half of the dark phase. While they are in the circulation, neutrophils undergo aging. Around *Zeitgeber* Time (ZT)5, *i.e.,* 5h after lights were turned on, blood neutrophils are mainly aged (Casanova-Acebes et al., 2013). While there is one study reporting more proinflammatory properties for aged neutrophils (Zhang et al., 2015), other studies show that these cells harbor reduced granule content, lower NET-forming capacities and decreased migratory properties to sites of inflammation (Adrover et al., 2019, 2020). At the same time, neutrophil aging is under circadian control. If *Bmal1* is missing in neutrophils, cells are constitutively fresh and, accordingly, they show different inflammatory

properties. As such, cells are more prone to infiltrate inflamed tissue after zymosan-induced peritonitis, an experimental model of sterile inflammation. In contrast, homeostatic clearing into tissues, which is attributed to aged cells, is impaired. Of note, the total number of neutrophils in blood remains rhythmic, indicating that this is regulated *via* mechanisms independent of the neutrophil circadian clock (Adrover et al., 2019). Additionally, cellular content of granules, phagocytic activity and the capacity to form NETs vary over the course of the day (Hriscu, 2005; Adrover et al., 2020) (**Figure 3**).

In summary, it is more and more acknowledged that the circadian clock has an impact on neutrophil physiology and pathophysiology. In particular, migratory processes seem to be subject to circadian regulation.

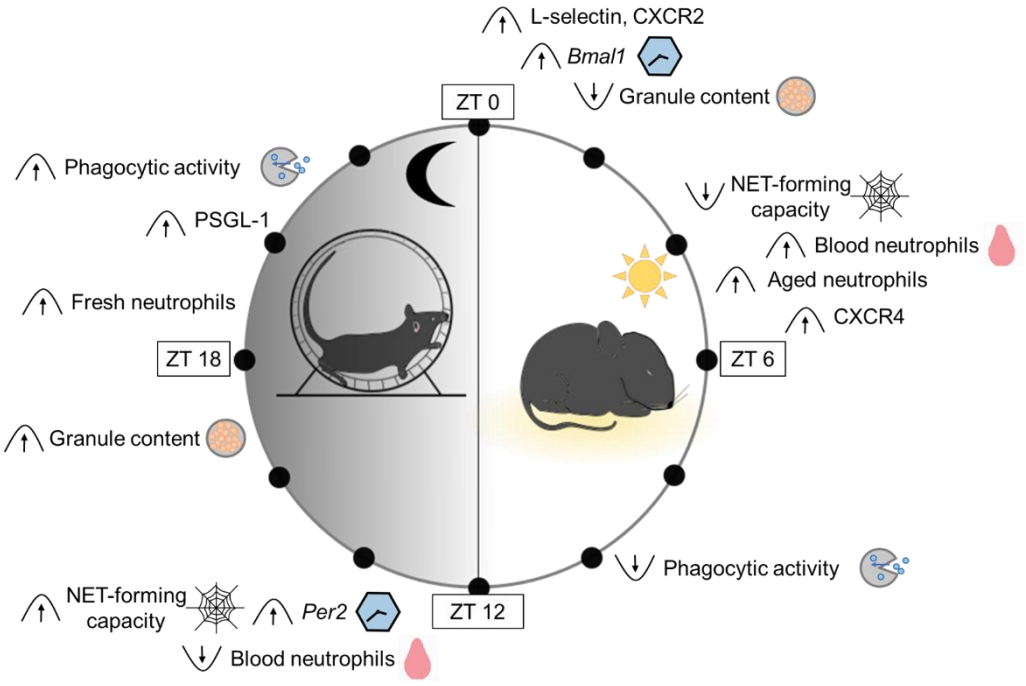

Figure 3: Murine neutrophils around the day. Abundance of neutrophils in the blood is changing over the course of the day. Lowest numbers are observed at the beginning of the active phase when cells are predominantly fresh. They peak at the beginning of the inactive phase, shortly before the peak of aged neutrophils. Expression of clock genes (*Bmal1*, *Per2*), migratory factors (CXCR2, CXCR4, PSGL-1, L-selectin) and effector functions (granule content, phagocytic activity, NET-forming capacity) also change over the course of the day. A curved line with an arrow pointing upwards indicates the peak, the same symbol with the arrow pointing downwards indicates the trough.

1.5. Hypothesis

The role of the circadian clock in macrophages in the context of metaflammation has been thoroughly described. The fact that there is crosstalk between macrophages and neutrophils and that neutrophils are often first responders in immune reactions makes this cell type an interesting target. Since infiltration of neutrophils into adipose tissue is likely a critical step in the initiation of metaflammation and migratory processes in neutrophils are controlled by the circadian clock, the aim of this work was to study the role of the neutrophil circadian clock in inflammatory processes in DIO. To this end, I generated a mouse line with *Bmal1* knockout specific in neutrophils (Neutrophil-*Bmal1* knockout (-BKO)) and studied metabolic and inflammatory parameters in these mice under HFD feeding.

Neutrophil numbers are constantly high in the spleen when they lack *Bmal1* (He et al., 2018). Furthermore, in sterile inflammatory conditions, *Bmal1*-deficient neutrophils have a higher tendency to infiltrate inflamed tissue (Adrover et al., 2019). Based on these results, I hypothesized that Neutrophil-BKO mice would exhibit higher neutrophil numbers in WAT during DIO. Owing to the facts that neutrophils further stimulate macrophage infiltration in the initiative phase of inflammation (Chertov et al., 1997; Soehnlein et al., 2008) and that macrophages are considered the main drivers of metaflammation and subsequent insulin resistance (Duan et al., 2018), I further hypothesized that Neutrophil-BKO mice on a HFD would be more prone to body weight gain, glucose intolerance and insulin resistance.

2. Materials and Methods

2.1. Animal experiments

All animal experiments were performed according to the German Law on Animal Welfare and the guidelines for animal research by the Federation of European Laboratory Animal Science Associations (FELASA). Before experiments were conducted, the experimental outline was subject to ethical assessment and to legal approval by the "Ministerium für Energiewende, Landwirtschaft, Umwelt, Natur und Digitalisierung" in Schleswig-Holstein. Experiments were performed under license numbers 4(58-5/19), 4(37-4/18), 4_2017-08-30, and 4_2020-09-23).

2.2. Generation of mice with neutrophil-specific knockout of *Bmal1*

Neutrophil-BKO mice were generated by crossing B6.Cg-Tg(S100A8-cre,-EGFP)1Ilw/J (*Mrp8-Cre*, Jackson Laboratory Stock No: 021614) mice to B6.129S4(Cg)-*Arntl*^{tm1Weit}/J (*Arntl*-flox or *Bmal1*-flox, Jackson Laboratory Stock No: 007668) mice. The genetic background of all mice was C57BL/6J. *Mrp8-Cre* mice were kindly donated by Prof. Dr. Christian Sadik, University of Lübeck. These mice express *Cre* recombinase under control of the neutrophil-specific *Mrp8* promoter (Passegué et al., 2004). *Bmal1*-flox mice were derived from the Institute's breeding at the University of Lübeck. These mice carry loxP sites around Exon 8 of the *Bmal1* gene so that this exon is excised in the presence of CRE recombinase (Kim et al., 2018). Exon 8 encodes for the bHLH domain that is responsible for DNA binding. Consequently, mutated protein is dysfunctional for circadian properties (Storch et al., 2007; Wang et al., 2013). When *Bmal1*-flox mice were crossed to *Mrp8-Cre* mice, the resulting offspring expressed mutated *Bmal1* specifically in neutrophils so that the circadian clock was disrupted in these cells.

2.2.1. Breeding of Neutrophil-BKO mice

Animals were generated and maintained in the animal facility of the University of Lübeck. For the first generation, homozygous *Bmal1*-flox mice were crossed to hemizygous *Mrp8-Cre* mice (**Figure 2**). The resulting offspring were heterozygous for *Bmal1*-flox and 50 % of them additionally expressed *Mrp8-Cre*. For the following generation, *Mrp8-Cre* positive mice from the first generation were again crossed to homozygous *Bmal1*-flox mice so that 50 % of the resulting offspring were homozygous for *Bmal1*-flox. Half of these animals expressed *Mrp8-Cre* (Neutrophil-BKO), the other half was negative for *Cre*

recombinase (Control animals). For maintenance of the line, Neutrophil-BKO and Control mice were mated, so that 50 % of the offspring were again Neutrophil-BKO and 50 % were Control animals.

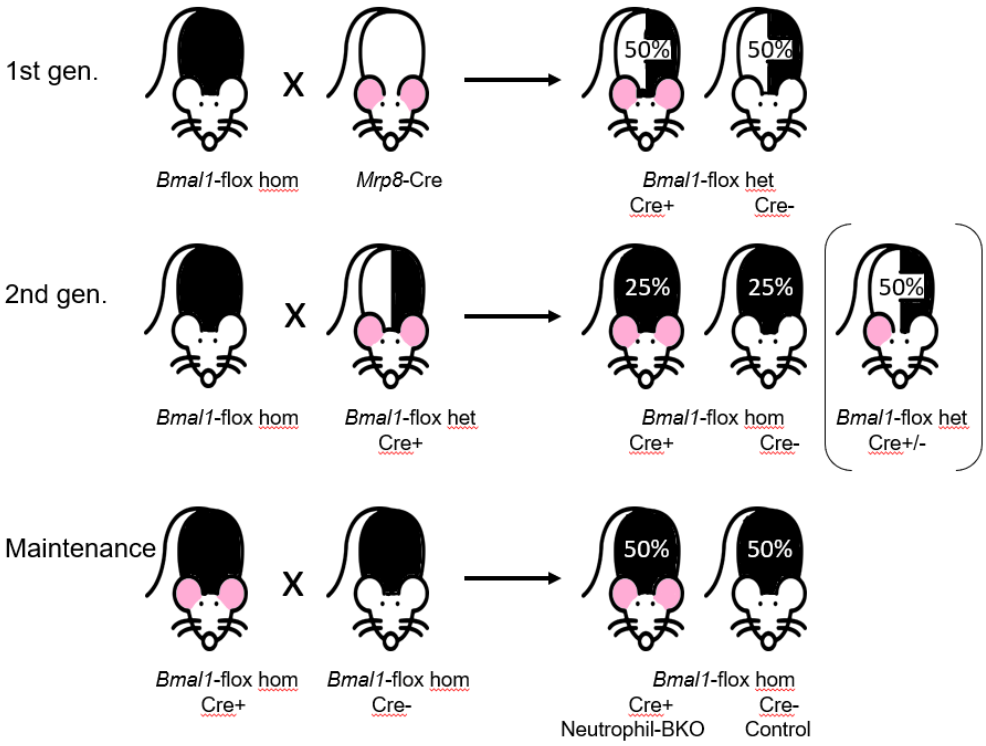

Figure 4: Breeding scheme to generate Neutrophil-BKO mice. In the first generation (gen.), homozygous (hom) *Bmal1*-flox mice were crossed to *Mrp8-Cre* mice. The resulting offspring that were heterozygous (het) for *Bmal1*-flox and expressed *Mrp8-Cre* were further crossed to homozygous *Bmal1*-flox mice (2nd gen.). 50 % of the offspring were already Control (*Bmal1*-flox hom, Cre-) or Neutrophil-BKO (*Bmal1*-flox hom, Cre+) mice. For maintenance, Neutrophil-BKO and Control animals were mated so that all resulting animals could be used for experiments. Black bodies indicate homozygous expression of *Bmal1*-flox, black-white bodies indicate heterozygous expression of *Bmal1*-flox, a white body represents wild type *Bmal1* alleles. Two pink ears represent hemizygous expression of *Mrp8-Cre*, one pink ear indicates that 50% of the corresponding mice are hemizygous for *Mrp8-Cre*.

2.2.2. Genotyping of Neutrophil-BKO mice

At the age of 3-4 weeks, animals were weaned, and ear biopsies were taken to discriminate the animals and to determine their genotype. Genomic DNA was extracted by the addition of 20 µL Lysis buffer (50 mM Tris/HCl pH 8.0, 10 nM Ethylenediaminetetraacetic acid (EDTA) pH 8.0, 2 mM NaCl, 1 % Sodium dodecyl sulphate) and 1 µL Proteinase K (10 mg/mL, Roche) to the ear biopsy. The reaction was incubated at 55 °C for 1 h, followed by addition of 500 µL Deionized water and deactivation at 95 °C for 10 min.

Genomic DNA was used as template to determine the *Bmal1*-flox genotype as well as the presence of *Cre* recombinase by polymerase chain reaction (PCR). The first animals were also checked for the correct *cre* allele by a locus-specific PCR.

2.2.2.1. Genotyping of *Bmal1*-flox

The following reagents were combined for the PCR reaction:

2.0 µL DNA template

2.0 µL 10X Ammonium buffer (Ampliqon)

1.0 µL $MgCl_2$ (25 mM, Ampliqon)

1.0 µL dNTPs (10 mM, ThermoFisher)

1.0 µL Primer *Bmal1* KO forward (10 µM, Eurofins)

1.0 µL Primer *Bmal1*-flox forward (10 µM, Eurofins)

2.0 µL Primer *Bmal1*-flox reverse (10 µM, Eurofins)

0.1 µL Taq polymerase (5 U/µL, Ampliqon)

9.9 µL Deinonized water

Primer sequences were

5' - CTC CTA ACT TGG TTT TTG TCT GT - 3' for *Bmal1* KO forward,

5' - ACT GGA AGT AAC TTT ATC AAA CTG -3' for *Bmal1*-flox forward and

5' - CTG ACC AAC TTG CTA ACA ATT A -3' for *Bmal1*-flox reverse.

PCR products were amplified in a reaction including initial denaturation at 94 °C for 3 min, followed by 35 cycles of 94 °C for 30 s, 59 °C for 1 min and 72 °C for 1 min. The reaction was completed by incubation at 72 °C for 5 min. Products were separated on a 1.5-% agarose gel and visualized with the help of SYBR Safe (Invitrogen) and the FastGene Blue/Green GelPic LED Box Imaging System (Nippon Genetics). Homozygous *Bmal1*-flox samples would show a band at 431 bp, heterozygous samples would show two bands at 327 bp and at 431 bp. In addition, the inclusion of the primer *Bmal1* KO forward allowed for the detection of knockout samples in which Exon 8 is excised. These samples would show a band at 570 bp. Under normal conditions, this band would not be expected in the samples, but it was detected occasionally so that it was always included in the genotyping process. Animals that showed this knockout band were excluded from experiments with three exceptions (two Neutrophil-BKOs and one Control), where the knockout allele was only detected after the experiment had started. Theoretically, this would not make a big difference since there was still one

intact allele that could be manipulated as desired. Still, the data were carefully checked for outliers. Since none of the three animals showed significant deviation from the other replicates, it was decided to include the animals in the analysis despite their differences in genotype.

2.2.2.2. Genotyping of *Cre*

DNA templates were generated as described above. The following reagents were combined for the PCR reaction:

1.0 µL DNA

2.0 µL 10X Standard buffer (Ampliqon)

0.4 µL dNTPs (10 mM, ThermoFisher)

1.2 µL Primer *Cre* forward (10 µM, Eurofins)

1.2 µL Primer *Cre* reverse (10 µM, Eurofins)

0.15 µL Taq polymerase (5 U/mL, Ampliqon)

14.05 µL Deionized water

Primer sequences were

5’ - CGA TGC AAC GAG TGA TGA GGT TCG - 3’ for *Cre* forward and

5’ - AGC ATT GCT GTC ACT TGG TCG TGG - 3’ for *Cre* reverse.

PCR products were amplified in a reaction including initial denaturation at 94 °C for 4 min, followed by 30 cycles of 94 °C for 30 s, 62 °C for 30 s and 72 °C for 30 s. The reaction was completed by incubation at 72 °C for 5 min. Products were separated on an agarose gel as described above. The presence of *Cre* was indicated by a band at 260 bp.

2.2.2.3. Locus-specific *Cre* genotyping

To ascertain that the *Cre* allele was correct, locus-specific *Cre* genotyping was performed for the first animals that founded the line and then repeated occasionally. This involved the following PCR reaction:

1.0 µL DNA

2.0 µL 10X Standard buffer (Ampliqon)

0.4 µL dNTPs (10 mM, ThermoFisher)

1.0 µL Primer oIMR1084 (10µM, Eurofins)

1.0 µL Primer oIMR1085 (10µM, Eurofins)

1.0 µL Primer oIMR7338 (10µM, Eurofins)

1.0 µL Primer oIMR7339 (10µM, Eurofins)

0.1 µL Taq polymerase (5 U/mL, Ampliqon)

12.5 µL Deionized water

Primer sequences were

5’ - GCG GTC TGG CAG TAA AAA CTA TC - 3’ for oIMR1084,

5’ - GTG AAA CAG CAT TGC TGT CAC TT - 3’ for oIMR1085,

5’ - CTA GGC CAC AGA ATT GAA AGA TCT - 3’ for oIMR7338 and

5’ - GTA GGT GGA AAT TCT AGC ATC ATC C - 3’ for oIMR7339.

PCR products were amplified in a reaction including initial denaturation at 94 °C for 3 min, followed by 35 cycles of 94 °C for 30 s, 62 °C for 1 min and 72 °C for 1 min. The reaction was completed by incubation at 72 °C for 5 min. Products were separated on an agarose gel as described above. If *Mrp8-Cre* was expressed hemizygously, a double band of 100 bp and 324 bp was visible. If animals were *Cre* negative, only the internal control band at 324 bp appeared. Compared to the *Cre* PCR described in section 2.2.2.2., this PCR has the advantage of including an internal control that assures that the PCR reaction has worked. However, the important band runs very low at only 100 bp, so that it can overlap with the primer cloud. For this reason, the general *Cre* PCR described in section 2.2.2.2. was used as the standard PCR to determine the presence of *Cre*.

2.3. Animal housing

All animals were kept in the animal facility of the University of Lübeck at room temperatures of 21 - 24 °C, humidity of 55 - 65 % and a light-dark cycle with 12 h light and 12 h darkness. In all experiments, the time of “lights on” is referred to ZT0 and the time of “lights off” as ZT12. Before

experiments, mice were housed in specific pathogen-free conditions in groups of up to 5 animals per cage in individually ventilated cages (SealSafe Plus GM 500, Tecniplast). They had *ad libitum* access to regular chow (breeding diet #1314, Altromin) and tap water. For the experiments, animals were transferred to the experimental unit. Here, they were kept in open cages (1284 L Eurostandard type II L, Tecniplast) and in light-tight cabinets where light conditions could be set individually. Whenever food intake was monitored (all HFD experiments and the corresponding short-term experiments with chow), mice were single-housed so that food intake could be related to a specific animal.

2.4. HFD feeding

At the age of 4-5 weeks, food was changed to HFD with 60 % of calories derived from fat (D12492i, Research Diets). Body weight and food consumption were measured weekly. Short-term HFD experiments were finished after one week of HFD feeding, whereas long-term HFD experiments included observation over 20-23 weeks after onset of HFD feeding. During long-term HFD experiments, two animals (one Neutrophil-BKO and one Control) were excluded because they did not develop obesity. One Neutrophil-BKO animal had to be excluded and sacrificed prematurely because of drastic loss of body weight caused by excessive growth of front teeth. One Neutrophil-BKO animal died during assessment of body composition so that body weight data could not be finalized, and the animal was excluded as well. In addition, one Neutrophil-BKO drastically lost weight without any apparent reason. According to ethical guidelines, it had to be sacrificed before the experiment was terminated.

For assessment of food intake, the food was weighed in weekly intervals. Only animals that participated in the whole experiment were considered. Some animals produced lots of food crumbs that were visible in the cage. If this was observed and food weight repeatedly exceeded 25 g per week (highest mean plus one standard deviation), animals were excluded from food intake measurements. This related to four Control and two Neutrophil-BKO animals in the long-term experiment. In the short-term experiment, two Control and one Neutrophil-BKO animal were excluded due to visible crumbs and high food intake.

2.5. Behavioral analyses

2.5.1. Measurements of locomotor activity

To detect locomotor activity, animals were single-housed and either placed in cages with a running-wheel (chow experiments) or with infrared detectors that were installed on top of the cages (HFD experiments). For running-wheel experiments, the number of wheel revolutions per time was recorded. Infrared detectors detected movements in their area as beam breaks per time. Both recordings were analyzed in 5-min intervals using the ClockLab system and software (ClockLab version 6.1.02, Actimetrics). One of the Neutrophil-BKO mice in chow experiments repeatedly blocked the running-wheel so that this mouse was excluded. One additional Neutrophil-BKO mouse was disturbed by regular opening of the cabinet due to a parallel experiment that required intervention every 12 h during the constant darkness (DD) phase. Locomotor activity periods therefore remained stable at 24 h. Since this was likely due to the interventions, this animal was excluded from period analysis.

2.5.2. Analyses of feeding rhythms

To analyze daily feeding rhythms, food of single-housed animals was weighed in 6-hour intervals over 30 h to get a profile spanning a whole 24-hour cycle. For minimal disturbance of the animals, time and noise during measurements were reduced as much as possible. When food was weighed during the dark phase, red light was used so that the circadian system was not disturbed.

Chow-fed animals were 18-23 weeks old when food profiles were set up. During HFD experiments, food profiles were generated at the beginning of HFD feeding (one week after start of HFD, age 5-6 weeks) and towards the end of the experiment (17-18 weeks after start of HFD, age 21-23 weeks).

2.6. Metabolic measurements

2.6.1. Glucose tolerance tests

Glucose tolerance tests were performed during long-term HFD feeding experiments, 15-16 weeks after start of HFD feeding. Tests were performed around ZT3 (± 30 min). Food was removed 16 h prior to the test so that animals were in a fasted state during the test. Initial blood glucose levels were determined by taking a drop of blood from the tail vein and measuring glucose concentration using a glucometer (ACCU-CHEK Aviva, Roche). Next, glucose solution was injected intraperitoneally (1.5 g/kg body weight, powdered D(+) glucose (ROTH) in 0.9 % NaCl (Braun)). Blood glucose measurements were repeated 15, 30, 60 and 120 min after the injection. At the end of the tests, animals were provided

with food again. From all the replicates, three Control animals were excluded from the analysis. Two of the animals came from the very first batch and their blood glucose levels never increased beyond 300 mg/dL, which was a clear deviation from all other replicates in both genotypes. It was therefore assumed that there was a technical problem with the injection, the glucose solution did probably not reach the intraperitoneal space. The third animal was excluded because it was classified as a non-responder in terms of developing obesity under HFD feeding.

2.6.2. Insulin tolerance tests

Since glucose and insulin tolerance tests both require repeated withdrawal of blood, mice were given one week of recovery between glucose and insulin tolerance tests. Therefore, insulin tolerance tests were performed 16-17 weeks after start of HFD feeding. The tests were performed in a similar way as the glucose tolerance tests, but food was removed only 4 h prior to the start. Insulin was injected at a concentration of 1 U/kg body weight. Human insulin stock solution (I9278, Sigma-Aldrich) was diluted with 0.9 % NaCl (Braun). The Control animal that did not respond to HFD feeding was also excluded from insulin tolerance test analysis. In addition, technical problems further reduced the total sample size of insulin tolerance tests: in one batch, the dilution of insulin was miscalculated so that the injected dose was too low (four Control and one Neutrophil-BKO animal). For one Control and two Neutrophil-BKO animals, glucose test stripes were missing to detect the last blood glucose value. All these animals were excluded from the analysis.

2.6.3. Body composition

Body composition of the animals was analyzed by nuclear magnetic resonance (minispec LF110, Bruker). Measurements were performed during week 16-17 of HFD feeding around ZT9 (± 30 min). Mice were immobilized in the measurement tube for a total time of 2 min. During that time, absolute amounts of free body fluid, fat mass, and lean mass were detected. Data were processed using the manufacturer's software (Measure minispec Plus NF, Bruker).

2.6.4. Indirect calorimetry

Oxygen consumption (VO_2) and carbon dioxide production (VCO_2) were analyzed using an open-circuit indirect calorimetry system (PhenoMaster, TSE Systems). The experiments were performed 14 - 16 weeks after onset of HFD feeding. One week before measurements started, mice were

accustomed to the drinking bottles used in the calorimetry system. Data on oxygen consumption and carbon dioxide production allowed for calculation of the respiratory exchange ratio (RER):

$$RER = \mathrm{VO2}/\mathrm{VCO2}$$

Data on oxygen consumption and RER were further used to calculate energy expenditure (Meyer et al., 2010):

$$Energy\ expenditure\ \left[\frac{kJ}{h}\right] = \ (4.44 + 1.43 * RER) * \mathrm{VO2} * 0.0036$$

Only the last day of measurement was used for analysis. In most cases, this was the seventh day. For one cohort, the calorimetry device recorded oxygen consumption and carbon dioxide production for only half of the channels. Therefore, measurements of four Control and two Neutrophil-BKO animals had to be terminated prematurely. Here, the fourth day was used for analysis. The calorimetry system collected data in 20-min intervals. Three consecutive data points were averaged to generate data with a time resolution of one hour.

2.7. Tissue and plasma collection

Mice were deeply anesthetized by intraperitoneal injection sodium pentobarbital (Narcoren, Boehringer Ingelheim, 320 mg/kg body weight). The injected solution additionally contained 1,000 U/mL sodium heparin (Rotexmedia, 10,000 U/kg body weight were injected) to prevent coagulation of blood. After careful evaluation of negative toe pinch reflexes, the thorax was opened. Blood was withdrawn from the right ventricle with the help of an insulin syringe (BD Biosciences). Blood samples were immediately transferred to EDTA-coated tubes (Sarstedt), which were stored on ice until centrifugation at 4 °C, 664 x g for 15 min. The supernatants (plasma) were frozen at -80 °C until further use.

Following blood collection, the circulation of the animals was perfused with 10 mL phosphate-buffered saline (PBS, Gibco). Next, the mice were decapitated, and the brains collected and immediately frozen on dry ice. When mice were sacrificed during their dark phase, these steps were performed under dim red light.

eWAT fat pads were carefully excised upstream of the epididymis. Additionally, inguinal subcutaneous (sc)WAT depots were collected from both sides. Adipose tissues were weighed and the lymph nodes of scWAT were excised. One eWAT and one scWAT fat pad were separately cut into small pieces and placed into ice-cold Adipose tissue dissociation buffer (see section 2.8.1.) for isolation of WBCs.

2.8. Analysis of adipose tissue immune cells

2.8.1. Isolation of immune cells out of adipose tissue

To quantify WBCs, neutrophils, and macrophages in adipose tissue, I followed a protocol for immune cell isolation that was adapted from Bapat and colleagues (Bapat et al., 2019). Adipose tissue depots were cut in small pieces and placed in Adipose tissue dissociation buffer containing 100 mM HEPES pH 7.4, 120 mM NaCl, 50 mM KCl, 5 mM Glucose, 1 mM $CaCl_2$, 1.5 % Bovine serum albumin (BSA) and 1 mg/mL Collagenase (Collagenase type I, gibco). Pieces of adipose tissue were placed into canonical tubes with 9 mL Dissociation buffer and incubated at 37 °C for 45 min, shaking at 250 rpm (Ecotron Incubator Shaker, Infors HT). The cell suspensions were then passed through 70-µm meshes (Miltenyi) and the flowthroughs incubated at room temperature for 10 min. During that time, floating adipocyte fractions separated from the SVC fractions below. These SVC fractions were collected with a pipette and transferred to fresh tubes for centrifugation (400 x g, 10 min, 4 °C). The supernatants were decanted, and the inverted tubes were dried on a paper towel. The pellets were then dissolved in 1 mL pre-chilled RPMI medium and transferred to 1.5-mL tubes. Cells were counted and up to 3M cells were stained for flow cytometry analysis.

2.8.2. Staining of adipose tissue-derived cells for flow cytometry

All centrifugation steps during this procedure were carried out at 300 x g for 5 min at room temperature. First, to change the medium to PBS, tubes were filled up with PBS, centrifuged, and the pellets resuspended in 100 µL PBS. Next, 4.0 µL Zombie NIR (live/dead stain coupled to a tandem fluorochrome composed of allophycocyanin (APC) and cyanine 7 (APC/Cy7), diluted 1:100 in PBS, **Table 1**) were added and incubated at room temperature in the dark for 15-30 min. Cells were then washed with 1 mL MACS buffer (PBS with 2 mM EDTA and 0.5 % BSA, pH 7.2) and centrifuged again. This time, the pellets were resuspended in 100 µL MACS buffer and 1.2 µL antibodies targeting Fcγ receptor (FCGR) 3 (CD16) and FCGR2 (CD32) were added (Fc block, diluted 1:10 in PBS, **Table 1**) and incubated at 4 °C for 5 min. After this incubation, antibodies directed against protein tyrosine phosphatase, receptor type, C (PTPRC, CD45), lymphocyte antigen 6 complex locus 6GD (Ly6G), integrin subunit α M (ITGM, CD11b), adhesion G protein-coupled receptor E1 (ADGRE1, F4/80), integrin subunit α X (ITGAX, CD11c) and macrophage mannose receptor (MMR, CD206) were directly added to the cell suspensions (**Table 1**). These antibodies were coupled to the fluorochromes fluorescein (FITC), brilliant violet 421 (BV421), peridinin chlorophyll protein - cyanine 5.5 (PerCP/Cy5), phycoerythrin (PE), APC and PE - Cyanine 7 (PE/Cy7) as specified below. The following volumes were used:

2.0 µL CD45-FITC (diluted 1:20 in PBS)

1,5 µL Ly6G-BV421

0.7 µL CD11b-PerCP/Cy5.5

1.75 µL F4/80-PE

0.7 µL CD11c-APC

4 µL CD206-PE/Cy7 (diluted 1:10 in PBS)

Antibodies were then incubated at 4 °C for 15-30 min. Subsequently, samples were washed with 1 mL MACS buffer to remove unbound antibodies. Samples were centrifuged again, and the pellets resuspended in 300 µL paraformaldehyde (1 % in PBS) to fix the cells until fluorescence activated cell sorting (FACS) measurements were performed on the following day.

Table 1: Details of products and antibodies that were used for FACS analysis

Name of the product/antibody	**Isotype**	**Clone**	**Company**	**Target cell/purpose**
Zombie NIR (APC/Cy7)	-	-	BioLegend	Dead cells
CD16/CD32 (Fc block)	-	-	BD Biosciences	Block unspecific binding
CD45-FITC	Rat IgG2b, κ	30-F11	BioLegend	WBCs
CD11b-PerCP/Cy5.5	Rat IgG2b, κ	M1/70	BioLegend	Neutrophils and macrophages
Ly6G-BV421	Rat IgG2a, κ	1A8	BioLegend	Neutrophils
F4/80-PE	Rat IgG2a, κ	BMS	BioLegend	Macrophages
CD11c-APC	Armenian hamster	N418	BioLegend	M1-like macrophages
CD206-PE/Cy7	Rat IgG2a, κ	C068C2	BioLegend	M2-like macrophages

2.8.3. Flow cytometry analysis

Samples that were prepared as described above were transferred to 5 mL flow cytometry tubes on the day of measurements. Immune cells were assessed using an LSR II or Canto II flow cytometry analyzer (BD Biosciences). The cytometers were compensated using single-stained compensation microbeads in combination with negative control beads (BD Biosciences). For Zombie-NIR, splenocytes were used

for compensation. For an equal proportion of live and dead cells, splenocytes were incubated at 60 °C for 5-10 min and then immediately placed on ice.

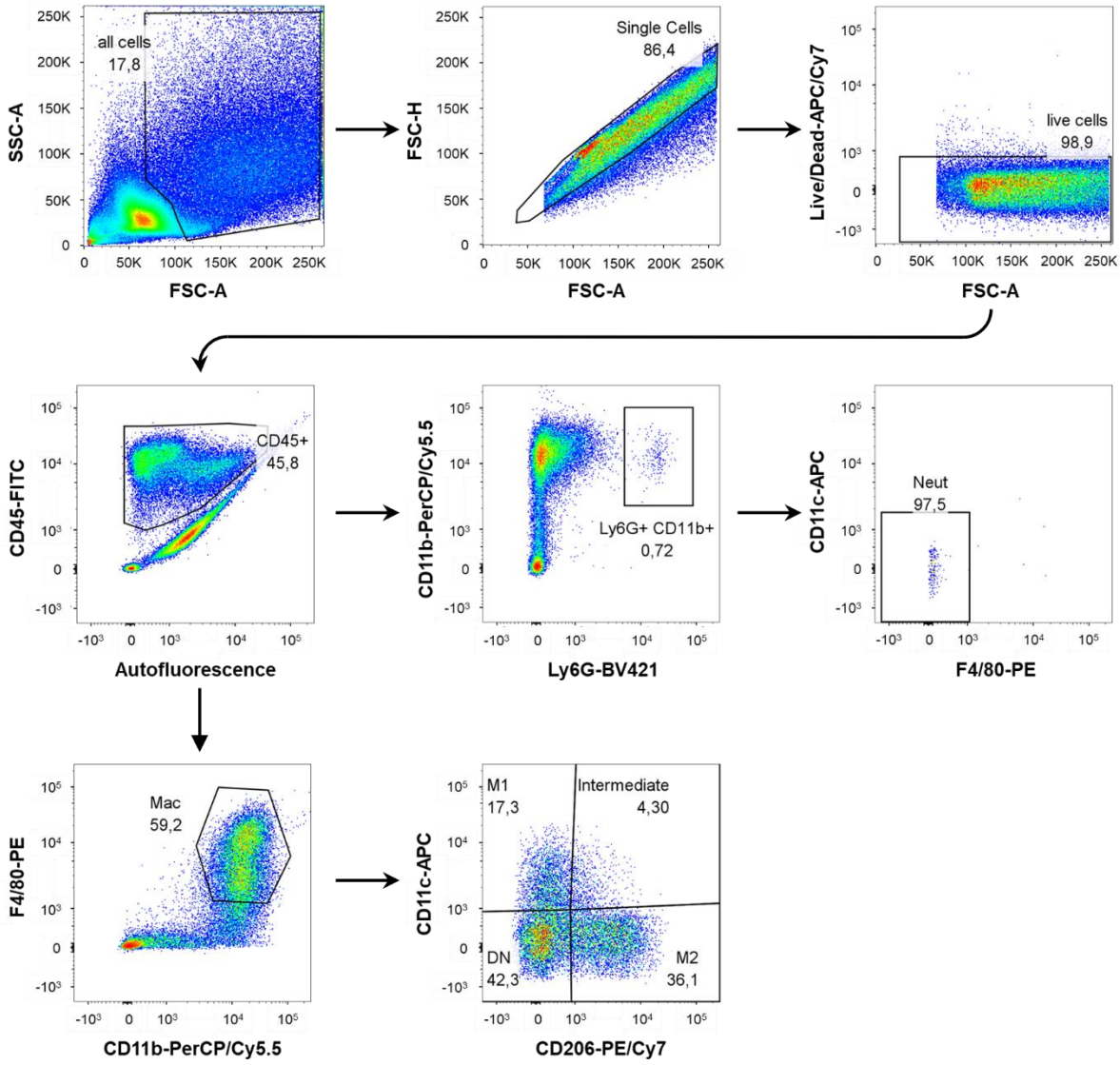

Figure 5: Gating hierarchy that was used to quantify WBCs, neutrophils, and macrophages. First, the cells of interest were separated from debris and dead cells in a forward scatter (FSC) – sideward scatter (SSC) panel. Following this, duplets were excluded in an FSC-FSC panel and live cells identified as being negative for the live/dead stain. From this population, CD45 positive cells (WBCs) were plotted against autofluorescence. WBCs were further categorized into neutrophils (Neut, positive for CD11b and Ly6G) and into macrophages (Mac, positive for F4/80 and CD11b). The final neutrophil population was identified by negative selection for F4/80 and CD11c. Macrophages were further categorized into M1-like (CD11c positive, CD206 negative) or M2-like (CD206 positive, CD11c negative) cells. Macrophages that expressed neither CD11c nor CD206 were classified double negative (DN).

The stainings allowed for quantification of WBCs, neutrophils, and macrophages, whereas macrophages were further distributed into M1-like and M2-like macrophages (**Table 1**, **Figure 5**). A dump channel was included to manage the high degree of autofluorescence that is typical of adipose tissue cells.

When stainings were established, isotype controls were used to exclude unspecific binding of the antibodies. Furthermore, fluorescence-minus-one controls helped to set the gates properly. Additionally, replicates with unstained control samples were measured in each batch.

2.9. Plasma measurements of leptin and adiponectin

Plasma levels of leptin and adiponectin were determined using sandwich enzyme-linked immunosorbent assay (ELISA) kits (mouse leptin ELISA kit and mouse adiponectin ELISA kit, both Crystal Chem) according to the manufacturer's instructions. Briefly, leptin or adiponectin were captured by specific antibodies that were coated on a microplate. Subsequently, a second specific antibody was added that bound to immobilized leptin or adiponectin. In case of adiponectin, this second antibody was biotinylated. It was further bound by a complex of streptavidin and horseradish peroxidase. In the leptin assay, the second antibody was bound by a third species-targeted antibody that was coupled to horseradish peroxidase. Addition of substrate solution initiated a colorimetric response that could be detected on a microplate spectrophotometer (450/630 nm, Epoch Microplate Spectrophotometer, BioTek instruments) in combination with Gen5 software (BioTek instruments). Plasma concentrations were interpolated from standard curves using GraphPad Prism 9 software (GraphPad).

2.10. Hematology

To determine blood cell counts, mice were sacrificed at ZT1 (± 30 min) by cervical dislocation and subsequent decapitation. Trunk blood was collected in EDTA-coated microvettes (Sarstedt) and analyzed on a scil Vet abc Plus+ hematology device (scil animal care company).

2.11. Isolation of neutrophils from bone marrow and blood

Neutrophils were isolated from blood and bone marrow for validation of the Neutrophil-BKO mouse model. For isolation of neutrophils from blood, mice were sacrificed by intraperitoneal injection of pentobarbital (320 mg/kg, Boehringer Ingelheim). In addition, sodium heparin (Rotexmedia,

10,000 U/kg body weight) was present in the injected solution to prevent coagulation. Blood was withdrawn from the right ventricle and transferred to EDTA-coated tubes. Red blood cells (RBCs) were lysed using RBC lysis buffer (BioLegend) according to the manufacturer's instructions. Briefly, blood samples were transferred to 50-mL canonical tubes and 10 mL of 1 X Lysis buffer were added. After incubation for 10 min at room temperature, tubes were filled up with MACS buffer (see 2.8.2.) and centrifuged at 350 x g, 5 min, 4 °C. The cell pellets were then resuspended in 300 µL PBS and stained as described for flow cytometry analysis (see 2.8.2.), but triple volumes were used. Samples were stained with the following reagents: Zombie-NIR, Fc block, CD45-FITC, Ly6G-BV421, CD11b-PercP/Cy5.5 (**Table 1**).

For isolation of neutrophils from bone marrow, mice were sacrificed by cervical dislocation followed by immediate decapitation. Femurs and tibias were isolated and cleared from muscle and connective tissue. Tips of the bones were cut off and the bone marrow flushed out with the help of a syringe and a 23 G cannula. Cells were collected in MACS buffer, filtered through 70-µm meshes (Miltenyi) and centrifuged at 350 x g for 5 min at 4 °C. The pellets were resuspended in 1 mL MACS buffer. Cells were then washed with PBS, resuspended in 300 µL PBS and stained as described for the samples derived from blood.

Blood and bone marrow samples were used to isolate neutrophils using a FACSAria III Flow Cytometer (BD Biosciences). Isolations were performed by staff from the Cell Analysis Core Facility of the University of Lübeck. The cytometer was compensated with a combination of unstained and single-stained neutrophil cell suspensions. Dead and duplet cells were excluded, and neutrophils selected as being positive for CD45, Ly6G and CD11b. Sorted cells were centrifuged at 300 x g for 5 min, the supernatants discarded, and the pellets frozen at -80 °C until further use.

2.12. RNA isolation and quantitative real-time (q)PCR

Total RNA was extracted from isolated neutrophils or from hypothalamic tissue. The hypothalamus was excised from frozen brains with a scalpel (Feather). The excised area was enclosed by the optic chiasm (rostral side) and by the mammillary bodies (caudal side). The samples were directly transferred to screw-cap tubes containing 500 µL TRIzol (ThermoFisher) and 5-6 ceramic beads (1.4-mm ceramic beads, Omni International). The tissue was homogenized in a bench homogenizer (Omni Bead Ruptor, Omni International) with the following settings: 1-2 cycles at a speed of 2.9 m/s, each cycle lasting 15-20 s with a break of 15 s in between cycles if two cycles were used. Neutrophil samples did not need mechanical homogenization so that 500 µL of TRIzol were directly added to frozen cell pellets and homogenized by pipetting up and down.

In both cases, the homogenates were incubated at room temperature for 5 min before 100 µL of chloroform were added (purity ≥ 99.5 %, Honeywell, ThermoFisher). Samples were then shaken vigorously and incubated for 5 min on ice, followed by centrifugation at 15,294 x g for 15 min at 4 °C. The upper aqueous phases containing RNA were combined with 250 µL isopropanol (Roth) and incubated at -20 °C for at least 30 min followed by centrifugation at 17,949 x g for 30 min at 4 °C. The RNA pellets were then washed twice with 500 µL ethanol (70 %) and centrifuged at 20,817 x g for 10 min at 4 °C. Pellets were air-dried for 5-10 min and dissolved in 16-25 µL deionized water. RNA concentrations and purities were determined by absorption at 260 and 280 nm on a spectrophotometer (Epoch Microplate Spectrophotometer, BioTek Instruments) and analyzed using Gen5 software (version 2.0, Bio Tek Instruments). Samples were either used directly for reverse transcription or frozen at -80 °C until further use.

cDNA was obtained from RNA using the High-capacity cDNA Reverse Transcription Kit (Applied Biosystems). Total RNA yield from neutrophil samples was very low (100-800 ng) so that up to 500 ng were used for reverse transcription. For hypothalamus samples, 2 µg total RNA were used. The corresponding volumes were topped up with Deionized water to 14.2 µL. Next, 5.8 µL master mix were added that contained 2 µL 10 X RT buffer, 0.8 µL 25 X dNTP mix, 2 µL 10 X Random hexamer RT primers and 1 µL MultiScribe reverse transcriptase.

Samples were incubated at 25 °C for 10 min, followed by 37 °C for 120 min and 85 °C for 5 min. cDNA was diluted 1:5 (neutrophils) or 1:10 (hypothalamus) with Deionized water and stored at -20 °C.

qPCR was performed using 5 µL Diluted cDNA, 5 µL Primer mix (1.4 µM, **Table 2**) and 10 µL Go-Taq qPCR Master Mix (Promega) on a 96-well plate (Multiplate PCR plates 96-well, Bio-Rad). Plates were sealed with adhesive tape (Biozym Biotech Trading) and measured in a real-time PCR detection system (CFX96 thermocycler, Bio-Rad). The following temperature conditions were used:

Temperature [°C]	Time	
94	5 min	
94	15 s	40 x
60	15 s	
72	20 s	
72	5 min	

Eukaryotic elongation factor 1 α *(Eef1α)* was used as housekeeping gene to normalize gene expression. Relative RNA levels were calculated using the ΔΔCT method (Livak and Schmittgen, 2001). Significant outliers, as determined by Grubb's tests with p-values below 0.05, were excluded from the analyses.

In knockout validation experiments, all samples with total RNA yield below 150 ng were excluded since data are getting unreliable with low RNA quantities. This affected one replicate from each genotype.

Table 2: Sequences of primers that were used for qPCR.

Target gene	Forward primer (5' → 3')	Reverse primer (5' → 3')
Agrp	ATGCTGACTGCAATGTTGCTG	CAGACTTAGACCTGGGAACTCT
Bmal1	AGAGGCGTCGGGACAAAATGAACAG	AACAGCCATCCTTAGCACGGTGA
Cartpt	CCCGAGCCCTGGACATCTA	GCTTCGATCTGCAACATAGCG
Eef1α	TGCCCCAGGACACAGAGACTTCA	AATTCACCAACACCAGCAGCAA
Il-6	GTGGCTAAGGACCAAGACCA	GGTTTGCCGAGTAGACCTCA
Mpo	TCCCACTCAGCAAGGTCTT	TAAGAGCAGGCAAATCCAG
Npy	ATGCTAGGTAACAAGCGAATGG	TGTCGCAGAGCGGAGTAGTAT
Pomc	ATGCCGAGATTCTGCTACAGT	TCCAGCGAGAGGTCGAGTTT
Tnf-α	GAAAAGCAAGCAGCCAACCA	CGGATCATGCTTTCTGTGCTC

2.13. Data analysis and statistics

Data are presented as means ± standard errors of the mean (SEMs). GraphPad prism software (Version 9.3.0., GraphPad) was used for statistical analyses. For comparison of one variable between two groups, unpaired t-tests were used. If standard deviations were not equal, Welch's correction was included. Two-way analysis of variance (ANOVA) with Bonferroni post-tests was applied for comparison of two variables (for example, time and genotype). Differences were considered statistically significant when p-values were below 0.05.

Analyses for circadian rhythmicity were performed using CircaCompare (Parsons et al., 2020). The corresponding package was installed and used in RStudio (version 1.4.1106, RStudio Inc.). To decide whether a dataset is significantly rhythmic, CircaCompare fits a cosinusoidal curve of user-defined period to the data. The period was set to 24 h and the significance threshold to 0.05. The corresponding code that was used can be found in the supplements (**Supplemental Figure S1**). If both genotypes showed rhythmic conditions, CircaCompare assessed differences in mesor, amplitude and phase. Again, differences with p-values below 0.05 were considered statistically significant.

3. Results

In this PhD thesis, I investigated the role of the circadian clock in neutrophils for DIO and metaflammation in mice. To this end, I generated Neutrophil-BKO mice and analyzed body weight and metabolic parameters after HFD feeding as well as adipose tissue infiltration of neutrophils and macrophages.

3.1. *Bmal1* is effectively reduced in Neutrophil-BKO mice

To test the influence of the neutrophil circadian clock on DIO and metaflammation, the Neutrophil-BKO mouse line was generated by crossing *Mrp8-Cre* mice to *Bmal1*-flox mice. For validation of the mouse model, mature neutrophils were isolated from blood and bone marrow by FACS. After exclusion of dead cells and duplets, neutrophils were selected based on expression of the leukocyte marker CD45 and the neutrophil markers CD11b and Ly6G. Immature neutrophils might not express Mrp8-driven *Cre* recombinase, hence they would not show recombination. These cells were identified by low or intermediate expression of Ly6G (Evrard et al., 2018) and excluded from analysis. Compared to Control levels (1.00 ± 0.33), *Bmal1* mRNA expression was significantly reduced to 0.20 ± 0.03 in neutrophils from Neutrophil-BKO mice (**Figure 6**).

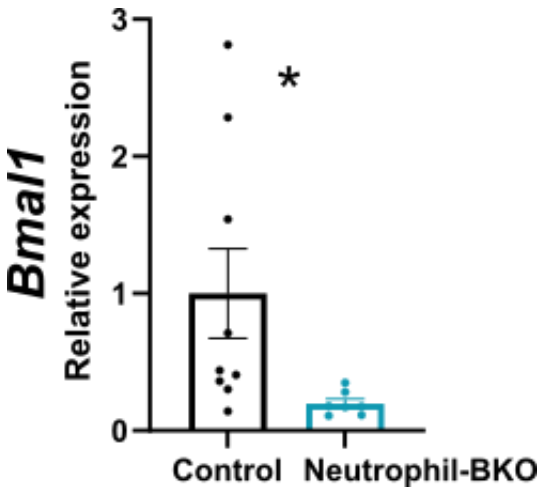

Figure 6: ***Bmal1* mRNA levels are significantly reduced in Neutrophil-BKO mice.** *Bmal1* mRNA levels from isolated neutrophils were measured by qPCR and normalized to expression levels of Controls. * $p < 0.05$ (unpaired t-test), n = 7/9 per genotype. Data are presented as means ± SEMs.

3.2. *Bmal1* knockout in neutrophils does not affect circadian locomotor activity or food intake rhythms

To test if *Bmal1* deletion in neutrophils affects the general organization of the circadian clock network, rhythms of locomotor activity and food intake were compared between Neutrophil-BKO and Control mice. For investigation of locomotor activity, mice were placed in cages with running-wheels and their activity was recorded in a 12h:12h light-dark regime (LD) and in DD. In LD, both genotpyes showed comparable locomotor activity patterns with high activity in the first half of the night and a decrease in the second half of the night. Upon release into DD, activity onsets shifted to earlier times every day. Of note, the Control actogram shows irregular activity onsets in DD. These were also observed for some of the Neutrophil-BKO mice (**Figure 7 A, B**). Neutrophil-BKO and Control mice showed 99.54 ± 0.18 % and 99.54 ± 0.13 % of their running-wheel activity during the night (dark phase), respectively. Accordingly, 0.46 ± 0.18 % (Neutrophil-BKOs) and 0.46 ± 0.13 % (Controls) of the daily activity counts were recorded during the day (light phase) (**Figure 7 C**). Locomotor activity periods were determined by χ^2 periodogram analysis. Animals showed LD periods of 24.02 ± 0.02 h (Neutrophil-BKOs) and 24.00 ± 0.00 h (Controls). Upon release into DD, free-running periods of 23.23 ± 0.14 h for Neutrophil-BKOs and 23.13 ± 0.09 h for Control mice were observed (**Figure 7D**). There was no significant genotype effect for any of the activity parameters that were assessed.

For analysis of food intake rhythms, food was weighed in LD at 6-hour intervals for one day (**Figure 7 E**). During the first half of the light phase (ZT0-6), Neutrophil-BKO and Control mice consumed 0.23 ± 0.23 % and 2.95 ± 1.37 % of their daily food intake, respectively. During the second half of the light phase (ZT6-12), food consumption increased to 10.34 ± 2.20 % (Neutrophil-BKOs) and 11.58 ± 2.45 % (Controls). Most of the food was consumed during the dark phase. From ZT12-18, Neutrophil-BKO animals consumed 53.27 ± 2.81 % of their food, compared to 46.76 ± 2.94 % for Controls. The second half of the dark phase was characterized by slightly lower food intake (36.16 ± 4.44 % for Neutrophil-BKOs and 37.71 ± 3.01 % for Controls). Feeding rhythm parameters (mesor, phase and amplitude) were not significantly different between genotypes (**Supplemental Table S1**).

It can therefore be concluded that knockout of *Bmal1* in neutrophils does not affect SCN-driven circadian rhythms of locomotor activity and food intake.

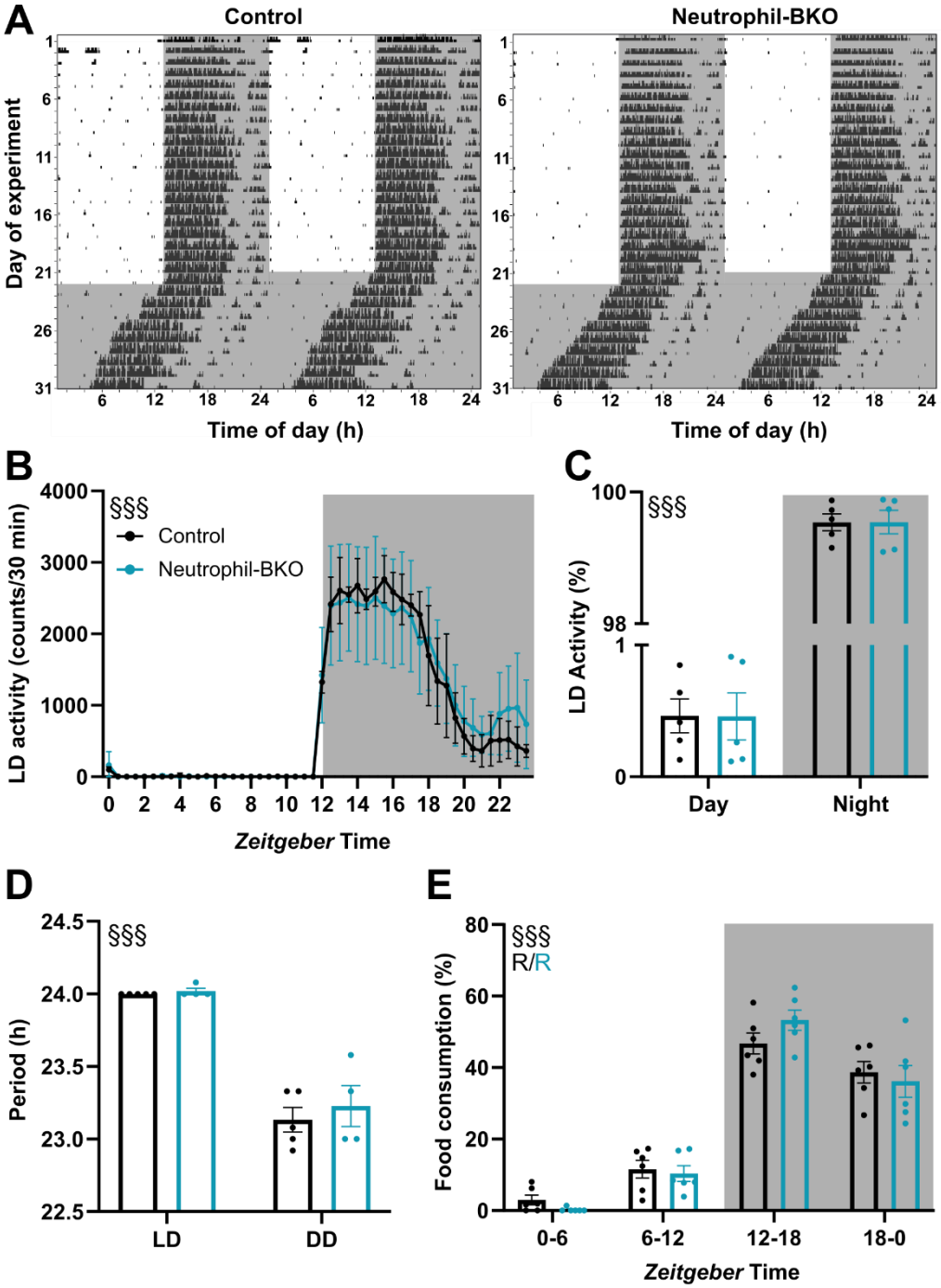

Figure 7: Locomotor activity and food intake rhythms are comparable between Neutrophil-BKO and Control animals. A: Representative double-plotted actograms of one Control and one Neutrophil-BKO mouse. Black bars represent activity. **B:** Activity profile averaged over 7 days in LD. n = 5 per genotype. **C:** Relative distribution of locomotor activity during day and night, averaged over 7 days in LD. n = 5 per genotype. **D:** Activity period analyzed across 8-17 days in LD and 6-9 days in DD. n = 4-5 per genotype. **E:** Relative food consumption in LD during a full 24-hour cycle. n = 6 per genotype. §§§ $p < 0.001$, time effect (B, C, E) or light schedule effect (D); two-way ANOVA. R: rhythmic ($p < 0.05$; CircaCompare). Grey-shaded areas indicate times with lights switched off. Data are presented as means ± SEMs.

3.3. Loss of *Bmal1* in neutrophils does not affect blood cell counts

To ensure that loss of *Bmal1* in neutrophils does not affect blood cell counts of immune cells, hematology measurements were performed. Blood of Neutrophil-BKO animals contained 9.93 ± 0.43 x 10^{12} RBCs/L, for Control mice this number was 9.57 ± 0.76 x 10^{12} RBCs/L. Abundance of platelets (PLT) was 0.87 ± 0.18 x 10^{12} cells/L and 0.95 ± 0.24 x 10^{12} cells/L for Neutrophil-BKOs and Controls, respectively. For WBCs, numbers were 3.47 ± 0.65 x 10^{9} cells/L for Neutrophil-BKOs and 3.15 ± 0.70 x 10^{9} cells/L for Controls (**Figure 8 A**). WBCs were further classified into lymphocytes (LYM), granulocytes (GRA, containing mostly neutrophils) and monocytes (MON). Neutrophil-BKO mice had 71.72 ± 3.30 % lymphocytes compared to 70.77 ± 4.07 % in Control mice. Granulocytes constituted 24.00 ± 3.12 % of WBCs in Neutrophil-BKOs and 25.40 ± 3.86 % in Controls. Lastly, monocytes accounted for 4.28 ± 0.42 % of WBCs in Neutrophil-BKOs and 3.83 ± 0.37 % of WBCs in Controls.

Controls and Neutrophil-BKOs did not show significant differences for any of the immune cell parameters that were analyzed so that it can be concluded that deletion of *Bmal1* in neutrophils does not influence blood immune cell counts.

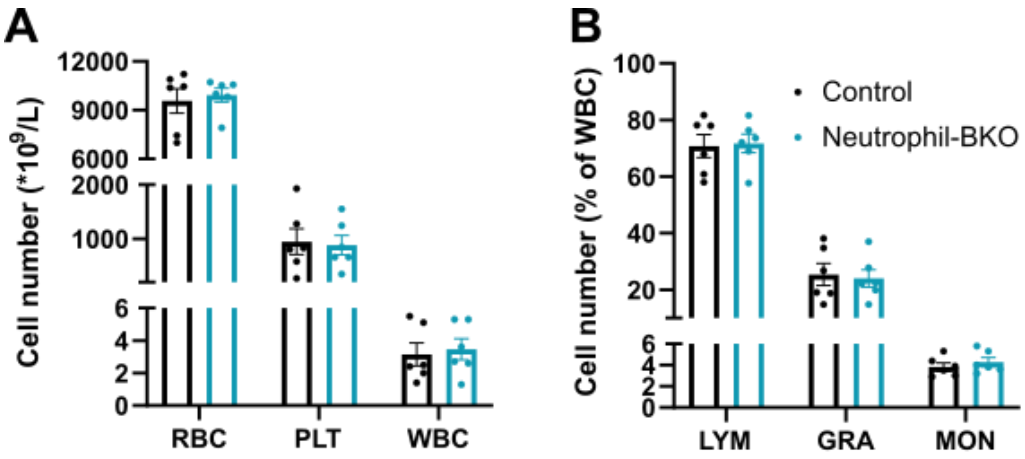

Figure 8: Loss of *Bmal1* in neutrophils does not affect immune cell counts in the blood. Blood samples were collected at ZT1. **A:** Absolute cell numbers of RBC, PLT and WBC. **B:** LYM, GRA and MON fractions are indicated as percentages of the WBC population. n = 6 per genotype. Data are presented as means ± SEMs.

3.4. Neutrophil-BKO animals show lower body weight gain and decreased adiposity after long-term feeding of HFD

To test the obesogenic effect of HFD on Neutrophil-BKO mice, animals were fed a HFD (60 % of calories from fat) for 20-23 weeks. At the beginning, body weight was 16.46 ± 0.26 g (Neutrophil-BKOs) or 18.17 ± 0.31 g (Controls) and there was no significant difference between genotypes. After 20 weeks of HFD feeding, Neutrophil-BKO and Control animals weighed 43.83 ± 1.40 g and 49.68 ± 0.75 g, respectively. Body weight of Neutrophil-BKO mice was significantly lower than that of Control mice from week 4 on (**Figure 9 A**). To analyze if lower body weight was accompanied by reduced growth, body length was measured at the end of the experiment. Neutrophil-BKO mice were significantly shorter than Controls (10.99 ± 0.06 cm compared to 11.34 ± 0.05 cm) (**Figure 9 B**).

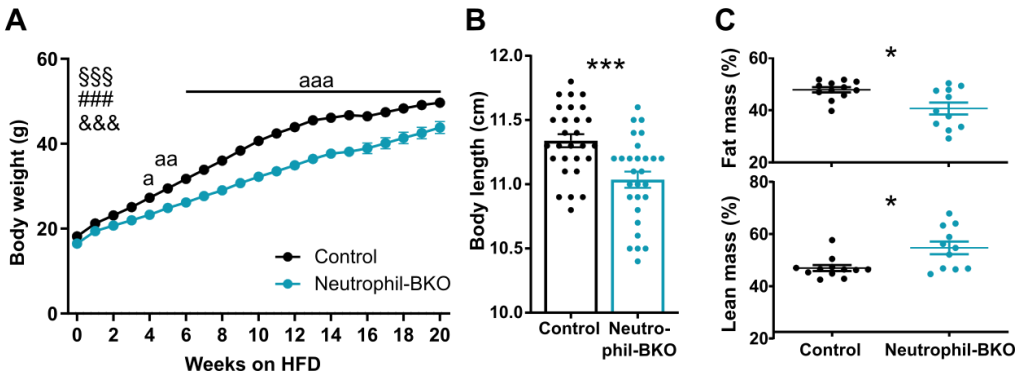

Figure 9: Neutrophil-BKO animals become less obese during long-term feeding of HFD. **A:** Body weight development during 20 weeks of HFD feeding. n = 28/31 per genotype. **B:** Body length that was measured at the end of the experiment. Length was taken from the tip of the mouth to the toes of stretched hind legs. n = 28 per genotype. **C:** Fat and lean mass in percent of body weight, analyzed by nuclear magnetic resonance measurements after 15-16 weeks of HFD feeding. n = 11/12 per genotype. ### $p < 0.001$ genotype effect, §§§ $p < 0.001$ time effect, &&& $p < 0.001$ interaction (two-way ANOVA). a $p < 0.05$, aa $p < 0.01$, aaa $p < 0.001$ (Bonferroni post-test). * $p < 0.05$ (unpaired t-test with Welch's correction for unequal variances). Data are presented as means ± SEMs.

In addition, fat and lean mass of the animals were analyzed by nuclear magnetic resonance measurements after 15-16 weeks of HFD feeding. Fat mass of Neutrophil-BKO animals was 40.65 ± 2.30 %, which was significantly lower than that of Control mice (47.84 ± 1.02 %). Conversely, lean mass was significantly higher for Neutrophil-BKO mice (54.71 ± 2.44 % for Neutrophil-BKOs *vs.* 46.98 ± 1.41 % for Controls) (**Figure 9 C**).

It can be therefore concluded that lower body weight of Neutrophil-BKOs after HFD feeding is associated with shorter body length and decreased adiposity.

3.5. Neutrophil-BKO animals show improved glucose tolerance and insulin sensitivity under HFD feeding

Glucose and insulin tolerance tests were used to analyze whether reduced adiposity during HFD feeding also improved metabolic function. Glucose tolerance and insulin sensitivity were tested by intraperitoneal injections of glucose and insulin and subsequent measurements of blood glucose levels (glucose or insulin tolerance test). At the beginning of the glucose tolerance test, fasting blood glucose levels were 165.23 ± 6.91 mg/dL for Neutrophil-BKOs and 198.5 ± 7.07 mg/dL for Controls. Upon injection of glucose, blood glucose levels strongly increased during the first 30 minutes for both genotypes, reaching 401.46 ± 10.94 mg/dL (Neutrophil-BKOs) or 399.75 ± 11.10 mg/dL (Controls). During the following 90 minutes, blood glucose steadily decreased again. This decrease was more pronounced in Neutrophil-BKO mice so that blood glucose levels were significantly lower at 60 and 120 minutes after injection. After 120 minutes, levels were almost back to baseline for Neutrophil-BKOs (213.46 ± 7.23 mg/dL), while Control animals still had increased values (288.58 ± 17.79 mg/dL) (**Figure 10 A**). The stronger decrease was also reflected in a significantly lower area under the curve for Neutrophil-BKO mice (36,340 ± 1,117 *vs.* 40,792 ± 1,199 (**Figure 10 B**).

These findings indicate that Neutrophil-BKO mice have a better ability to balance their blood glucose levels under HFD conditions. The stronger decline after glucose injection could be explained either by a higher secretion of insulin and/or by a higher insulin sensitivity.

To test whether changes in glucose tolerance in Neutrophil-BKOs were due to altered insulin sensitivity, an insulin tolerance test was performed. Before insulin was injected, blood glucose levels were comparable for both genotypes (205.33 ± 8.17 mg/dL for Neutrophil-BKOs and 219.11 ± 9.98 mg/dL for Controls). As expected, insulin injection caused a rapid decrease of blood glucose levels during the first 30 minutes, reaching 140.78 ± 12.91 mg/dL for Neutrophil-BKOs and 166.33 ± 8.23 mg/dL for Controls. During the remaining 90 minutes of the test, blood glucose levels stabilized and increased again. This increase was slower for Neutrophil-BKO mice so that these mice showed significantly lower levels at 120 minutes (163.56 ± 11.37 mg/dL *vs*. 214.78 ± 17.24 mg/dL in Controls) (**Figure 10 C**). As for the glucose tolerance test, the area under the curve was significantly smaller for Neutrophil-BKOs (18,726 ± 1,277) compared to Controls (22,679 ± 1,003) (**Figure 10 D**). Since all animals received the same amount of insulin relative to their body weight, a smaller area under the curve reflects higher sensitivity to insulin. It can be therefore concluded that Neutrophil-BKO animals have a better insulin sensitivity during long-term HFD feeding.

Altogether, Neutrophil-BKO mice show an ameliorated DIO phenotype. They gain less weight, and they retain higher glucose tolerance and insulin sensitivity under HFD conditions.

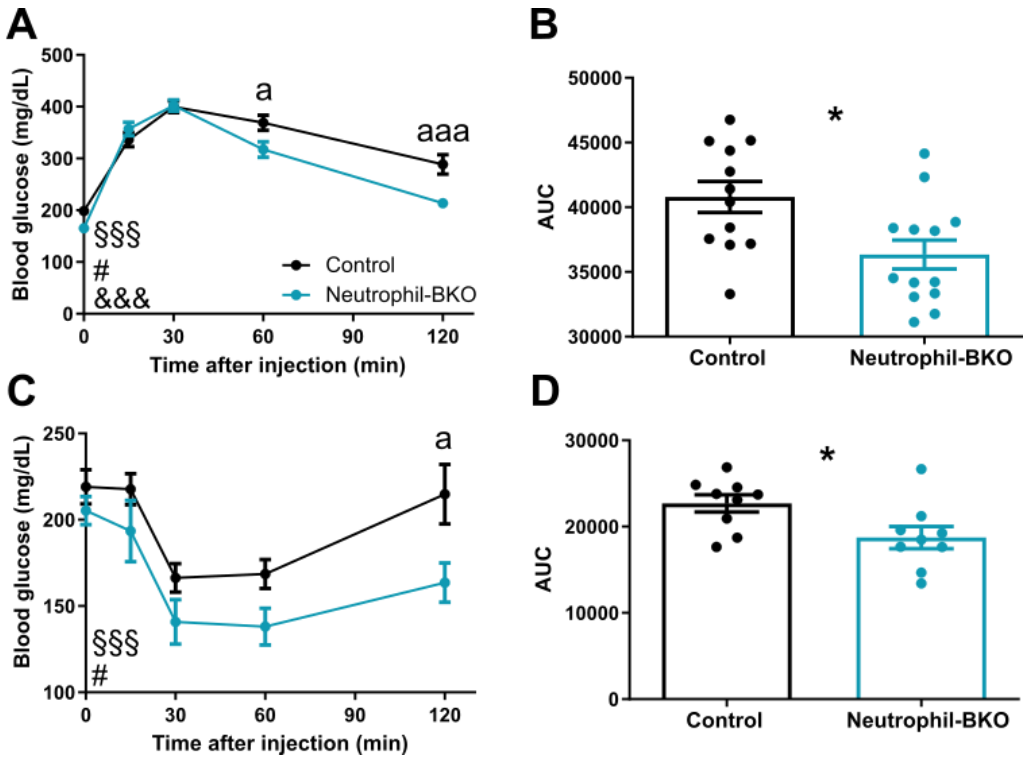

Figure 10: Glucose and insulin tolerance are enhanced in Neutrophil-BKOs after long-term HFD feeding. **A:** Blood glucose levels after intraperitoneal injection of glucose (glucose tolerance test). The test was performed 15-16 weeks after onset of HFD feeding and started at ZT3.5 **B:** Glucose area under the curve (AUC) during glucose tolerance test. **C:** Blood glucose levels after intraperitoneal injection of insulin (insulin tolerance test). The test was performed 16-17 weeks after onset of HFD feeding and started at ZT3.5 **D:** Glucose AUC during insulin tolerance test. n = 13/14 per genotype (A & B), n = 9 per genotype (C & D). # $p < 0.05$ genotype effect, §§§ $p < 0.001$ time effect, &&& $p < 0.001$ interaction (two-way ANOVA). a $p < 0.05$, aaa $p < 0.001$ (Bonferroni post-test). * $p < 0.05$ (unpaired t-test). Data are presented as means ± SEMs.

3.6. Food intake is reduced in Neutrophil-BKO mice during long-term feeding of HFD, but locomotor activity and energy metabolism are not altered

Energy balance of Neutrophil-BKO mice was analyzed in more detail to clarify if differences in food intake, locomotor activity, energy consumption or metabolism of macronutrients might contribute to reduced body weight gain of Neutrophil-BKO mice in DIO.

Food intake was quantified every week during 20 weeks of HFD feeding. In accordance with the lower body weight gain that was observed, food intake of Neutrophil-BKO mice was slightly but significantly reduced. Over the course of the experiment, Neutrophil-BKO mice consumed 388.97 ± 7.69 g of food, compared to Controls that ate 409.47 ± 5.75 g. The difference in cumulative food intake was significant from week 15 onwards (**Figure 11 A**). Of note, body weight of Neutrophil-BKO mice was significantly

lower after 4 weeks already (see **Figure 9 A**). Still, food intake needs to be considered as a factor that might contribute to lower body weight in Neutrophil-BKOs.

It is known that metabolic outcome is not only influenced by the amount of food that is consumed but also by timing of food intake. To see whether food intake rhythms were altered, food consumption was analyzed in daily profiles at the beginning (after 1 week) and towards the end (after 17-18 weeks) of HFD feeding. Already after one week of HFD feeding, food intake rhythms were dampened compared to observations on normal chow in both genotpyes (**Figure 7 E**, **Figure 11 B**, **Supplemental Figure S2 A, B**). On HFD, mice consumed 13.65 ± 1.14 % (Neutrophil-BKOs) and 13.99 ± 2.08 % (Controls) of their daily food during the first half of the light phase (ZT0-6). Between ZT6 and ZT12, food intake increased to 22.82 ± 0.91 % (Neutrophil-BKOs) and to 21.23 ± 3.03 % (Controls). Highest food consumption was observed during the first half of the dark phase (ZT12-18), when Neutrophil-BKO mice ate 41.20 ± 1.59 % and Control mice 36.12 ± 3.58 % of their food. From ZT18-0, the remaining 22.23 ± 1.69 % (Neutrophil-BKOs) and 28.54 ± 4.06 % (Controls) were consumed. Altogether, about a third of the total food was consumed during the light phase, but there was no significant difference between genotypes. Again, feeding rhythm parameters were not different between genotypes (**Figure 11 B**, **Supplemental Table S1**).

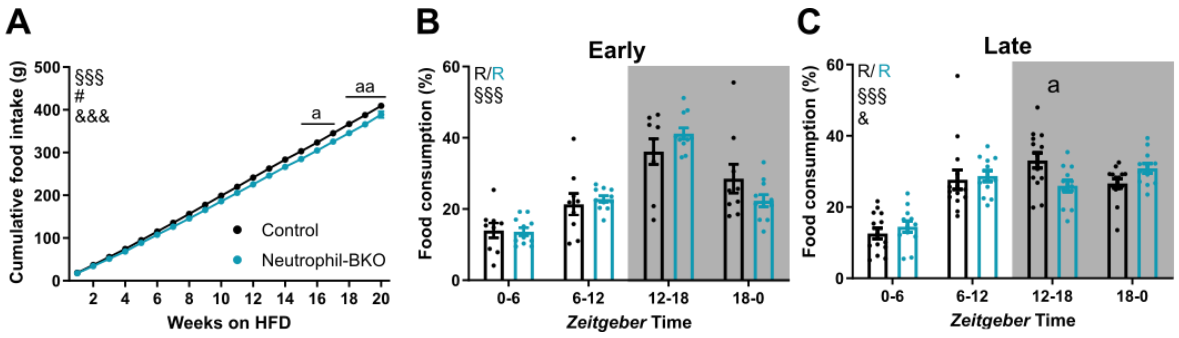

Figure 11: Food consumption is reduced in Neutrophil-BKO mice after long-term HFD feeding. **A:** Cumulative food intake during 20 weeks of HFD feeding. n = 27 per genotype. **B:** Relative food consumption over the course of one day during an early phase of the experiment (1 week after onset of HFD feeding). n = 9/11 per genotype. **C:** Relative food consumption over the course of one day at a late stage of HFD feeding (17-18 weeks after start). n = 12/14 per genotype. §§§ $p < 0.001$ time effect, # $p < 0.05$ genotype effect, & $p < 0.05$ and &&& $p < 0.001$ interaction (two-way ANOVA). a $p < 0.05$, aa $p < 0.01$ (Bonferroni post-test). R: rhythmic ($p < 0.05$; CircaCompare). Grey-shaded areas indicate times with lights switched off. Data are presented as means ± SEMs.

After 17-18 weeks of HFD feeding, food intake rhythms had dampened even further. Neutrophil-BKO and Control mice consumed 14.49 ± 1.57 % and 12.59 ± 1.49 % of their food during the first half of the light phase (ZT0-6), respectively. From ZT6-12, these numbers increased to 28.70 ± 1.55 % (Neutrophil-

BKOs) and 27.70 ± 2.72 % (Controls). Together, food intake during the light phase comprised around 40 % of the daily food intake. Between ZT12 and ZT18, Neutrophil-BKO mice ate 25.96 ± 1.64 % and Control mice 33.10 ± 2.13 %. During the second half of the dark phase, food intake was 30.86 ± 1.36 % for Neutrophil-BKOs and 26.62 ± 1.31 % for Controls. There was no overall genotype effect, but food consumption was significantly lower for Neutrophil-BKO mice from ZT12-18. Both Neutrophil-BKO and Control mice preserved their circadian rhythm of food intake. However, the amplitude was significantly reduced for Neutrophil-BKO animals (**Figure 11 C**, **Supplemental Table S1**).

In summary, cumulative food intake over the course of 20 weeks on HFD was reduced for Neutrophil-BKO mice. With extended time on HFD, food intake of Neutrophil-BKOs was decreased especially during the first half of the dark phase.

For information on energy utilization of the mice, I measured locomotor activity, oxygen consumption, and carbon dioxide production. Furthermore, RER was calculated. This measure confers information on the type of macronutrients that were metabolized.

Locomotor activity was detected by passive infrared sensors that were installed atop the cages. Activity was monitored continuously throughout the experiment. Time frames of one week were selected at the beginning and at the end of HFD feeding for quantification of activity. Over the course of the experiment, total daily activity decreased from an average of $8.68 \pm 0.85 * 10^3$ counts/day to $6.29 \pm 0.79 * 10^3$ counts/day in Neutrophil-BKO animals. A similar reduction of locomotor activity was observed for Controls ($9.12 \pm 0.64 * 10^3$ counts/day in the beginning vs. $5.29 \pm 0.80 * 10^3$ counts/day in the end) (**Figure 12 A, B**). Total activity was not different between Neutrophil-BKO and Control mice.

At the early stage, Neutrophil-BKO mice showed 11.03 ± 1.24 % of their activity during the day (light phase), compared to 9.41 ± 0.74 % for Control mice. Accordingly, 88.97 ± 1.24 % or 90.59 ± 0.74 % of locomotor activity were observed during the night (dark phase) (**Figure 12 C**). At the late stage, activity during the day accounted for 11.95 ± 2.41 % of the total activity (Neutrophil-BKOs) or for 14.61 ± 2.97 % (Controls). Likewise, 88.03 ± 2.41 % or 85.39 ± 2.97 % of activity was detected during the night (**Figure 12 D**). Distribution of light and dark activity was not different between genotypes, neither at the early nor at the late stage. Controls showed a slight but non-significant increase in daytime activity from the early to the late stage (**Supplemental Figure S2 C, D**). Compared to chow-fed animals, relative daytime activity increased under HFD feeding while relative nighttime activity decreased. Differences between genotypes were non-significant under all conditions that were analyzed (**Figure 7 C**, **Figure 12 C, D**, **Supplemental Figure S2 C, D**).

In summary, there is no indication of genotype differences in locomotor activity, neither during chow feeding nor during exposure to HFD.

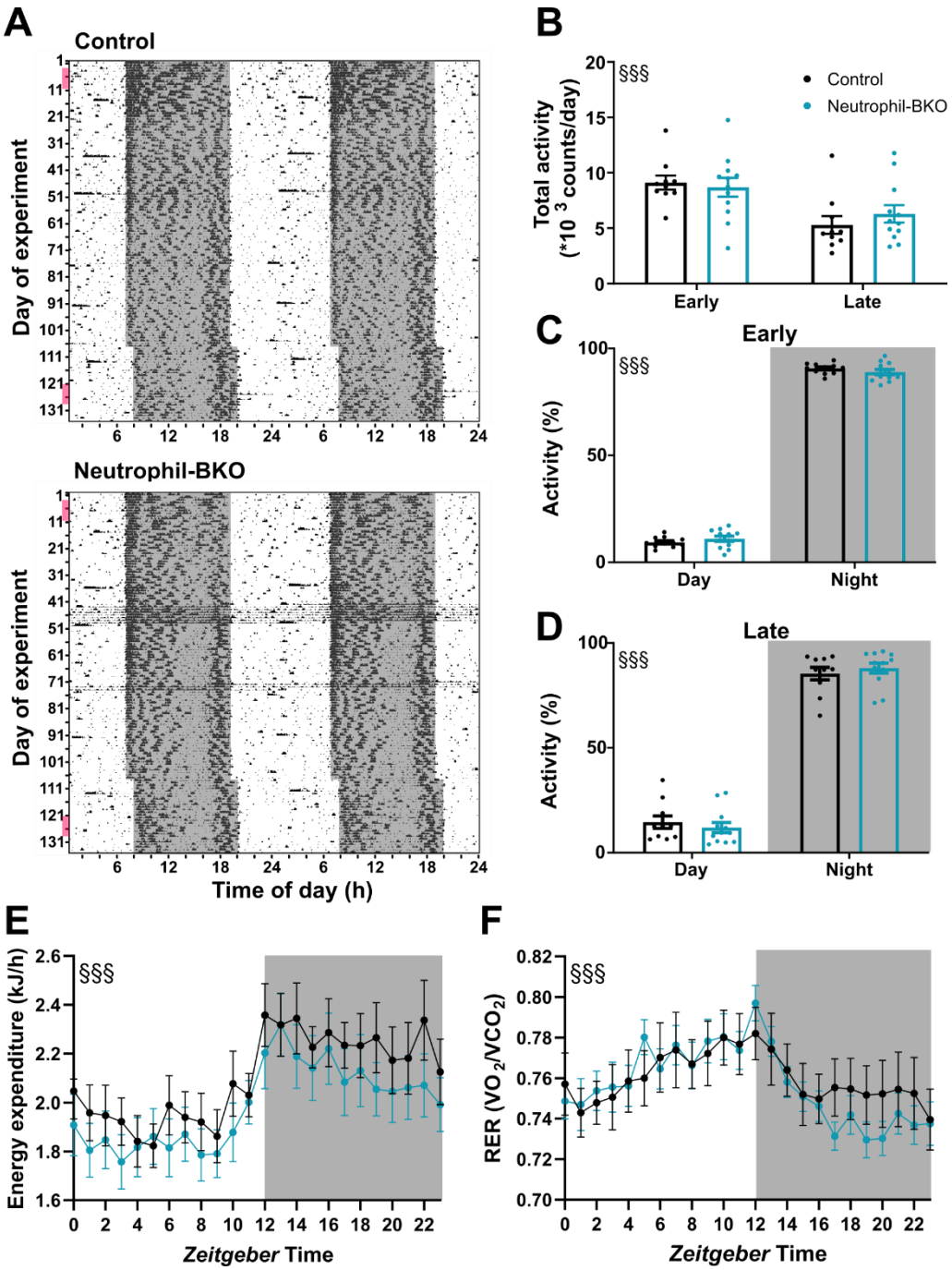

Figure 12: Locomotor activity and energy metabolism are not different during long-term HFD feeding. **A:** Representative double-plotted actograms of one Control and one Neutrophil-BKO mouse. Black bars represent activity. Pink bars along the left axis indicate time frames that were used for more detailed analysis at an early or a late time of the experiment. **B:** Total activity per day during the early and late time of the experiment. Data were averaged over 7 days that are indicated by pink bars in (A). n = 10-12 per genotype. **C, D:** Distribution of activity over day and night during the early (C) or late (D) time of the experiment. Data were averaged over 7 days that are indicated by pink bars in (A). n = 10-12 per genotype. **E:** Energy expenditure that was determined from indirect calorimetry measurements 14-16 weeks after start of HFD feeding. n = 8/10 per genotype. **F:** RER that was determined from indirect calorimetry measurements 14-16 weeks after start of HFD feeding. n = 8/10 per genotype. §§§ $p < 0.001$ time effect (two-way ANOVA). Grey-shaded areas indicate times with lights switched off. Data are presented as means ± SEMs.

To analyze energy metabolism of the mice, animals were observed in an indirect calorimetry system 14-16 weeks after start of HFD feeding. This system detected oxygen consumption and carbon dioxide production, which allowed for calculation of energy expenditure and RER. Energy expenditure changed over the course of the day: it was low during the light phase and high during the dark phase (**Figure 12 E**). This is in accordance with higher locomotor activity during the dark phase. There was no significant difference between genotypes, even though energy expenditure of Neutrophil-BKOs seems to be permanently lower than that of Control animals. However, total daily energy expenditure was not different between genotypes (**Supplemental Figure S3**).

RER also changed over the course of the day. An RER of 1 is observed when energy is purely derived from carbohydrates, while fat metabolism results in an RER of 0.7 (Patel et al., 2021). The high content of fat in the diet was resembled in low RER values. However, during the light phase, when less food was consumed, there was a steady increase in RER. In the dark, higher consumption of HFD resulted in decreased RER values (**Figure 12 F**). This trend was similarly observed for both genotypes and there was no significant genotype effect.

From the experiments described above, it can be concluded that locomotor activity and energy metabolism are comparable between Neutrophil-BKO and Control mice on HFD. Therefore, it is unlikely that these factors contribute to differences in body weight development that were observed under HFD conditions. At the same time, food intake was slightly but significantly lower in Neutrophil-BKO mice so that it is possible that lower energy intake contributes to a lower body weight gain.

3.7. Infiltration of neutrophils into WAT is not altered in Neutrophil-BKO mice

Obesity is accompanied by infiltration of neutrophils into adipose tissue. Neutrophils participate in metaflammation and thereby influence metabolic outcome (Lee and Lee, 2014; Lee and Olefsky, 2021; Talukdar et al., 2012; Chai et al., 2019). Since deletion of *Bmal1* in neutrophils might alter migratory behavior of these cells, neutrophil numbers in adipose tissue were analyzed by FACS. To this end, SVCs were isolated from fat pads and stained with antibodies against cell type-specific markers. Two different types of adipose tissue were analyzed: eWAT, representative of visceral adipose tissue, and inguinal scWAT, representative of subcutaneous adipose tissue. Neutrophils were quantified relative to the number of WBCs. Therefore, the WBC fraction was analyzed first to characterize the baseline. WBCs were identified by their expression of CD45.

In eWAT, the highest WBC numbers for Neutrophil-BKO mice were observed at ZT13 (62.49 ± 5.95 %) and the lowest at ZT7 (51.59 ± 7.71 %). WBC numbers did not significant 24-hour rhythms in Neutrophil-BKO mice. In comparison, Control mice showed a rhythmic regulation of WBC numbers

with a peak at ZT7 (54.91 ± 9.17 %) and a trough at ZT19 (37.86 ± 1.90 %). Controls showed a trend to reduced WBC numbers at ZT 13 and ZT 19, but there was no significant difference between genotypes, neither at these times nor in the general comparison (**Figure 13 A**).

In scWAT, the number of WBCs was non-rhythmic for both groups. Both, Neutrophil-BKO and Control mice had the highest and lowest cell counts at ZT13 and ZT19, respectively (48.54 ± 5.12 % and 39.43 ± 2.58 % for Neutrophil-BKOs, 46.51 ± 5.78 % and 42.10 ± 2.13 % for Controls). Again, there was no significant difference between genotypes (**Figure 13 A**).

Since both groups showed comparable numbers of WBCs in both tissues, these numbers can be used as baseline for subsequent analysis of further immune cell populations. However, it needs to be considered that WBC numbers of Controls show significant rhythms in eWAT, while this is not the case for Neutrophil-BKO mice.

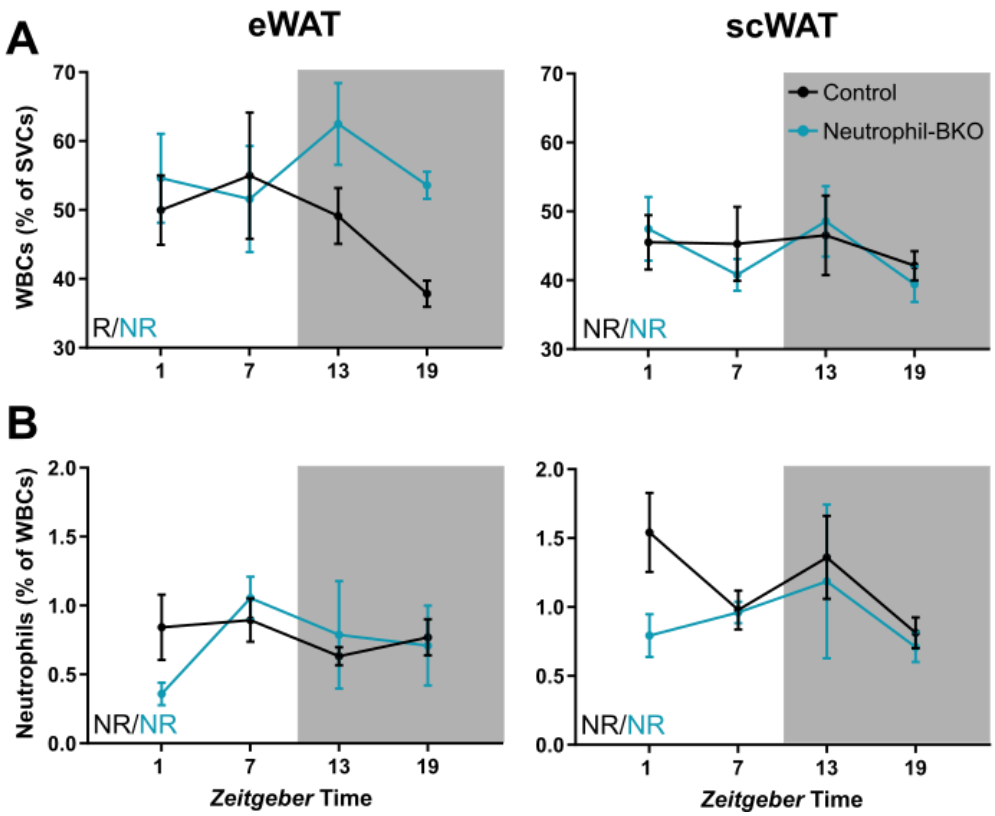

Figure 13: Numbers of WBCs and neutrophils are comparable in eWAT and scWAT after long-term HFD feeding. **A:** Number of WBCs in eWAT, (left) and scWAT (right). Cell counts are indicated as percentage of the SVCs that were isolated from adipose tissue and analyzed by flow cytometry. **B:** Numbers of neutrophils as percentage of WBCs in eWAT (left) and scWAT (right). n = 7/8 per condition. Tissues were harvested at the end of long-term HFD feeding. R: rhythmic ($p < 0.05$), NR: non-rhythmic (CircaCompare). Grey-shaded areas indicate times with lights switched off. Data are presented as means ± SEMs.

Neutrophils constitute a small fraction of WBCs in adipose tissue. They were identified as being positive for the markers Ly6G and CD11b and negative for macrophage markers F4/80 and CD11c. In eWAT, neutrophil numbers in Neutrophil-BKO mice varied from 0.35 ± 0.08 % at ZT1 to 1.05 ± 0.16 % at ZT7. Control mice had similar levels with a minimum of 0.63 ± 0.07 % at ZT13 and a maximum of 0.89 ± 0.16 % at ZT7. There was no significant difference between genotypes and both profiles did not show significant 24-hour rhythms (**Figure 13 B**). Of note, using SVCs as baseline yielded comparable results for numbers and rhythms of neutrophils in eWAT so the result is not biased by rhythm differences in WBC numbers (**Supplemental Figure S4 A**).

In scWAT, neutrophil numbers in Neutrophil-BKO mice were highest at ZT13 (1.19 ± 0.56 %) and lowest at ZT19 (0.71 ± 0.11 %). For Control animals, peak neutrophil count was reached at ZT1 (1.54 ± 0.29 %) and the minimum at ZT19 (0.81 ± 0.11 %). Again, genotypes were not significantly different and none of the profiles was significantly rhythmic. In conclusion, there are no genotype-related differences in the number of neutrophils in none of the tissues that were analyzed.

Next, to study whether different polarization of neutrophils might contribute to the different phenotypes, I analyzed expression of CD206, a potential marker of neutrophils with anti-inflammatory properties (Cuartero et al., 2013). An increase of CD206 positive neutrophils was expected for Neutrophil-BKO mice that have a better metabolic outcome. However, neutrophils that were isolated from adipose tissue were negative for CD206 to almost 100 % for both genotypes (data not shown). It is therefore likely that deletion of *Bmal1* in neutrophils influences metabolic state more indirectly *via* other mechanisms.

3.8. Neutrophil-BKO mice harbor elevated macrophage numbers in adipose tissue and more M2-like macrophages in eWAT

Macrophages are the main effector cells in metaflammation and there are reports on interaction between neutrophils and macrophages (Bouchery and Harris, 2019; Talukdar et al., 2012; Chen et al., 2014; Braza et al., 2018). Therefore, the next step was to quantify macrophage numbers of Neutrophil-BKO mice in adipose tissue under HFD conditions. Since macrophages can acquire pro- and anti-inflammatory properties in metaflammation, the distribution of the corresponding phenotypes was analyzed as well.

Macrophages were identified by their co-expression of F4/80 and CD11b. Levels in eWAT fluctuated between 61.04 ± 6.23 % at ZT1 and 33.69 ± 6.84 % at ZT7 for Neutrophil-BKOs. For Control animals, the maximum was 50.50 ± 7.39 % at ZT1 and the minimum 31.73 ± 5.32 % at ZT7. There was no

significant difference between genotypes. For both genotypes there were large differences between minimum and maximum levels of macrophages. However, the profiles did not show significant 24-hour rhythms (**Figure 14 A**). Since the baseline of WBCs showed differences in rhythmicity between Neutrophil-BKO and Control animals, the number of macrophages was also analyzed relative to SVCs. In this analysis, the profiles did not show significant 24-hour rhythms either, but macrophage numbers were slightly and significantly increased in Neutrophil-BKOs (**Supplemental Figure S4 B**).

Similarly, scWAT displayed slightly elevated levels of macrophages in Neutrophil-BKO mice. Numbers were overall higher than in eWAT with the highest values observed at ZT1 (66.26 ± 4.96 % for Neutrophil-BKOs and 55.38 ± 2.27 % for Controls). Macrophage numbers were lowest at ZT7 in Neutrophil-BKO mice (54.20 ± 3.72 %) and at ZT13 in Controls (48.50 ± 5.12 %). Of note, macrophage numbers were significantly rhythmic in Neutrophil-BKO mice but not in Controls (**Figure 14 A**).

For analysis of macrophage polarization, M1-like macrophages were characterized as being positive for CD11c and negative for CD206. Opposite criteria were used for M2-like macrophages, *i.e*., those cells were negative for CD11c and positive for CD206 (Trim et al., 2018; Lee and Olefsky, 2021). In eWAT, there were differences in the abundance of M1-like and M2-like populations between the two genotypes. Macrophages in Neutrophil-BKO mice contained a lower percentage of M1-like cells (15.00 ± 1.05 % compared to 23.29 ± 1.71 % in Controls). At the same time, the fraction of M2-like cells was elevated (41.75 ± 3.11 % vs. 23.77 ± 1.95 % in Controls). In addition, relative eWAT fat pad weights were higher in Neutrophil-BKO mice (3.89 ± 0.21 % *vs.* 2.57 ± 0.16 %) (**Figure 14 B, C**). In contrast, macrophages in scWAT did not show genotype-related differences in their polarization state. In Neutrophil-BKO mice, 7.37 ± 0.82 % of the macrophages were classified as M1-like, compared to 8.97 ± 0.90 % in Controls. Similarly, 65.42 ± 3.66 % M2-like macrophages were detected in Neutrophil-BKOs, while the number was 59.75 ± 3.05 % in Control animals. The weight of scWAT in relation to body weight was comparable between the two groups (3.84 ± 0.22 % in Neutrophil-BKOs and 4.13 ± 0.14 % in Controls) (**Figure 14 B, D**). Data on macrophage polarization are presented as averages over the whole 24-hour cycle. However, differences that were observed were also obvious in profiles with a time resolution of 6 h (**Supplemental Figure S4 C, D**).

In summary, Neutrophil-BKO mice showed higher macrophage numbers in scWAT. In eWAT, macrophage numbers were significantly higher in Neutrophil-BKOs as well, but only if SVCs were used as baseline. Furthermore, the relation of M1-like and M2-like macrophages was altered in eWAT. Neutrophil-BKO mice had more anti-inflammatory M2-like macrophages, while proinflammatory M1-like macrophages were less prevalent. These results indicate that loss of *Bmal1* in neutrophils might influence the polarization state of macrophages, at least in eWAT.

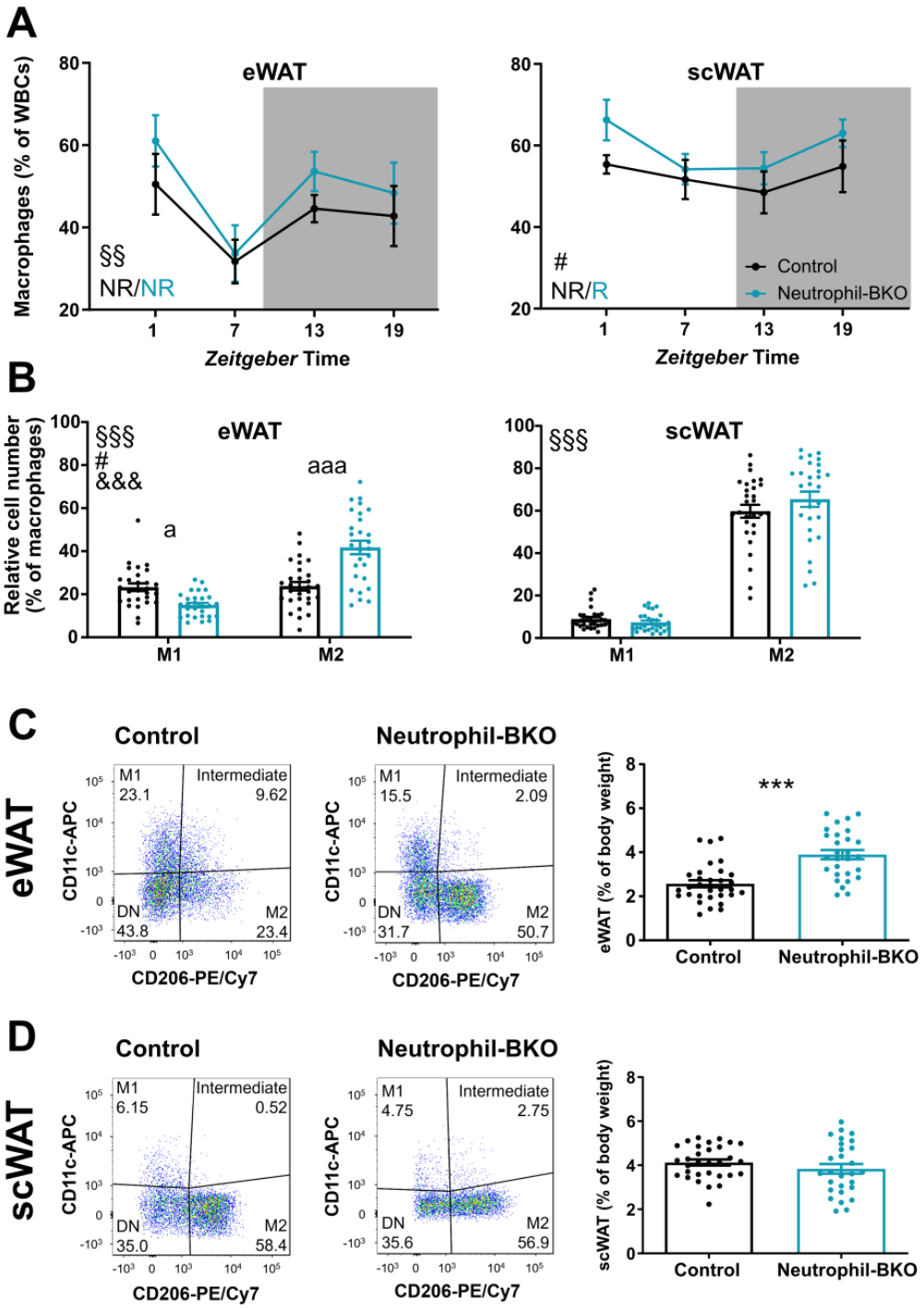

Figure 14: Neutrophil-BKO mice show increased macrophage numbers in scWAT and altered macrophage polarization in eWAT after long-term HFD feeding. A: Number of macrophages as percentage of WBCs in eWAT (left) and scWAT (right). n = 7/8 per condition. **B:** Number of M1-like or M2-like macrophages as percentage of all macrophages. Data were averaged across the whole 24-hour cycle. n = 28/29 per genotype. **C, D:** Representative images from macrophage analysis and fat pad weight of eWAT (C) or scWAT (D). n = 28/31 per genotype. M1: M1-like macrophages, M2: M2-like macrophages, DN: double negative. §§ $p < 0.01$ time effect, §§§ $p < 0.001$ polarization effect, # $p < 0.05$ genotype effect, &&& $p < 0.001$ interaction (two-way ANOVA). a $p < 0.05$, aaa $p < 0.001$ (Bonferroni post-test). *** $p < 0.001$ (unpaired t-test). R: rhythmic ($p < 0.05$), NR: non-rhythmic (CircaCompare). Grey-shaded areas indicate times with lights switched off. Data are presented as means ± SEMs.

3.9. Reduced body weight gain and food intake are already observed after one week on HFD, but not on chow diet

Two findings that were described above could be relevant for the metabolic phenotype that was observed in Neutrophil-BKO mice: reduced food intake and altered macrophage polarization that favors anti-inflammatory M2-like macrophages in eWAT. Since neutrophils are commonly described as early responder and effector cells in immune responses, it would be expected to observe the relevant effect early after onset of HFD feeding. Therefore, a short-term experiment was set up in which mice received HFD for one week. Body weight and food intake were observed and immune cells in adipose tissue were analyzed as in the long-term experiment.

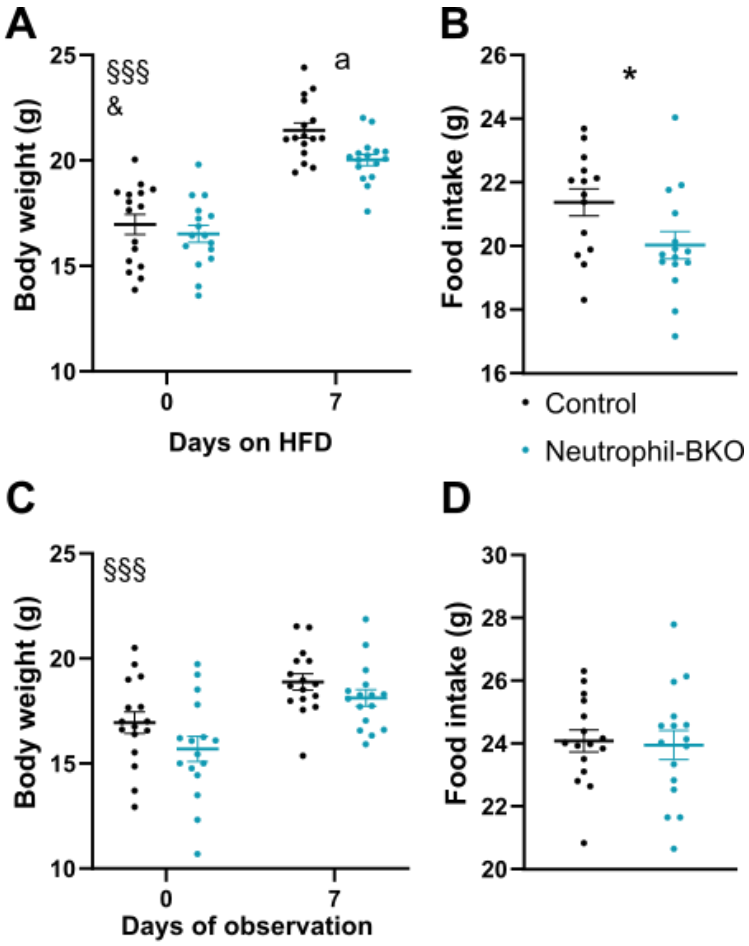

Figure 15: Body weight and food intake are reduced in Neutrophil-BKO mice already after one week of HFD. **A:** Body weight at the beginning and at the end of one week of HFD feeding. Age at start: 4-5 weeks. n = 16 per genotype. **B:** Food intake during one week of HFD feeding. n = 14/15 per genotype. **C:** Body weight at the beginning and at the end of one week of chow feeding. Age at start: 4-5 weeks. n = 16 per genotype **D:** Chow intake during one week. n = 16 per genotype. §§§ $p < 0.001$ time effect, & $p < 0.05$ interaction (two-way ANOVA). a $p < 0.05$ (Bonferroni post-test). * $p < 0.05$ (unpaired t-test). Data are presented as means ± SEMs.

At the start of the experiment, body weights in the two groups were comparable (16.52 ± 0.41 g for Neutrophil-BKO mice and 16.97 ± 0.48 g for Control animals). After one week on HFD, however, body weight was significantly lower in Neutrophil-BKO mice (20.03 ± 0.27 g *vs.* 21.43 ± 0.35 g) (**Figure 15 A**). Decreased body weight was accompanied by significantly lower food intake during that week. Neutrophil-BKO mice ate 20.03 ± 0.43 g and Control mice 21.37 ± 0.43 g (**Figure 15 B**).

To exclude that Neutrophil-BKO mice generally gain less weight and consume less food, the same experiment was performed with normal chow diet. Here, body weight was comparable between genotypes both at the beginning and at the end of the experiment (beginning: 15.69 ± 0.60 g for Neutrophil-BKOs and 16.94 ± 0.52 g for Controls, end: 18.12 ± 0.39 g for Neutrophil-BKOs and 18.88 ± 0.38 g for Controls) (**Figure 15 C**). Likewise, food intake was not significantly different. Neutrophil-BKO mice consumed 23.95 ± 0.46 g and Control mice ate 24.08 ± 0.35 g (**Figure 15 D**).

Thus, it can be concluded that differences in body weight and food intake are especially related to HFD feeding and that lower HFD intake might contribute to the body weight phenotype that was observed.

3.10. Numbers of neutrophils and macrophages are not different after one week of HFD feeding

To address whether the status of immune cells in adipose tissue is comparable between long-term and short-term HFD feeding, adipose tissue was analyzed for immune cells after one week on HFD. Again, the number of WBCs was used as a baseline, so this population was characterized first. Numbers of WBCs in eWAT were highest at ZT1 for Neutrophil-BKO mice (54.55 ± 3.53 %) and at ZT13 for Control animals (53.20 ± 1.84 %). The lowest WBC numbers were measured at ZT19 for Neutrophil-BKOs (43.55 ± 3.72 %) and at ZT7 for Controls (43.35 ± 6.88 %) (**Figure 16 A**). Thus, the range was very similar between the genotypes. None of the profiles was significantly rhythmic.

In scWAT, WBC numbers were generally lower than in eWAT. Maximum numbers were 35.00 ± 2.37 % for Neutrophil-BKOs and 34.63 ± 1.63 % for Controls, both at ZT13. Lowest numbers were 28.03 ± 2.47 % (Neutrophil-BKOs, ZT19) and 24.75 ± 1.68 % (Controls, ZT7). Again, the range was similar and both profiles did not show significant 24-hour rhythms. However, there was a significant effect of time for WBC numbers in scWAT, indicating that values were different over time (**Figure 16 A**). This must be considered when using WBCs as baseline in further analyses for scWAT. Altogether, WBC numbers were comparable between genotypes, so they are suitable as baseline for subsequent analyses.

Alike the situation after long-term HFD feeding, neutrophils accounted for a small fraction of WBCs in eWAT. Highest numbers were detected at ZT1, when Neutrophil-BKO mice had 0.98 ± 0.16 % neutrophils and Control animals 1.48 ± 0.19 % (**Figure 16 B**). Lowest values were measured at ZT13 for Neutrophil-BKOs (0.47 ± 0.16 %) and at ZT19 for Controls (0.75 ± 0.05 %), respectively. In contrast to long-term HFD samples, a circadian rhythm was detected for both genotypes. However, rhythm parameters (mesor, amplitude and phase) were not different between Neutrophil-BKOs and Controls (**Supplemental Table S1**).

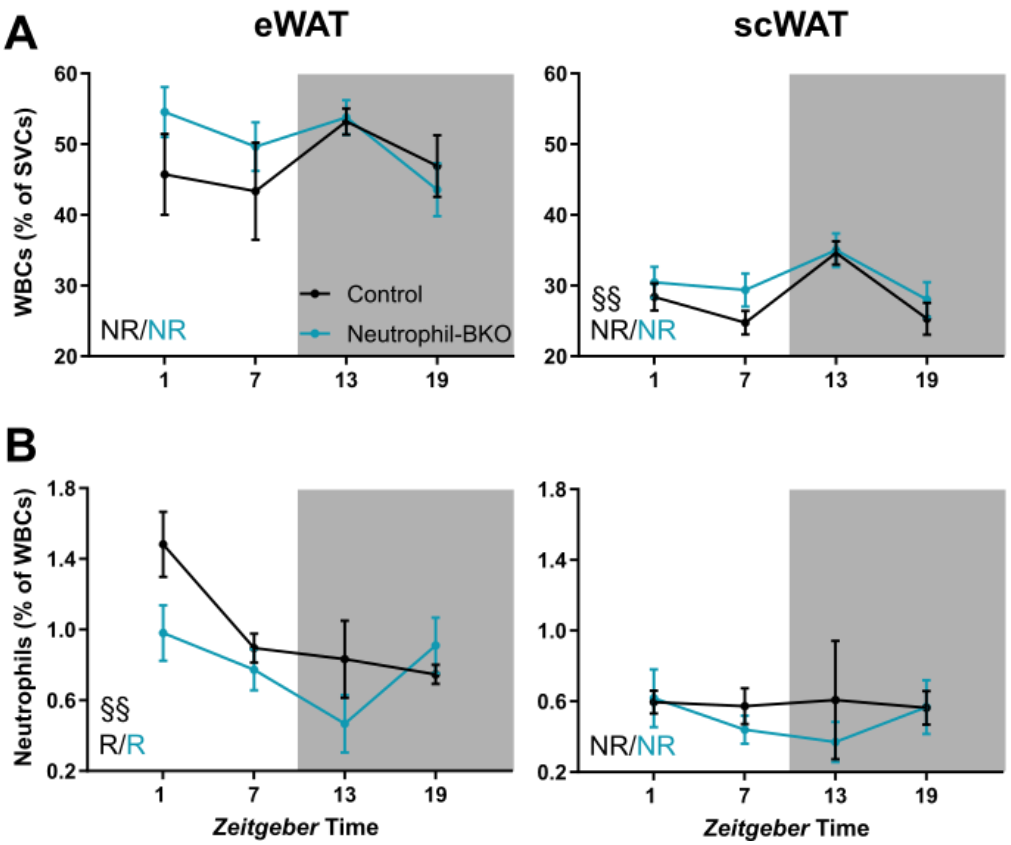

Figure 16: Numbers of WBCs and neutrophils are comparable in eWAT and scWAT after short-term HFD feeding. **A:** Numbers of WBCs in eWAT (left) and scWAT (right). Cell counts are indicated as percentage of the SVCs that were isolated from adipose tissue and analyzed by flow cytometry. **B:** Numbers of neutrophils as percentage of WBCs in eWAT (left) and scWAT (right). n = 3-5 per condition. §§ $p < 0.01$ time effect (two-way ANOVA). R: rhythmic ($p < 0.05$), NR: non-rhythmic (CircaCompare). Grey-shaded areas indicate times with lights switched off. Data are presented as means ± SEMs.

In scWAT, neutrophil numbers were reduced compared to the numbers found in eWAT and after long-term HFD feeding. The maximum number was 0.61 ± 0.34 % (ZT13) for Neutrophil-BKOs and 0.62 ± 0.16 % (ZT1) for Controls (**Figure 16 B**). Lowest percentages were detected at ZT13 (0.37 ± 0.11 %, Neutrophil-BKOs) and at ZT19 (0.56 ± 0.09 %, Controls). The profiles did not show

significant 24-hour rhythms. This result was independent of the baseline, as there were no significant rhythms either when neutrophils were analyzed in relation to SVCs (**Supplemental Figure S5 A**).

In summary, neutrophil numbers exhibited circadian oscillations in eWAT for both genotypes, but there was no genotype-related difference regarding WBC or neutrophil numbers in adipose tissue after one week of HFD feeding.

Next, macrophages were analyzed in the samples generated after one week of HFD feeding. In eWAT, macrophages constituted 51.75 ± 1.79 % (ZT7) up to 58.00 ± 1.29 % (ZT13) of WBCs in Neutrophil-BKO mice. In Controls, macrophages accounted for 50.58 ± 3.96 % (ZT7) up to 56.10 ± 5.40 % (ZT19) of WBCs. Both profiles did not show significant 24-hour rhythms and there was no significant genotype effect (**Figure 17 A**).

In scWAT, macrophage numbers were rhythmic for both genotypes with at peak at ZT7 (Neutrophil-BKOs: 65.50 ± 3.14 %, Controls: 68.58 ± 2.56 %) and a trough at ZT19 (Neutrophil-BKOs: 53.68 ± 2.95 %, Controls: 48.53 ± 4.79 %). There was no significant genotype effect for macrophage fractions in eWAT and rhythm parameters were comparable between genotypes (**Figure 17 A**, **Supplemental Table S1**). Of note, macrophage rhythms were not observed when SVCs were used as baseline (**Supplemental Figure S5 B**).

Next, the fractions of M1-like and M2-like macrophages were quantified. In eWAT of Neutrophil-BKO mice, 15.24 ± 0.75 % of macrophages were M1-like and 37.15 ± 2.93 % were M2-like. This corresponded to 15.37 ± 1.02 % M1-like macrophages and 37.87 ± 3.35 % M2-like macrophages in Controls. Numbers were very similar and there was no significant difference between genotypes. This result contrasts with findings in long-term experiments, where M1-like macrophages were reduced, and M2-like macrophages were increased in Neutrophil-BKO mice.

In scWAT, Neutrophil-BKO mice showed 4.97 ± 0.44 % M1-like and 53.10 ± 3.75 % M2-like macrophages. Similarly, Controls showed 5.53 ± 0.45 % M1-like and 56.10 ± 2.78 % M2-like macrophages. Differences between genotypes were not significant (**Figure 17 B**).

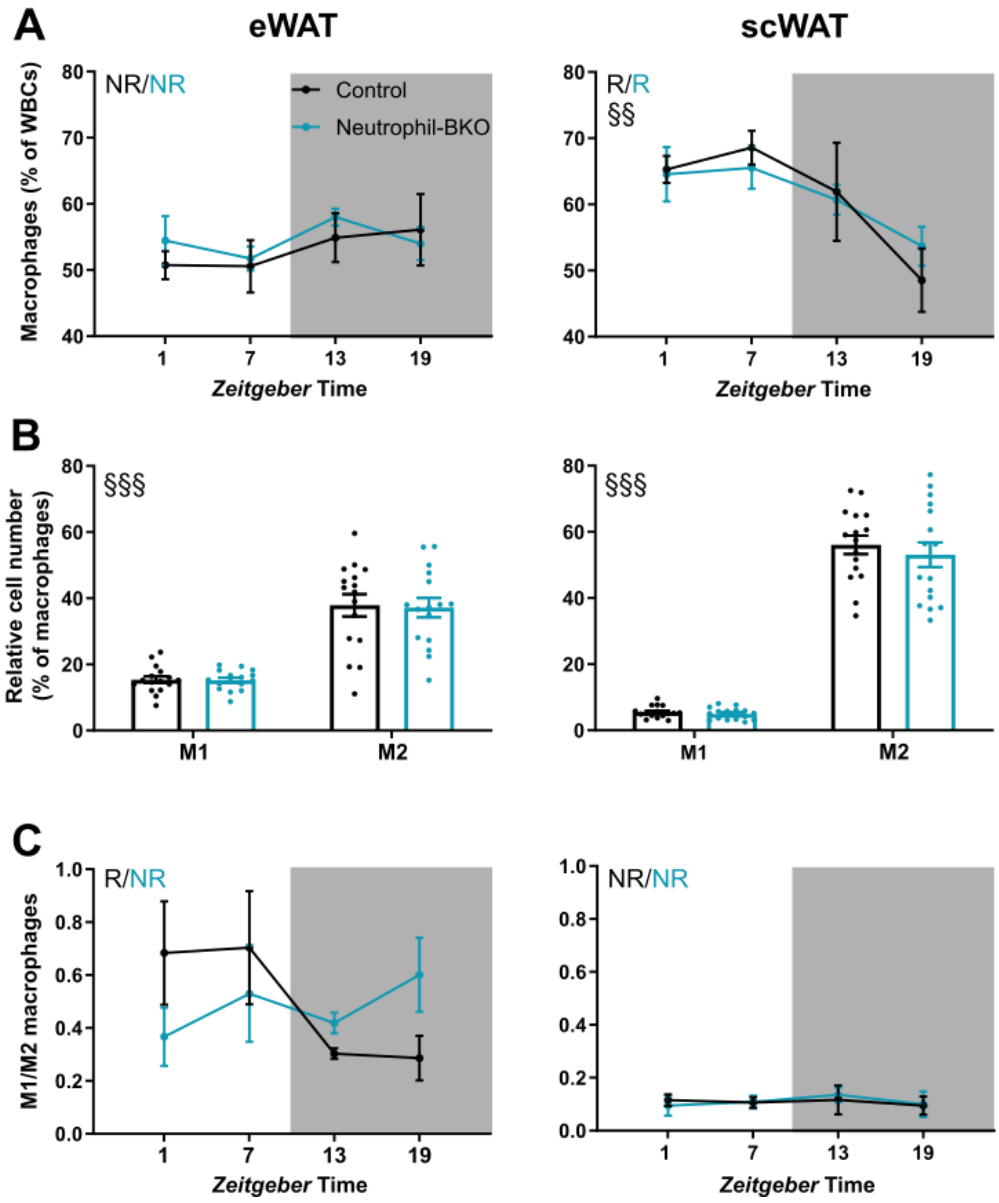

Figure 17: Macrophage numbers and polarization states are not altered after short-term HFD feeding. **A:** Number of macrophages as percentage of WBCs in eWAT (left) and scWAT (right). n = 3-5 per condition. **B:** Number of M1-like or M2-like macrophages as percentage of all macrophages. Data were averaged across the whole 24-hour cycle. n = 16 per genotype **C:** Ratio between M1-like and M2-like macrophages in 6-hour intervals across the 24-hour cycle. n = 3-5 per condition. §§ $p < 0.01$ time effect, §§§ $p < 0.001$ polarization effect (two-way ANOVA). R: rhythmic ($p < 0.05$), NR: non-rhythmic (CircaCompare). Grey-shaded areas indicate times with lights switched off. Data are presented as means ± SEMs.

Of note, the ratio of M1-like and M2-like macrophages in eWAT displayed significant circadian rhythmicity in Controls, but not in Neutrophil-BKO animals. Neutrophil-BKO ratios were highest at ZT19 (0.60 ± 0.14) and lowest at ZT1 (0.37 ± 0.11). Control ratios showed significant 24-hour rhythms with a peak at ZT7 (0.70 ± 0.21) and a trough at ZT19 (0.29 ± 0.08) (**Figure 17 C**). This rhythm was evoked by rhythmic levels of M2-like macrophages while M1-like macrophages were not significantly rhythmic

(**Supplemental Figure S5 C, D**). In scWAT, both genotypes showed non-rhythmic ratios of M1-like and M2-like macrophages. Neutrophil-BKO values varied from 0.10 ± 0.05 at ZT19 to 0.14 ± 0.03 at ZT13, while Controls showed values between 0.10 ± 0.03 at ZT19 and 0.12 ± 0.06 at ZT13 (**Figure 17 C**).

Altogether, abundance and polarization of macrophages in adipose tissue were influenced by the duration HFD feeding. After one week on HFD, macrophage numbers were not different between genotypes, while long-term exposure to HFD led to elevated macrophage numbers in scWAT and, depending on the baseline, also in eWAT. Moreover, macrophage polarization was not different between genotypes after short-term HFD feeding, except for a significantly rhythmic M2-like population in eWAT of Controls that was not observed Neutrophil-BKO mice. In contrast, long-term HFD reduced the number of M1-like macrophages in eWAT in both genotypes. Accordingly, M2-like macrophages were elevated in this condition.

As a conclusion, two effects are observed in long-term HFD experiments that might explain lower body weight of Neutrophil-BKO mice: decreased food intake and altered macrophage polarization in eWAT. Of these, only decreased food intake is already observed after one week on HFD.

3.11. Plasma levels of leptin and adiponectin are not altered

To identify potential sources of altered food intake, plasma levels of leptin and adiponectin were determined. Both adipokines are involved in inflammatory pathways and in hypothalamic food intake regulation(Rasmussen et al., 2006; Kubota et al., 2007; Valassi et al., 2008; La Cava, 2017) so they might be altered in Neutrophil-BKO mice and therefore influence food intake.

Plasma levels of leptin and adiponectin were determined by ELISA. After one week on HFD, plasma of Neutrophil-BKO mice contained 7.13 ± 0.45 ng/mL leptin, comparable to Controls with 8.52 ± 1.04 ng/mL. After long-term exposure to HFD, leptin levels increased massively to 86.55 ± 7.97 ng/mL for Neutrophil-BKOs and to 96.83 ± 4.71 ng/mL for Controls (**Figure 18 A**). There was no significant difference between genotypes.

Similarly, adiponectin levels were comparable for both genotypes. After one week on HFD, plasma samples of Neutrophil-BKO mice contained 3.87 ± 0.10 µg/mL adiponectin, which was comparable to levels in Controls (4.25 ± 0.22 µg/mL). During long-term exposure to HFD, levels increased slightly to 6.86 ± 0.31 µg/mL (Neutrophil-BKOs) and 6.27 ± 0.31 µg/mL (Controls) (**Figure 18 B**). Of note, leptin and adiponectin were not significantly rhythmic in all conditions that were analyzed (**Supplemental Figure S6**) so it can be excluded that differences in circadian rhythms play a role.

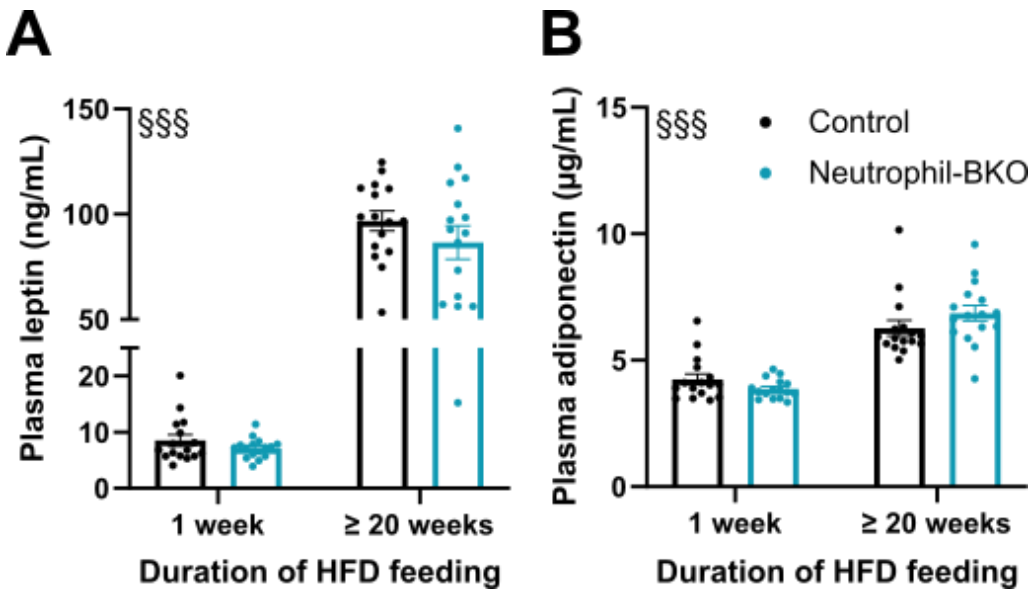

Figure 18: Plasma levels of leptin and adiponectin are not altered. A: Plasma leptin was determined by ELISA. **B:** Plasma adiponectin as determined by ELISA. n = 16 per condition. §§§ $p < 0.001$ duration of HFD (two-way ANOVA). Data are presented as means ± SEMs.

3.12. mRNA expression levels of orexigenic and anorexigenic peptides in the hypothalamus are not altered

Leptin levels in plasma were not altered between genotypes. However, HFD feeding is known to induce central leptin resistance so it might thus be possible that the same levels of leptin induce different responses in the hypothalamus in the two genotypes. To test this, expression of *Pomc*, *Cartpt*, *Agrp* and *Npy* were analyzed by qPCR from hypothalamic tissue.

POMC and CART are anorexigenic, *i.e.,* they suppress food intake (Valassi et al., 2008). If they are responsible for lower food intake in Neutrophil-BKO mice, increased levels would be expected. After one week of HFD, *Pomc* expression in Neutrophil-BKO mice was highest at ZT13 (1.03 ± 0.10), compared to 1.17 ± 0.37 in Controls. Expression levels were also similar at all other times and there was no circadian rhythmicity. After long-term exposure to HFD, *Pomc* expression in Neutrophil-BKO mice varied from 0.78 ± 0.07 at ZT19 to 2.71 ± 1.22 at ZT7. Similarly, Control mice showed expression levels between 0.66 ± 0.03 at ZT13 and 1.14 ± 0.48 at ZT7. Both profiles did not show significant 24-hour rhythms and there was no significant difference between genotypes (**Figure 19 A**).

Cartpt showed similar mRNA expression levels in both genotypes as well. One week of HFD feeding resulted in relative expression levels between 0.84 ± 0.05 (ZT13) and 1.02 ± 0.09 (ZT19) for Neutrophil-BKOs and in levels between 0.83 ± 0.03 (ZT13) and 1.00 ± 0.06 (ZT1) for Controls. After long-term HFD feeding, expression levels were generally higher with the minimum being 1.38 ± 0.05 (ZT7) for

Neutrophil-BKOs and 1.32 ± 0.07 (ZT1) for Controls. Neither short-term nor long-term samples showed significant 24-hour rhythms of *Cartpt* expression (**Figure 19 B**).

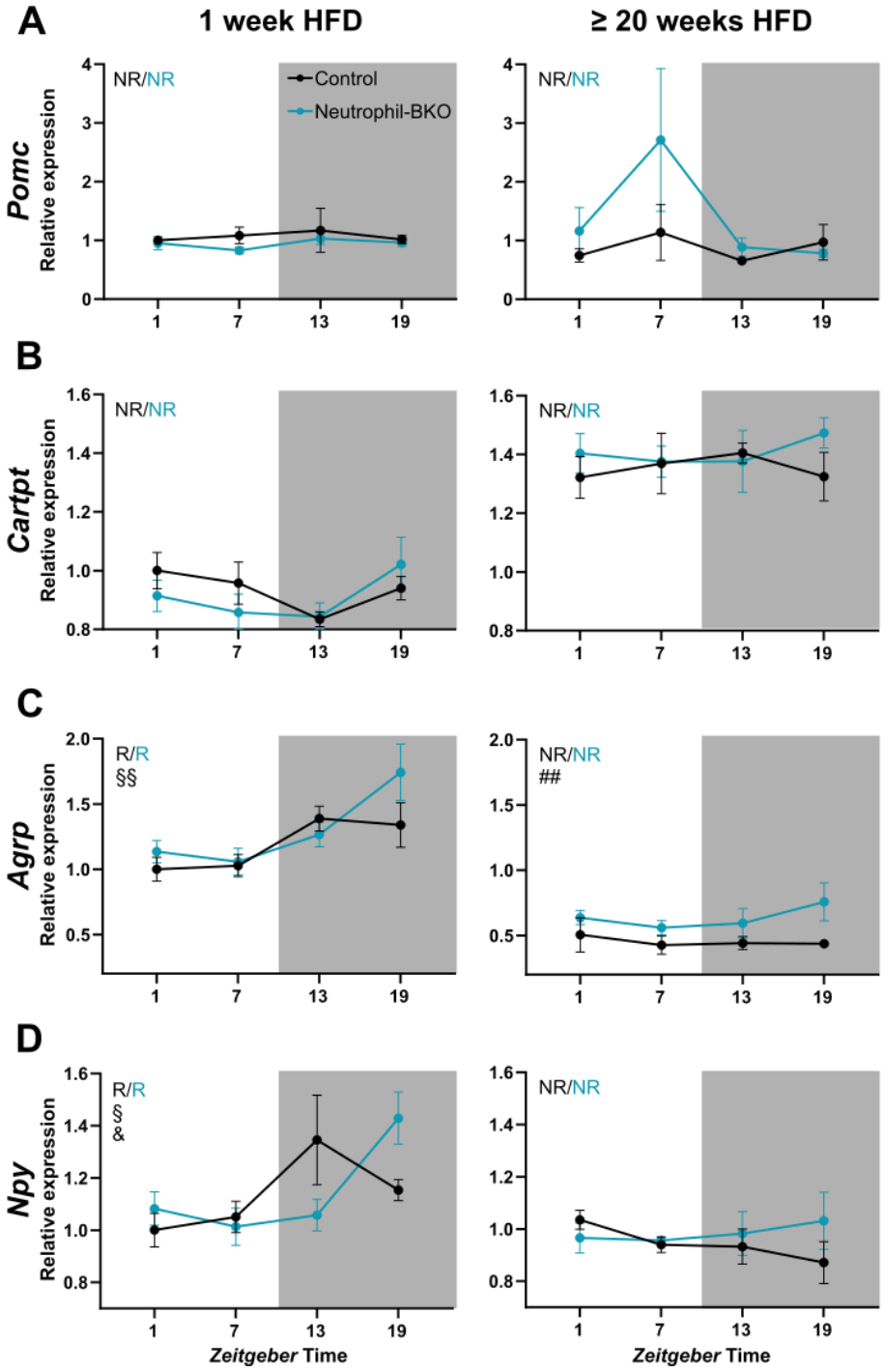

Figure 19: mRNA expression of anorexigenic and orexigenic peptides in hypothalamus is not altered except for *Agrp*. Relative expression of *Pomc* (**A**), *Cartpt* (**B**), *Agrp* (**C**) and *Npy* (**D**) for samples that were collected after one week on HFD (left) or after 20-23 weeks on HFD (right). All values were normalized to Control expression levels at ZT1 after one week on HFD. n = 3-5 per condition. § $p < 0.05$, §§ $p < 0.01$ time effect; ## $p < 0.01$ genotype effect; & $p < 0.05$ interaction (two-way ANOVA). R: rhythmic ($p < 0.05$), NR: non-rhythmic (CircaCompare). Grey-shaded areas indicate times with lights switched off. Data are presented as means ± SEMs.

In contrast to POMC and CART, AGRP and NPY have orexigenic effects, i.e., they induce food intake (Valassi et al., 2008). If they are responsible for lower food intake in Neutrophil-BKO mice, it would be expected to see decreased levels. *Agrp* expression was similar between Neutrophil-BKOs and Controls after one week on HFD. Neutrophil-BKO mice had expression levels that varied from 1.06 ± 0.10 at ZT7 to 1.74 ± 0.22 at ZT19. For Control animals, *Agrp* expression was lowest at ZT1 (1.00 ± 0.09) and highest at ZT13 (1.39 ± 0.10). Both genotypes showed rhythmic 24-hour expression profiles (**Figure 19 C**). However, even though minimum and maximum expression levels occurred at different times, there was no significant difference in mesor, phase nor amplitude (**Supplemental Table S1**).

Long-term exposure to HFD reduced *Agrp* expression to maximum levels of 0.76 ± 0.15 (ZT19) for Neutrophil-BKOs and 0.51 ± 0.13 (ZT1) for Controls. The rhythms that were observed after one week of HFD were not detectable anymore, but Neutrophil-BKO mice had significantly higher expression levels than Control animals (**Figure 19 C**).

The second orexigenic peptide, *Npy*, was also rhythmically expressed after one week on HFD, but expression levels were not different between genotypes. Neutrophil-BKO mice had lowest *Npy* expression at ZT7 (1.01 ± 0.07) and highest levels at ZT19 (1.43 ± 0.10). In contrast, minimum expression for Controls was observed at ZT1 (1.00 ± 0.06) and highest levels were detected at ZT13 (1.35 ± 0.17) (**Figure 19 D**). Even though this timing might suggest different phasing, there was no significant difference in phase, mesor nor amplitude (**Supplemental Table S1**).

Long-term exposure to HFD ablated rhythms of *Npy* expression. Neutrophil-BKO mice showed levels from 0.96 ± 0.01 (ZT7) to 1.03 ± 0.11 (ZT19), while for Control mice the minimum and maximum expression levels were 0.87 ± 0.08 (ZT19) and 1.04 ± 0.04 (ZT1), respectively. There was no significant difference between genotypes (**Figure 19 D**).

All in all, a significant difference between genotypes was only observed for *Agrp* expression after long-term exposure to HFD. However, expression was increased in Neutrophil-BKO mice, which does not explain lower food intake since AGRP stimulates feeding. Therefore, it can be concluded that differential expression of (an)orexigenic peptides in the hypothalamus cannot be responsible for reduced HFD food intake of Neutrophil-BKO animals.

3.13. Proinflammatory genes are not altered in the hypothalamus, but rhythms of neutrophil infiltration might be affected by the deletion of *Bmal1*

In addition to inflammation in adipose tissue, obesity goes along with an increase of inflammatory processes in the brain, especially in the hypothalamus (De Souza et al., 2005; Thaler et al., 2012). To clarify whether an altered inflammatory state might contribute to differences in food intake, expression of the proinflammatory cytokines *Tnf-α* and *Il-6* was measured in hypothalamic tissue.

Following one week of HFD feeding, *Tnf-α* expression varied over the day from 0.38 ± 0.05 (ZT13) to 1.69 ± 0.86 (ZT7) in Neutrophil-BKO mice and from 0.80 ± 0.23 (ZT13) to 1.36 ± 0.28 (ZT19) in Control mice. A similar range of expression levels was observed after long-term HFD feeding. Neutrophil-BKO mice showed minimum and maximum levels of 0.69 ± 0.08 (ZT13) and 0.91 ± 0.19 (ZT1), respectively, while values for Controls varied from 0.66 ± 0.08 at ZT13 to 1.00 ± 0.07 at ZT1. There was no significant difference between genotypes, but statistical analysis was hindered by large variation between replicates, especially after short-term HFD. However, *Tnf-α* expression was rhythmic for Neutrophil-BKOs after one-week HFD feeding and for Controls after long-term exposure to HFD (**Figure 20 A**).

After one week of HFD, expression patterns of *Il-6* were very similar to those of *Tnf-α*. Lowest *Il-6* levels were detected at ZT13 (0.45 ± 0.03 for Neutrophil-BKOs and 0.83 ± 0.25 for Controls). Neutrophil-BKO mice showed highest expression at ZT7 (1.69 ± 0.83), while highest Control levels were detected at ZT19 (1.15 ± 0.25). In contrast to *Tnf-α*, long-term exposure to HFD slightly reduced expression levels of *Il-6*. Maximum values of 0.48 ± 0.05 (ZT19) and 0.61 ± 0.12 (ZT7) were detected for Neutrophil-BKOs and Controls, respectively. Expression values were relatively stable over time. Lowest levels were 0.40 ± 0.03 (ZT13) for Neutrophil-BKOs and 0.41 ± 0.05 (ZT19) for Controls. There was no significant difference between genotypes, but statistical analysis was again hindered by large variation between replicates, especially after short-term HFD. No significant circadian rhythm was detected for *Il-6* in any condition (**Figure 20 B**).

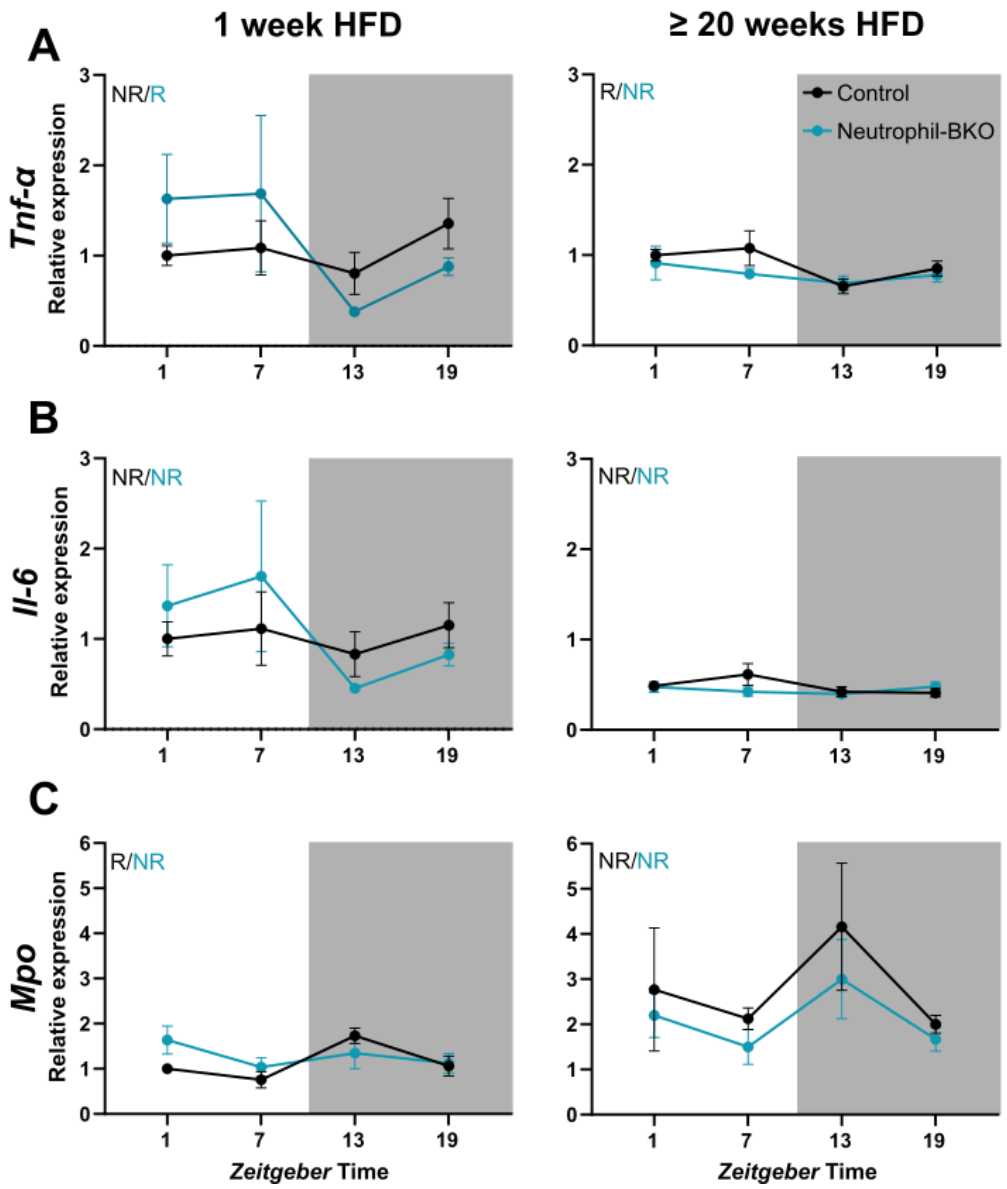

Figure 20: mRNA expression of inflammation-related genes in hypothalamus is not altered. Relative expression of *Tnf-α* (**A**), *Il-6* (**B**) and *Mpo* (**C**) for samples that were collected after one week on HFD (left) or after 20-23 weeks on HFD (right). All values were normalized to Control expression levels at ZT1 after one week on HFD. n = 3-5 per condition. R: rhythmic ($p < 0.05$), NR: non-rhythmic (CircaCompare). Grey-shaded areas indicate times with lights switched off. Data are presented as means ± SEMs.

Since there were no significant differences between genotypes, these results do not give an indication of an altered inflammatory state in the hypothalamus. However, it is debated whether neutrophils from the periphery infiltrate hypothalamic tissue during metaflammation (Buckman et al., 2014; Yang et al., 2019). Loss of *Bmal1* in neutrophils might directly influence central infiltration of these cells and thereby directly mediate changes in hypothalamic food intake regulation. Therefore, *Mpo* expression was assessed in hypothalamic tissue.

Interestingly, *Mpo* was detectable in the hypothalamus of mice that received HFD. Neutrophil-BKO mice showed relative mRNA levels ranging from 1.04 ± 0.21 (ZT7) to 1.64 ± 0.31 (ZT1) after one week of HFD feeding. Similarly, *Mpo* expression in Controls varied from 0.76 ± 0.18 (ZT7) to 1.73 ± 0.17 (ZT13). Long-term HFD feeding was accompanied by a rise of *Mpo* expression in the hypothalamus. Highest expression was detected at ZT13 (3.00 ± 0.88 for Neutrophil-BKOs and 4.16 ± 1.41 for Controls) and values did not drop below 1.50 ± 0.39 for Neutrophil-BKOs or 2.00 ± 0.20 for Controls (both ZT19). There was no significant difference in mRNA expression levels of the two genotypes. However, Control animals showed rhythmic *Mpo* expression after one week of HFD while no significant 24-hour rhythms were detected for Neutrophil-BKO mice and after long-term exposure to HFD (**Figure 20 C**). Loss of *Mpo* rhythmicity in Neutrophil-BKO mice after one week on HFD might point at non-rhythmic neutrophil infiltration into hypothalamic tissue.

When all *Zeitgeber* Times were anlayzed together, both genotypes showed significant increase of *Mpo* expression after long-term HFD feeding compared to short-term HFD (**Supplemental Figure S7 A**). In addition, the increase was less pronounced in Neutrophil-BKO mice (**Supplemental Figure S7 B**), indicating that recruitment of neutrophils into hypothalamic tissue might be attenuated in Neutrophil-BKO mice after long-term HFD feeding.

Together, mRNA expression of *Tnf-α* and *Il-6* did not indicate differences in inflammatory state of the hypothalamus. Differences in *Mpo* expression might indicate altered rhythms and magnitudes of neutrophil infiltration into the hypothalamus upon HFD feeding.

4. Discussion

In our modern world, artificial light, constant availability of food and increasing demands of shift work foster a lifestyle that is more and more uncoupled from the natural environment. While this allows for more flexibility, it imposes the risk of circadian disruption, *i.e.*, the dissociation of internal and external 24-hour rhythms. Since circadian and metabolic systems are highly interconnected, circadian disruption has severe consequences on metabolic health (Depner et al., 2014; McHill and Wright, 2017; Fatima and Rana, 2020; Mason et al., 2020). This effect is clearly observed in people working regular night shifts. These people have a significantly increased risk of obesity and related comorbidities such as cardiovascular disease and T2DM (Wang et al., 2011; Kecklund and Axelsson, 2016; Vetter et al., 2018; Torquati et al., 2018).

In obese patients, adipose tissue exhibits chronic low-grade inflammation (termed metaflammation) that spreads *via* the circulation to other peripheral organs and to the brain (Gregor and Hotamisligil, 2011; Zatterale et al., 2019). Inflammatory signaling promotes the progression of insulin resistance and T2DM (Hotamisligil et al., 1993; Nakatani et al., 2004; Shoelson et al., 2003; Arkan et al., 2005; Blüher et al., 2009; Burhans et al., 2018). Intense research identified macrophages as the main cellular players in metaflammation. While resident macrophages in adipose tissue of lean patients exhibit mainly anti-inflammatory properties, obesity leads to a phenotypic switch towards proinflammatory macrophages that are responsible for metaflammation. At the same time, macrophage numbers in adipose tissue increase drastically (Lumeng et al., 2007b; Oh et al., 2012; Lee and Lee, 2014; Li et al., 2015; Lee and Olefsky, 2021). Early events in metaflammation also involve neutrophil infiltration into adipose tissue within 3 days after onset of HFD feeding (Elgazar-Carmon et al., 2008; Talukdar et al., 2012). Neutrophil effector proteins like NE and MPO influence insulin sensitivity (Talukdar et al., 2012; Chai et al., 2019). Therefore, adipose tissue infiltration by neutrophils might be a critical step in the onset of metaflammation, especially since neutrophils closely interact with macrophages (Chertov et al., 1997; Soehnlein et al., 2008; Tam et al., 2020).

Numerous functions of macrophages are controlled by the circadian clock (Keller et al., 2009; Kitchen et al., 2020). Deletion of *Bmal1* in murine macrophages exacerbates adipose tissue inflammation and leads to increased body weight and impaired glucose tolerance in DIO (Nguyen et al., 2013). In neutrophils, a connection between the circadian clock and migratory properties was described (He et al., 2018). Despite the close interaction between neutrophils and macrophages, the influence of the neutrophil circadian clock on metaflammation has not been analyzed to date. It was the aim of this thesis to investigate this influence. To this end, a mouse line harboring a *Bmal1* mutation in neutrophils was created (Neutrophil-BKO mice). Metabolism of Neutrophil-BKO mice was challenged by HFD

feeding to assess body weight development, metabolic state, and immune cell populations in adipose tissue. Unlike hypothesized, absence of the molecular clock in neutrophils resulted in a less pronounced obesity phenotype, reduced food intake, and a healthier metabolic state under HFD feeding. More surprisingly, these changes were not accompanied by alterations in number or rhythms of neutrophils in adipose tissue. However, Neutrophil-BKO mice showed increased numbers of anti-inflammatory macrophages in eWAT. Together with reductions in food intake, this effect might explain the observed differences in body weight and metabolic state.

4.1. Generation and circadian characterization of Neutrophil-BKO mice

To investigate the role of the neutrophil circadian clock in DIO, I generated a mouse line with neutrophil-specific null-mutation of *Bmal1*. To this end, *Bmal1*-flox mice were crossed to *Mrp8-Cre* mice. *Bmal1* RNA expression in the resulting Neutrophil-BKO mice was reduced by approximately 80 % (**Figure 6**). This refelcts a clear and significant downregulation, but it also suggests that about 20 % of targeted cells remained without recombination. In the literature, recombination efficiency of the *Mrp8-Cre* line was analyzed in a study together with 12 other different driver lines that target myeloid cells. Depending on the reservoir that was assessed, *Mrp8*-driven *Cre* recombinase was expressed in 80-90 % of all neutrophils (Abram et al., 2014), which corresponds closely to the results presented in this thesis. In addition, the authors of this publication also estimated off-target effects in other immune cell populations by evaluating *Cre* expression in various immune cells of innate and adaptive immunity. Highest expression in non-neutrophil cells was found in monocytes/macrophages (about 20 %) and in peripheral blood B cells (about 10 %). Besides *Mrp8-Cre*, there are two other mouse lines available that drive expression of *Cre* recombinase in neutrophils: *LysM-Cre* and *Ly6G-Cre*. However, *LysM-Cre* mice are less neutrophil-specific with *Cre*-mediated recombination in nearly 100 % of macrophages (Abram et al., 2014), and *Ly6G-Cre* mice were generated by a knock-in approach that deletes expression of LY6G, an important surface antigen for neutrophil detection (Hasenberg et al., 2015). For these reasons, *Mrp8-Cre* was selected as the optimal driver line to target neutrophils for my experiments.

An initial assessment of locomotor activity and food intake rhythms in Neutrophil-BKO mice was necessary to confirm that these SCN-driven functions of the circadian clock were unaffected. As expected, Neutrophil-BKO mice showed normal rhythms of locomotor activity and food intake in LD and a free-running period in DD that was shorter than 24 h **(Figure 7**). Of note, both genotypes showed free-running periods of around 23.2 h in DD (**Figure 7 D**), while this period is reported to be 23.6 - 23.8 h in C57BL/6J mice (Schwartz and Zimmerman, 1990). Since both strains that were crossed to generate Neutrophil-BKO mice were of C57BL/6J origin, strain-specific differences cannot account for these unusually short periods. Both genotypes, Controls and Neutrophil-BKOs, were similarly

affected, so it is unlikely that *Mrp8*-driven expression of *Cre* is responsible for this effect. However, there are examples of studies reporting short free-running periods of C57/BL6 mice, albeit under slightly modified experimental conditions. Periods of around 23.5 h are reported when mice are kept in constant dim red light (Abe et al., 1989) and blinded C57/BL6 mice show free-running periods of around 23.3 h (Ebihara et al., 1986). The variability of free-running periods can be explained by genetic drift in C57/BL6 mice. Since Neutrophil-BKO mice showed DD periods that were shorter than LD periods and since there was no difference between genotypes, the experiment allows to conclude that circadian control of locomotor activity is unaffected in Neutrophil-BKO mice.

In addition to short periods in DD, some mice showed irregular activity onsets in DD. This was most obvious for Control animals (**Figure 7 A**), but it was also observed in some Neutrophil-BKO mice. An additional experiment would be necessary to clarify if this is reproducible or whether it was a finding of a single experiment that was confounded by factors such as noise.

Furthermore, immune cell numbers in blood were comparable between Neutrophil-BKOs and Controls (**Figure 8**) and they were in the range of described reference values (StemCell Technologies, 2021). Altogether, Neutrophil-BKO mice showed marked reduction of *Bmal1* expression in neutrophils. SCN-driven circadian parameters and immune cell numbers in the blood were unaffected by the mutation.

4.2. Loss of *Bmal1* function in neutrophils protects against DIO

Neutrophil-BKO mice that were exposed to HFD gained less body weight compared to Control animals. This effect was observed already after one week of HFD (**Figure 15 A**), and it persisted during extended HFD feeding of 20 weeks (**Figure 9 A**). Interestingly, significant differences in body weight were not observed on normal chow (**Figure 15 C**), which is why further metabolic characterizations were only performed with HFD-fed animals.

Lower body weight of Neutrophil-BKO mice after HFD was accompanied by significantly reduced fat mass (**Figure 9 C**) and improved glucose and insulin tolerance (**Figure 10**). These results collectively demonstrate that neutrophil-specific deficiency of *Bmal1* confers beneficial effects on metabolic state under HFD challenge. This effect was surprising since conditional *Bmal1* deficiency in various other tissues aggravates DIO. While global *Bmal1* knockout mice on a HFD show impaired glucose and fat metabolism but no marked changes in body weight (Shimba et al., 2011; Kennaway et al., 2013), liver-specific loss of *Bmal1* leads to higher body weight and metabolic impairments on HFD feeding (Jacobi et al., 2015). Similarly, *Bmal1* knockout in adipocytes aggravates body weight gain (Paschos et al., 2012), and *Bmal1* deficiency in pancreatic beta cells aggravates insulin resistance (Rakshit et al., 2016).

Most notably, loss of *Bmal1* in macrophages enhances inflammation of adipose tissue, accompanied by elevated body weight and enhanced glucose intolerance (Nguyen et al., 2013). All these results point at a protective role of BMAL1 against detrimental processes related to metaflammation.

However, *Bmal1* deficiency in skeletal muscle (Wada et al., 2018) and in the intestine (Yu et al., 2021) reduces body weight gain and metabolic impairments in DIO similar to what was observed for *Bmal1* deficiency in neutrophils. These studies suggest that BMAL1 exerts tissue-specific roles for metabolic processes so that it may be difficult to target in obesity therapies. However, neutrophils are easily accessible in the blood and might therefore be suitable as a target of cell-specific therapeutic interventions.

Of note, Neutrophil-BKO mice showed significantly reduced body length along with lower body weight after long-term HFD feeding (**Figure 9 B**). This observation might point at a growth phenotype in addition to the metabolic phenotype that was characterized here. Body growth is influenced by nutritional, environmental, genetic and hormonal factors (Lui et al., 2015). In my experiments, environmental conditions and food composition were completely identical and highly controlled, so I can exclude these factors. Mice differed genetically in the presence or absence of *Cre* recombinase expression in neutrophils, but this difference does not suggest an influence on growth. However, hormones such as growth hormone or insulin-like growth factor 1 might be altered due to genetic differences. Release of growth hormone is controlled *via* the hypothalamic-pituitary axis, while insulin-like growth factor 1 is produced in the liver upon stimulation by growth hormone (Ashpole et al., 2015). There is no indication of *Mrp8* expression, and therefore recombination, in the brain (Allen Brain Atlas, 2021), but *Mrp8* might be expressed in the liver during embryonic development (MGI - Mouse Gene Expression Database, 2021). Therefore, it is theoretically possible that there is some degree of recombination in this tissue, which might in turn affect the expression of insulin-like growth factor 1. However, if there was recombination in the liver, (partial) loss of *Bmal1* in this tissue would be the consequence and the opposite body weight phenotype should be observed upon HFD feeding (Jacobi et al., 2015). Hence, it seems unlikely that *Mrp8-Cre* drives recombination in the liver. In addition, body length was only significantly shorter when mice received HFD (**Figure 9 B**, **Supplemental Figure S8**), which is why a general growth deficit of Neutrophil-BKO mice is unlikely. The mechanism behind diet-dependent body length effects remains unclear. Of note, Control mice that received HFD showed significant increases of body length compared to Controls on chow. This effect was not observed for Neutrophil-BKO mice (**Supplemental Figure S8**). HFD feeding is associated with growth inductions in juvenile mice (Wu et al., 2011b; Machnicki et al., 2022). This effect seems to be attenuated in Neutrophil-BKO mice. However, since Neutrophil-BKO mice also exhibit decreased fat mass and improved glucose and insulin tolerance, it can be concluded that the obesogenic effect of HFD is different for Neutrophil-BKO and Control mice.

Since differences in body weight and metabolic health can be caused by altered locomotor activity or energy metabolism, these parameters were analyzed, but no differences were found between Neutrophil-BKO and Control mice. It is obvious, though, that HFD feeding leads to a reduction of total activity (**Figure 12 D**). This effect was described in the literature (Barzel et al., 2015; Wong et al., 2015) and it was comparable between genotypes. Therefore, I can conclude that changes in locomotor activity and energy metabolism are not responsible for the improved outcome of Neutrophil-BKO mice in DIO experiments.

4.3. Neutrophil numbers or rhythms are not altered in adipose tissue

My initial hypothesis postulated that *Bmal1* knockout in neutrophils would affect the number of neutrophils in adipose tissue upon HFD feeding. This was based on the assumption that infiltration of adipose tissue by neutrophils was rhythmic in Control mice, as demonstrated for tissues like liver, lung, and spleen. It was further assumed that loss of *Bmal1* would ablate this rhythm, since this was observed for clock-deficient neutrophils in the spleen (He et al., 2018). These previous findings highlighted the role of the circadian clock in neutrophils for rhythmic tissue migration and supported the initial hypothesis. In contrast, my results show that neutrophil numbers in adipose tissue were not different between Neutrophil-BKO and Control animals (**Figure 13 B**, **Figure 16 B**). Moreover, presence of neutrophils was rhythmic for both genotypes in eWAT after short-term HFD feeding (**Figure 16 B**), but rhythms were lost after extended HFD feeding (**Figure 13 B**). Altogether, the genotype did not influence the number of neutrophils in adipose tissue in my experimental setup. Therefore, body weight and metabolic outcome of DIO seem to be independent of the degree of neutrophil infiltration into adipose tissue. This was unexpected for several reasons. Firstly, a proportional relationship between the number of neutrophils in adipose tissue and the degree of body weight gain and metaflammation has been described previously (Talukdar et al., 2012; Varol et al., 2014). Secondly, neutrophil functions are rather proinflammatory. Secretion of cytokines and activation of macrophages suggest that neutrophils promote metaflammation so their presence would aggravate body weight gain and insulin resistance (Soehnlein et al., 2008; Amulic et al., 2012; Lee and Lee, 2014). Furthermore, deletion or inhibition of the neutrophil-derived proteins MPO and NE reduce body weight gain and improve metabolic state (Chai et al., 2019; Talukdar et al., 2012). From this it can be inferred that the presence of neutrophils and the expression of these proteins may negatively influence DIO.

However, in a similar direction to my results, dissociation between the number of neutrophils in adipose tissue and metabolic state has previously been reported. Naringenin treatment reduces HFD-stimulated infiltration of neutrophils, while it does not affect body weight after two weeks on HFD in

mice (Tsuhako et al., 2020). Thus, the role of neutrophils in DIO seems to be more complex than a direct proportional relationship and further research will be necessary to fully elucidate neutrophil functions in this context. An important aspect might be neutrophil heterogeneity, the capacity of neutrophils to acquire different phenotypes. Basic principles are only starting to be understood (Liew and Kubes, 2019; Ng et al., 2019). More detailed knowledge could unravel potential connections between the severity of DIO and the phenotype neutrophils in adipose tissue, rather than just their number. In my experiments, expression of CD206 by neutrophils was assessed as a potential marker for neutrophils with anti-inflammatory properties (Cuartero et al., 2013). However, CD206 was almost indetectable in my experimental conditions (data not shown). It is still unknown whether this is the correct marker for heterogenous neutrophil populations in the context of DIO and it is unclear whether the procedure of immune cell isolation and staining might influence expression levels of CD206 in neutrophils. Therefore, more information will be necessary to allow for final conclusions on the heterogeneity of neutrophils in DIO.

Another surprising finding is that rhythms of neutrophils in adipose tissue were not different between genotypes, even though the neutrophil circadian clock was shown to regulate tissue migration (He et al., 2018; Adrover et al., 2019). This might be explained by tissue-specific differences between previously analyzed tissues (*e.g.*, liver, lung, and spleen) and WAT that was studied here. There are only few studies available that analyze the presence of neutrophils in adipose tissue. Adrover and colleagues reported that homeostatic clearance of neutrophils into adipose tissue is reduced when *Bmal1* is knocked out (Adrover et al., 2019). The study also reports increased tendency of *Bmal1*-deficient neutrophils to migrate towards sites of acute inflammation. However, both conditions were only analyzed at one time point (ZT5), and it remains unclear whether neutrophils show rhythmic migration into adipose tissue under conditions of chronic inflammation. One further publication reports that homeostatic neutrophil numbers in WAT are not different between ZT5 and ZT13 (Casanova-Acebes et al., 2018). In line with this, the results presented in this thesis suggest that neutrophil numbers in adipose tissue are not rhythmic during DIO. The only exception was found in eWAT after one week of HFD feeding. Here, rhythmic neutrophil numbers were detected for both genotypes. However, these rhythms were not detectable anymore after extended HFD feeding. This might be related to HFD-induced dampening of rhythms as it was reported for clock gene expression in adipose tissue (Kohsaka et al., 2007).

The fact that neutrophil-specific deletion of *Bmal1* does not lead to genotype-specific changes in numbers or rhythms of neutrophils in adipose tissue implies that the circadian clock in neutrophils has a minor role in this context. He and colleagues demonstrated that leukocyte clocks and the microenvironment both contribute to rhythmic infiltration of immune cells (He et al., 2018). It might therefore be possible that adipose tissue-derived signals dominate neutrophil-derived signals or both

act in a functionally redundant way. This would result in comparable cell counts between Neutrophil-BKO and Control mice as it was observed in this thesis.

The influence of the neutrophil circadian clock on migratory behavior might be more pronounced in other tissues. As such, steady-state numbers of neutrophils have been shown to follow a circadian pattern in the liver (He et al., 2018; Crespo et al., 2020). Neutrophils in the liver were further demonstrated to influence hepatic clock gene expression and thereby affect triglyceride levels in this organ (Crespo et al., 2020). It would be interesting to investigate how the circadian clock in neutrophils influences these interactions and how processes in the liver might contribute to the ameliorated phenotype of Neutrophil-BKO in DIO.

4.4. Neutrophil-BKO mice harbor increased macrophage levels in adipose tissue and increased numbers of M2-like macrophages in eWAT

Neutrophil numbers in adipose tissue were not influenced by the deletion of *Bmal1* in neutrophils. Considering that neutrophils contribute to the recruitment of macrophages, it is therefore not surprising that short-term HFD feeding did not lead to altered macrophage numbers either (**Figure 17 A**). After long-term HFD feeding, however, macrophage fractions were increased for Neutrophil-BKOs in scWAT. In eWAT, increased macrophage numbers were only observed when SVCs were used as baseline (**Figure 14 A**, **Supplemental Figure S4 B**). Findings of elevated macrophage numbers in Neutrophil-BKO mice might seem counterintuitive because the presence of macrophages is associated with detrimental effects in metaflammation and with impaired metabolic function. However, I found that macrophages in scWAT were predominantly anti-inflammatory, M2-like. The same was observed for macrophages of Neutrophil-BKO mice in eWAT (**Figure 14 B**, **Figure 17 B**). Therefore, it is unlikely that they strongly promote metaflammation. In contrast, they might have beneficial effects. Hence, elevated macrophage numbers in adipose tissue of Neutrophil-BKO mice do not conflict with the improved metabolic outcome that was observed.

Interestingly, the polarization phenotype of macrophages in eWAT was different between genotypes after long-term HFD feeding. Neutrophil-BKO mice harbored significantly increased percentages of M2-like macrophages, while the M1-like fraction was significantly reduced (**Figure 14 B, C**). These changes are consistent with reduced body weight gain and improved metabolic phenotype of the mice.

A connection between neutrophils and macrophage polarization has been described before. On the one hand, neutrophil-derived heparin-binding protein has been reported to interact with monocytes in infections with *Streptococcus pyogenes*. This interaction stimulates expression of the

proinflammatory cytokines IL-6, IL-1β and TNF-α (Påhlman et al., 2006). On the other hand, further studies describe an anti-inflammatory influence of neutrophils. During helminth infections, neutrophils are required for macrophages to acquire an M2-like phenotype that mediates resistance to further infections. Mechanistically, IL-13 that is secreted by neutrophils is involved in macrophage polarization (Chen et al., 2014). Similarly, neutrophil-derived colony-stimulating factor 1 promotes M2-like macrophages in the context of tolerance to transplanted organs (Braza et al., 2018). Furthermore, neutrophils can reduce the release of TNF-α from macrophages *in vitro* by decreasing NF-κB signaling (Marwick et al., 2018). Even in the context of DIO, neutrophils seem to influence macrophage polarization. In mice that lack NE, a neutrophil-derived protease, DIO leads to reduced numbers of M1-like macrophages and elevated levels of M2-like macrophages in eWAT (Talukdar et al., 2012).

In most of these studies, neutrophil-macrophage crosstalk enhances M2-like macrophages. However, the effects are attributed to different effector molecules, and it remains unknown whether these molecules are under circadian control. It might be interesting to test whether expression patterns are altered in the absence of *Bmal1*.

After one week on HFD, however, M2-like macrophages were not altered yet (**Figure 17 B**). Since neutrophils are early effector cells in inflammatory reactions and body weight changes were already obvious at this stage (**Figure 15 A**), it was assumed that the relevant mechanism could also be detected at this time. This might suggest that altered polarization after long-term HFD feeding is a secondary effect, rather than part of the mechanism leading to reduced body weight gain. However, absence of altered macrophage polarization after one week of HFD might also be related to compensatory mechanisms that reduce inflammatory parameters at this stage. Such an effect was described for inflammatory markers in the hypothalamus (Thaler et al., 2012).

Interestingly, M2-like macrophages in eWAT displayed circadian changes in Controls that were not observed for Neutrophil-BKOs after one week of HFD feeding (**Supplemental Figure S5 D**). Loss of rhythmicity in Neutrophil-BKO mice indicates that the neutrophil circadian clock might influence rhythms of M2-like macrophages. However, M2-like macrophages were non-rhythmic for both genotypes after long-term exposure to HFD (**Supplemental Figure S4 D**). Either this is due to gradual loss of rhythmicity that goes along with HFD feeding (Kohsaka et al., 2007) or it argues against a role of the neutrophil circadian clock in rhythms of M2-like macrophages.

Comparing the two different adipose tissue depots that have been analyzed in this project, eWAT seems to be more involved in inflammatory processes that might influence the phenotype. Since eWAT represents VAT, this is consistent with reports on visceral obesity being more detrimental for metabolic health than accumulation of subcutaneous fat (Gealekman et al., 2011), partly because VAT is more

involved in metaflammation processes (Fried et al., 1998; Fain et al., 2004; Murano et al., 2008; Joe et al., 2009; Lee et al., 2016; Hwang et al., 2019).

Interestingly, eWAT tissue weight was higher in Neutrophil-BKOs than in Controls (**Figure 14 C**), which might be related to increased cellular stress, immune activation and, as a result, decreased glucose tolerance and insulin sensitivity (Cinti et al., 2005; Jernås et al., 2006). In case of Neutrophil-BKOs, the anti-inflammatory polarization of macrophages might compensate for this effect so that tissue expansion is not critical in this situation.

However, increased expansion of eWAT in Neutrophil-BKO mice contrasts with the finding that total fat mass was reduced in these animals (**Figure 9 C**). Weight of scWAT was comparable to Controls (**Figure 14 D**), so there must be other depots with decreased fat mass. Identifying these depots might also give interesting hints on the mechanism leading to reduced fat mass and healthier metabolic state in Neutrophil-BKO mice.

4.5. HFD intake is reduced in Neutrophil-BKO animals

As pointed out above, an influence of neutrophils on macrophage polarization might be part of the mechanism underlying the observed body weight and metabolic phenotypes. However, food intake was reduced in Neutrophil-BKO mice (**Figure 11 A**, **Figure 15 B**) and this factor might also contribute to decreased body weight gain and improved metabolic outcome. In contrast to results for altered macrophage polarization, food intake was already reduced after one week of HFD feeding (**Figure 15 B**, **Figure 17 B**). Since neutrophils are considered early effector cells in immune reactions (Amulic et al., 2012; Fine et al., 2019) and they infiltrate adipose tissue already 3 days after onset of HFD feeding (Elgazar-Carmon et al., 2008; Talukdar et al., 2012), the observation of this early effect makes food intake a strong candidate to explain the beneficial effects for Neutrophil-BKO mice.

4.5.1. Neutrophil-BKO mice do not show altered mRNA expression of neuropeptides that regulate food intake

Further experiments were performed to gain mechanistic insights on food intake regulation. However, no evidence was found for alterations, neither on the level of adipokines that might influence food intake (**Figure 18**) nor on the level of transcripts of hypothalamic peptides that are involved in appetite regulation (**Figure 19**). Interpretation of the results for mRNA expression of hypothalamic peptides were complicated by high variation within replicates, which might be related to technical limitations. The hypothalamus was manually excised from frozen tissue as described before (Li et al., 2014), This

technique allows for subsequent analysis of other brain structures, because the remaining brain stays intact and frozen. However, it bears the risk of including various amounts of surrounding non-hypothalamic tissue, thereby increasing the variability of samples. To overcome this, hypothalamic tissue could be dissected from brain sections (Kernie et al., 2000; Paschos et al., 2012). Alternatively, immunofluorescence staining or *in situ* hybridization might be used in future experiments for more spatial information on expression in different subregions of the hypothalamus. Furthermore, immunofluorescence stainings would allow for assessment of protein levels which might deviate from mRNA expression that was analyzed here.

Among all hypothalamic peptide transcripts that were analyzed, only *Agrp* showed genotype-related differences. After long-term exposure to HFD, expression of this gene was increased in Neutrophil-BKO mice (**Figure 19 C**). AGRP is orexigenic, *i.e.*, it stimulates food intake. Increased *Agrp* expression would therefore be associated with higher food intake. Since food intake is decreased in Neutrophil-BKO mice, it is possible that upregulation of *Argp* is a compensatory effect to prevent even lower food intake.

When comparing gene expression after short-term and long-term HFD feeding, *Cartpt* was increased after long-term feeding, while *Agrp* was decreased (**Figure 19**). These results are in line with a report of increased expression of anorexigenic peptides and decreased levels of orexigenic peptides upon HFD feeding (Kohsaka et al., 2007).

Altogether, data presented in this thesis do not provide evidence for altered regulation of food intake at the level of hypothalamic neuropeptide transcripts. It cannot be excluded that there are effects downstream of these transcripts – *e.g.*, at the level of the neuropeptides themselves – that were not analyzed to date, so it is still possible that hypothalamic regulation of food intake is altered in Neutrophil-BKO mice.

4.5.2. Inflammatory state of the hypothalamus is not altered, but rhythms of neutrophil migration might be affected

HFD feeding is associated with hypothalamic inflammation, characterized by increased expression levels of *Il-6* and *Tnf-α* (De Souza et al., 2005; Milanski et al., 2009; Thaler et al., 2012). Inflammation is linked to increased food intake and body weight (Thaler et al., 2012; Valdearcos et al., 2014; Douglass et al., 2017). Expression of *Il-6* and *Tnf-α* mRNA was assessed to analyze a potential contribution to reduced food intake and body weight gain of Neutrophil-BKO mice. No differences were found between Controls and Neutrophil-BKOs (**Figure 20 A, B**). These results do not point at differences in inflammatory state of the hypothalamus that would lead to reduced food intake of Neutrophil-BKO

mice. However, it cannot be excluded that other cytokines are affected. For example, *Il-1β* was shown to be involved in inflammatory processes in the brain (Douglass et al., 2017; Pflieger et al., 2018b), even though other studies found no or only moderate regulation of this cytokine in DIO (Thaler et al., 2012; Valdearcos et al., 2014).

Microglia have been considered the main cell type being involved in central inflammation upon HFD feeding (Jeong et al., 2013; Thaler et al., 2012; Valdearcos et al., 2014). However, also peripheral immune cells seem to infiltrate the brain during DIO and contribute to central inflammation (Buckman et al., 2014; Jeong et al., 2013; Yang et al., 2019). In this project, neutrophil infiltration into the hypothalamus was indirectly assessed by detection of *Mpo* mRNA expression. Circadian rhythms were observed for Controls after short-term HFD feeding, but not for Neutrophil-BKOs (**Figure 20 C**). Compared to sort-term HFD feeding, long-term exposure to HFD led to increased *Mpo* expression levels for both genotypes, but the increase was less pronounced in Neutrophil-BKO mice (**Supplemental Figure S7**). MPO is described to be specific for neutrophils (Schultz et al., 1965; Dunn et al., 1968; Ji et al., 2007, 2008; Jeong et al., 2010), even though there are reports of *Mpo* expression in microglia (Gray et al., 2007), monocytes and macrophages (Stackowicz et al., 2020). Therefore, it needs to be considered that other cell types might be detected in this analysis. More experiments are necessary for direct evidence that neutrophils are present in the hypothalamus. This could be achieved by immunofluorescence stainings or by FACS analysis of hypothalamic tissue. Furthermore, circadian rhythms of *Mpo* could be related to rhythmic *Mpo* expression or to rhythmic presence of neutrophils within the hypothalamus. Further experiments using alternative techniques would allow for stronger conclusions here.

In summary, my findings suggest that neutrophils infiltrate hypothalamic tissue, but further experiments are necessary to verify that *Mpo* is neutrophil-derived and to discriminate between rhythmic *Mpo* expression and rhythmic neutrophil infiltration. In any case, *Mpo* expression seems to be influenced by the neutrophil circadian clock since *Mpo* is no longer rhythmic in Neutrophil-BKO mice after short-term HFD feeding and the increase of *Mpo* expression upon long-term HFD feeding is dampened in Neutrophil-BKO mice. However, it remains unclear how neutrophils in the hypothalamus might affect food intake or hypothalamic inflammation in accordance with the results of this thesis. Interestingly, it was shown that the chemokine CXCL12 is induced by HFD feeding in rats and that it stimulates food intake *via* induction of the orexigenic neuropeptide enkephalin in the paraventricular nucleus of the hypothalamus (Poon et al., 2016). Since CXCR4, the receptor for CXCL12, is expressed on the surface of neutrophils and its levels change diurnally (Adrover et al., 2019), there might be a connection worth exploring in future experiments. This is especially interesting since differences in food intake become obvious only upon HFD feeding (**Figure 15**) and CXCL12 is induced by HFD.

During this project, it was assumed that an early effect is responsible for the improved DIO phenotype of Neutrophil-BKO mice. Given the role of neutrophils as early effector cells and the early body weight differences, it appears very likely that such early events determine the long-term outcome. However, it is possible that neutrophil effects in metaflammation are not limited to the early phase but remain important at later stages. In particular, neutrophils have been attributed a role in clearing debris in sterile inflammation (Oved et al., 2021), an effect that would be relevant at later stages.

4.6. Unaddressed factors that could influence DIO outcome in Neutrophil-BKO mice

In the experiments presented in this thesis, reduced food intake and altered polarization of macrophages were identified as two potential factors contributing to improved resistance of Neutrophil-BKO mice against DIO. However, it is still possible that other factors are involved that were not addressed so far.

As such, neutrophils are known to form NETs to attack pathogens (Papayannopoulos, 2018; Rada, 2019), but NET formation was also described in conditions of sterile inflammation like ischemia, autoimmunity, or cancer (Cui et al., 2012; Huang et al., 2015; Jorch and Kubes, 2017; Kim et al., 2019). The capacity to release NETs has been shown to change over the day (Adrover et al., 2020). NETs are detected in blood of obese patients (D'Abbondanza et al., 2019) and NET inhibition can prevent DIO-associated endothelial damage in mice (Wang et al., 2018). However, inhibition of NET formation does not reduce adipose tissue inflammation or DIO-induced insulin sensitivity (Braster et al., 2016). Hence, it was not investigated in this project.

Another factor that might be involved in the phenotype of Neutrophil-BKO mice is KLF2. This myeloid factor negatively regulates inflammatory activation of monocytes, in part by inhibiting NF-kB activation (Das 2006). HFD consumption leads to decreased KLF2 levels and loss of *Klf2* aggravates metaflammation in peripheral and central tissues (Sweet 2020). However, *Klf2* is described to be expressed in monocytes, so it would not be affected by neutrophil-specific deletion of *Bmal1*. Nonetheless, it might be interesting to analyze whether it is also expressed in neutrophils. In that case, circadian regulation of *Klf2* would be an interesting target to study.

Time-of-day dependent changes of neutrophil granule content have been reported (Adrover et al., 2020) and granule components such as MPO are relevant for the production of ROS (Amulic et al., 2012). Similarly, at least in human neutrophils, it was shown that the ROS-producing capacity of neutrophils changes across the day (Ella et al., 2018). In the context of obesity, ROS are associated with

mitochondrial dysfunction which may exacerbate metaflammation (de Mello et al., 2018). It might be possible that ROS levels are reduced in Neutrophil-BKO mice, thereby contributing to the improved outcome of DIO that was observed. However, it was previously shown that stimulated ROS production in neutrophils that lack *Bmal1* does not differ from wild type neutrophils (Adrover et al., 2019), indicating that time-of-day dependent ROS production might be regulated independent of the neutrophil-intrinsic circadian clock.

Deletion of NE is associated with decreased body weight gain, improved insulin sensitivity and increased numbers of M2-like macrophages in eWAT during HFD feeding (Talukdar et al., 2012). These findings are comparable to the results presented here for Neutrophil-BKO mice so that it might be interesting to study the influence of the circadian clock on expression or activity of NE. The promotor region of NE does not contain a canonical E-box, so direct transcriptional control by BMAL1:CLOCK is unlikely. Nonetheless, it is possible that NE is influenced by the circadian clock *via* different pathways.

4.7. Conclusions and outlook

In this PhD thesis, the role of the neutrophil circadian clock for progression of DIO was investigated for the first time. Lack of *Bmal1* in neutrophils resulted in reduced body weight gain as well as reduced fat mass. In accordance with this, glucose tolerance and insulin sensitivity were improved. Of note, only male mice were used in this study. Extending the results to female mice would allow for more general conclusions.

Two factors were identified that can provide a link between the phenotype and the underlying mechanism. Firstly, food intake was reduced in Neutrophil-BKO mice. Secondly, a higher percentage of anti-inflammatory macrophages was found in eWAT. Follow-up experiments are necessary to further identify mechanistic details how these factors contribute to reduced body weight gain and improved metabolic phenotype. It is possible that there is no single factor that is responsible for the improved DIO phenotype of Neutrophil-BKO mice, but that several factors collectively promote these beneficial effects.

Changes in food intake are already noticeable after one week of HFD feeding. However, in the long-term experiment, significant differences in food intake are evident later than significant differences in body weight (**Figure 9 A**, **Figure 11 A**). Still, food intake has high potential to explain the differences in body weight and metabolic outcome since it directly influences energy balance. Food intake regulation was analyzed on the level of adipokines (leptin and adiponectin), of hypothalamic neuropeptides (*Pomc*, *Cartpt*, *Agrp*, *Npy*) and of hypothalamic inflammation (*Il-6*, *Tnf-α*, *Mpo*). Except for *Mpo*

expression, none of the analyses revealed a clear link to explain how the neutrophil circadian clock might be involved in the reduction of food intake upon HFD feeding. Differences in *Mpo* rhythmicity might indicate differences in neutrophil infiltration of the hypothalamus. Potential interference with hypothalamic CXCL12 might be subject to further investigation.

Likewise, an influence of the neutrophil circadian clock on macrophage polarization is a potential starting point for further experiments. Macrophage polarization towards the anti-inflammatory type in Neutrophil-BKO mice might have a strong protective potential against adverse metabolic effects of DIO. To unveil further mechanistic details, it could be investigated whether there is circadian expression of NE and other neutrophil-derived factors that have been described to influence macrophage polarization (heparin binding protein, IL-13, and colony-stimulating factor 1). In addition, *in vitro* stimulation experiments might show whether absence of the circadian clock in neutrophils alters the susceptibility of macrophages to be polarized into M1-like or M2-like cells.

Independent of the mechanism underlying the observed metabolic phenotypes, Neutrophil-BKO mice represent a model in which a targeted manipulation improves resistance to DIO, as demonstrated by reduced body weight gain and improved glucose tolerance and insulin sensitivity. If this manipulation can be translated to the human situation, it might open new strategies for clinical interventions in obesity and therefore help to control related health problems. However, in the clinic situation we are confronted with patients that are already obese, while the experiments presented here studied the onset and progression of obesity in the presence of *Bmal1* deletion in neutrophils. A first step in converging these two situations could be an inducible mouse model in which *Bmal1* is only knocked out in neutrophils when animals are already obese. This could be achieved either by inducible expression of *Cre* recombinase (Feil et al., 2009) or by intravenous injection of targeted nanoparticles (Liu et al., 2018). If this intervention reduces body weight and improves glucose tolerance and insulin sensitivity of the mice, it represents a manipulation of high therapeutic potential. As such, the results of this PhD thesis might pave the way for new therapeutic interventions to overcome obesity as a global health problem of modern societies.

References

Abe, H., Kida, M., Tsuji, K., and Mano, T. (1989). Feeding cycles entrain circadian rhythms of locomotor activity in CS mice but not in C57BL/6J mice. Physiol Behav *45*, 397–401.

Abram, C.L., Roberge, G.L., Hu, Y., and Lowell, C.A. (2014). Comparative analysis of the efficiency and specificity of myeloid-Cre deleting strains using ROSA-EYFP reporter mice. Journal of Immunological Methods *408*, 89–100.

Adlanmerini, M., Nguyen, H.C., Krusen, B.M., Teng, C.W., Geisler, C.E., Peed, L.C., Carpenter, B.J., Hayes, M.R., and Lazar, M.A. (2021). Hypothalamic REV-ERB nuclear receptors control diurnal food intake and leptin sensitivity in diet-induced obese mice. J Clin Invest *131*.

Adrover, J.M., Del Fresno, C., Crainiciuc, G., Cuartero, M.I., Casanova-Acebes, M., Weiss, L.A., Huerga-Encabo, H., Silvestre-Roig, C., Rossaint, J., Cossío, I., et al. (2019). A Neutrophil Timer Coordinates Immune Defense and Vascular Protection. Immunity.

Adrover, J.M., Aroca-Crevillén, A., Crainiciuc, G., Ostos, F., Rojas-Vega, Y., Rubio-Ponce, A., Cilloniz, C., Bonzón-Kulichenko, E., Calvo, E., Rico, D., et al. (2020). Programmed “disarming” of the neutrophil proteome reduces the magnitude of inflammation. Nat Immunol *21*, 135–144.

Akashi, M., and Takumi, T. (2005). The orphan nuclear receptor RORalpha regulates circadian transcription of the mammalian core-clock Bmal1. Nat Struct Mol Biol *12*, 441–448.

Allen Brain Atlas, 2021: https://mouse.brain-map.org/gene/show/19964, accessed December 16, 2021

Allenbach, C., Zufferey, C., Perez, C., Launois, P., Mueller, C., and Tacchini-Cottier, F. (2006). Macrophages induce neutrophil apoptosis through membrane TNF, a process amplified by Leishmania major. J Immunol *176*, 6656–6664.

Amin, T., and Mercer, J.G. (2016). Hunger and Satiety Mechanisms and Their Potential Exploitation in the Regulation of Food Intake. Curr Obes Rep *5*, 106–112.

Amulic, B., Cazalet, C., Hayes, G.L., Metzler, K.D., and Zychlinsky, A. (2012). Neutrophil function: from mechanisms to disease. Annu. Rev. Immunol. *30*, 459–489.

Anafi, R.C., Lee, Y., Sato, T.K., Venkataraman, A., Ramanathan, C., Kavakli, I.H., Hughes, M.E., Baggs, J.E., Growe, J., Liu, A.C., et al. (2014). Machine learning helps identify CHRONO as a circadian clock component. PLoS Biol *12*, e1001840.

Arble, D.M., Bass, J., Laposky, A.D., Vitaterna, M.H., and Turek, F.W. (2009). Circadian timing of food intake contributes to weight gain. Obesity (Silver Spring) *17*, 2100–2102.

Arjona, A., and Sarkar, D.K. (2005). Circadian Oscillations of Clock Genes, Cytolytic Factors, and Cytokines in Rat NK Cells. The Journal of Immunology *174*, 7618–7624.

Arkan, M.C., Hevener, A.L., Greten, F.R., Maeda, S., Li, Z.-W., Long, J.M., Wynshaw-Boris, A., Poli, G., Olefsky, J., and Karin, M. (2005). IKK-beta links inflammation to obesity-induced insulin resistance. Nat Med *11*, 191–198.

Aroca-Crevillén, A., Adrover, J.M., and Hidalgo, A. (2020). Circadian Features of Neutrophil Biology. Front Immunol *11*, 576.

Aryal, R.P., Kwak, P.B., Tamayo, A.G., Gebert, M., Chiu, P.-L., Walz, T., and Weitz, C.J. (2017). Macromolecular Assemblies of the Mammalian Circadian Clock. Mol. Cell *67*, 770-782.e6.

Aschoff, J., Fatranská, M., Giedke, H., Doerr, P., Stamm, D., and Wisser, H. (1971). Human circadian rhythms in continuous darkness: entrainment by social cues. Science *171*, 213–215.

Ashpole, N.M., Sanders, J.E., Hodges, E.L., Yan, H., and Sonntag, W.E. (2015). GROWTH HORMONE, INSULIN-LIKE GROWTH FACTOR-1 AND THE AGING BRAIN. Exp Gerontol *68*, 76–81.

Athens, J.W., Haab, O.P., Raab, S.O., Mauer, A.M., Ashenbrucker, H., Cartwright, G.E., and Wintrobe, M.M. (1961). Leukokinetic studies. IV. The total blood, circulating and marginal granulocyte pools and the granulocyte turnover rate in normal subjects. J Clin Invest *40*, 989–995.

Azevedo, P.G. de, Miranda, L.R., Nicolau, E.S., Alves, R.B., Bicalho, M.A.C., Couto, P.P., Ramos, A.V., Souza, R.P. de, Longhi, R., Friedman, E., et al. (2021). Genetic association of the PERIOD3 (PER3) Clock gene with extreme obesity. Obes Res Clin Pract *15*, 334–338.

Bae, K., Jin, X., Maywood, E.S., Hastings, M.H., Reppert, S.M., and Weaver, D.R. (2001). Differential functions of mPer1, mPer2, and mPer3 in the SCN circadian clock. Neuron *30*, 525–536.

Balsalobre, A., Brown, S.A., Marcacci, L., Tronche, F., Kellendonk, C., Reichardt, H.M., Schütz, G., and Schibler, U. (2000). Resetting of circadian time in peripheral tissues by glucocorticoid signaling. Science *289*, 2344–2347.

Bapat, S.P., Liang, Y., and Zheng, Y. (2019). Characterization of Immune Cells from Adipose Tissue. Curr Protoc Immunol *126*, e86.

Barclay, J.L., Shostak, A., Leliavski, A., Tsang, A.H., Jöhren, O., Müller-Fielitz, H., Landgraf, D., Naujokat, N., van der Horst, G.T.J., and Oster, H. (2013). High-fat diet-induced hyperinsulinemia and tissue-specific insulin resistance in Cry-deficient mice. Am J Physiol Endocrinol Metab *304*, E1053-1063.

Barrett, R.K., and Takahashi, J.S. (1995). Temperature compensation and temperature entrainment of the chick pineal cell circadian clock. J Neurosci *15*, 5681–5692.

Barzel, B., Lim, K., Burke, S.L., Armitage, J.A., and Head, G.A. (2015). Specific role of dietary fat in modifying cardiovascular and locomotor activity 24-h rhythms. Chronobiology International *32*, 668–676.

Baumann, A., Gönnenwein, S., Bischoff, S.C., Sherman, H., Chapnik, N., Froy, O., and Lorentz, A. (2013). The circadian clock is functional in eosinophils and mast cells. Immunology *140*, 465–474.

Beck-Schimmer, B., Schwendener, R., Pasch, T., Reyes, L., Booy, C., and Schimmer, R.C. (2005). Alveolar macrophages regulate neutrophil recruitment in endotoxin-induced lung injury. Respir Res *6*, 61.

Berson, D.M., Dunn, F.A., and Takao, M. (2002). Phototransduction by retinal ganglion cells that set the circadian clock. Science *295*, 1070–1073.

Blüher, M., Bashan, N., Shai, I., Harman-Boehm, I., Tarnovscki, T., Avinaoch, E., Stumvoll, M., Dietrich, A., Klöting, N., and Rudich, A. (2009). Activated Ask1-MKK4-p38MAPK/JNK stress signaling pathway in human omental fat tissue may link macrophage infiltration to whole-body Insulin sensitivity. J Clin Endocrinol Metab *94*, 2507–2515.

Bode, B., Shahmoradi, A., Taneja, R., Rossner, M.J., and Oster, H. (2011). Genetic interaction of Per1 and Dec1/2 in the regulation of circadian locomotor activity. J Biol Rhythms *26*, 530–540.

Bolinder, J., Kager, L., Ostman, J., and Arner, P. (1983). Differences at the receptor and postreceptor levels between human omental and subcutaneous adipose tissue in the action of insulin on lipolysis. Diabetes *32*, 117–123.

Bollinger, T., Leutz, A., Leliavski, A., Skrum, L., Kovac, J., Bonacina, L., Benedict, C., Lange, T., Westermann, J., Oster, H., et al. (2011). Circadian clocks in mouse and human CD4+ T cells. PLoS One *6*, e29801.

Borregaard, N., and Cowland, J.B. (1997). Granules of the Human Neutrophilic Polymorphonuclear Leukocyte. Blood *89*, 3503–3521.

Bouchery, T., and Harris, N. (2019). Neutrophil-macrophage cooperation and its impact on tissue repair. Immunol. Cell Biol.

Braster, Q., Silvestre Roig, C., Hartwig, H., Beckers, L., den Toom, M., Döring, Y., Daemen, M.J., Lutgens, E., and Soehnlein, O. (2016). Inhibition of NET Release Fails to Reduce Adipose Tissue Inflammation in Mice. PLoS ONE *11*, e0163922.

Braza, M.S., Conde, P., Garcia, M., Cortegano, I., Brahmachary, M., Pothula, V., Fay, F., Boros, P., Werner, S.A., Ginhoux, F., et al. (2018). Neutrophil derived CSF1 induces macrophage polarization and promotes transplantation tolerance. Am. J. Transplant. *18*, 1247–1255.

Brestoff, J.R., Kim, B.S., Saenz, S.A., Stine, R.R., Monticelli, L.A., Sonnenberg, G.F., Thome, J.J., Farber, D.L., Lutfy, K., Seale, P., et al. (2015). Group 2 innate lymphoid cells promote beiging of white adipose tissue and limit obesity. Nature *519*, 242–246.

Brown, S.A., Zumbrunn, G., Fleury-Olela, F., Preitner, N., and Schibler, U. (2002). Rhythms of mammalian body temperature can sustain peripheral circadian clocks. Curr Biol *12*, 1574–1583.

Buckman, L.B., Hasty, A.H., Flaherty, D.K., Buckman, C.T., Thompson, M.M., Matlock, B.K., Weller, K., and Ellacott, K.L.J. (2014). Obesity induced by a high-fat diet is associated with increased immune cell entry into the central nervous system. Brain Behav Immun *35*, 33–42.

Buhr, E.D., and Takahashi, J.S. (2013). Molecular components of the Mammalian circadian clock. Handb Exp Pharmacol 3–27.

Buijs, R.M., Chun, S.J., Niijima, A., Romijn, H.J., and Nagai, K. (2001). Parasympathetic and sympathetic control of the pancreas: a role for the suprachiasmatic nucleus and other hypothalamic centers that are involved in the regulation of food intake. J Comp Neurol *431*, 405–423.

Buijs, R.M., van Eden, C.G., Goncharuk, V.D., and Kalsbeek, A. (2003). The biological clock tunes the organs of the body: timing by hormones and the autonomic nervous system. J Endocrinol *177*, 17–26.

Bunger, M.K., Wilsbacher, L.D., Moran, S.M., Clendenin, C., Radcliffe, L.A., Hogenesch, J.B., Simon, M.C., Takahashi, J.S., and Bradfield, C.A. (2000). Mop3 is an essential component of the master circadian pacemaker in mammals. Cell *103*, 1009–1017.

Burhans, M.S., Hagman, D.K., Kuzma, J.N., Schmidt, K.A., and Kratz, M. (2018). Contribution of Adipose Tissue Inflammation to the Development of Type 2 Diabetes Mellitus. Compr Physiol *9*, 1–58.

Busino, L., Bassermann, F., Maiolica, A., Lee, C., Nolan, P.M., Godinho, S.I.H., Draetta, G.F., and Pagano, M. (2007). SCFFbxl3 controls the oscillation of the circadian clock by directing the degradation of cryptochrome proteins. Science *316*, 900–904.

Camacho, F., Cilio, M., Guo, Y., Virshup, D.M., Patel, K., Khorkova, O., Styren, S., Morse, B., Yao, Z., and Keesler, G.A. (2001). Human casein kinase Idelta phosphorylation of human circadian clock proteins period 1 and 2. FEBS Lett *489*, 159–165.

Cano, P., Jiménez-Ortega, V., Larrad, A., Reyes Toso, C.F., Cardinali, D.P., and Esquifino, A.I. (2008). Effect of a high-fat diet on 24-h pattern of circulating levels of prolactin, luteinizing hormone, testosterone, corticosterone, thyroid-stimulating hormone and glucose, and pineal melatonin content, in rats. Endocrine *33*, 118–125.

Cao, X., Yang, Y., Selby, C.P., Liu, Z., and Sancar, A. (2021). Molecular mechanism of the repressive phase of the mammalian circadian clock. Proc Natl Acad Sci U S A *118*.

Carroll, J.F., Thaden, J.J., Wright, A.M., and Strange, T. (2005). Loss of diurnal rhythms of blood pressure and heart rate caused by high-fat feeding. Am J Hypertens *18*, 1320–1326.

Casanova-Acebes, M., Pitaval, C., Weiss, L.A., Nombela-Arrieta, C., Chèvre, R., A-González, N., Kunisaki, Y., Zhang, D., van Rooijen, N., Silberstein, L.E., et al. (2013). Rhythmic modulation of the hematopoietic niche through neutrophil clearance. Cell *153*, 1025–1035.

Casanova-Acebes, M., Nicolás-Ávila, J.A., Li, J.L., García-Silva, S., Balachander, A., Rubio-Ponce, A., Weiss, L.A., Adrover, J.M., Burrows, K., A-González, N., et al. (2018). Neutrophils instruct homeostatic and pathological states in naive tissues. J Exp Med *215*, 2778–2795.

Chai, W., Aylor, K., Liu, Z., Gan, L.-M., Michaëlsson, E., and Barrett, E. (2019). Inhibiting myeloperoxidase prevents onset and reverses established high fat diet -induced microvascular insulin resistance. Am. J. Physiol. Endocrinol. Metab.

Chakravarti, A., Rusu, D., Flamand, N., Borgeat, P., and Poubelle, P.E. (2009). Reprogramming of a subpopulation of human blood neutrophils by prolonged exposure to cytokines. Lab Invest *89*, 1084–1099.

Chen, G.Y., and Nuñez, G. (2010). Sterile inflammation: sensing and reacting to damage. Nat Rev Immunol *10*, 826–837.

Chen, F., Wu, W., Millman, A., Craft, J.F., Chen, E., Patel, N., Boucher, J.L., Urban, J.F., Kim, C.C., and Gause, W.C. (2014). Neutrophils prime a long-lived effector macrophage phenotype that mediates accelerated helminth expulsion. Nat. Immunol. *15*, 938–946.

Chertov, O., Ueda, H., Xu, L.L., Tani, K., Murphy, W.J., Wang, J.M., Howard, O.M., Sayers, T.J., and Oppenheim, J.J. (1997). Identification of human neutrophil-derived cathepsin G and azurocidin/CAP37 as chemoattractants for mononuclear cells and neutrophils. J Exp Med *186*, 739–747.

Cinamon, G., Shinder, V., Shamri, R., and Alon, R. (2004). Chemoattractant signals and beta 2 integrin occupancy at apical endothelial contacts combine with shear stress signals to promote transendothelial neutrophil migration. J Immunol *173*, 7282–7291.

Cinti, S., Mitchell, G., Barbatelli, G., Murano, I., Ceresi, E., Faloia, E., Wang, S., Fortier, M., Greenberg, A.S., and Obin, M.S. (2005). Adipocyte death defines macrophage localization and function in adipose tissue of obese mice and humans. J Lipid Res *46*, 2347–2355.

Claustrat, B., Brun, J., and Chazot, G. (2005). The basic physiology and pathophysiology of melatonin. Sleep Med Rev *9*, 11–24.

Coomans, C.P., van den Berg, S.A.A., Lucassen, E.A., Houben, T., Pronk, A.C.M., van der Spek, R.D., Kalsbeek, A., Biermasz, N.R., Willems van Dijk, K., Romijn, J.A., et al. (2013). The suprachiasmatic nucleus controls circadian energy metabolism and hepatic insulin sensitivity. Diabetes *62*, 1102–1108.

Cowland, J.B., and Borregaard, N. (1999). Isolation of neutrophil precursors from bone marrow for biochemical and transcriptional analysis. J Immunol Methods *232*, 191–200.

Crespo, M., Gonzalez-Teran, B., Nikolic, I., Mora, A., Folgueira, C., Rodríguez, E., Leiva-Vega, L., Pintor-Chocano, A., Fernández-Chacón, M., Ruiz-Garrido, I., et al. (2020). Neutrophil infiltration regulates clock-gene expression to organize daily hepatic metabolism. Elife *9*, e59258.

Creux, N., and Harmer, S. (2019). Circadian Rhythms in Plants. Cold Spring Harb Perspect Biol *11*, a034611.

Cuartero, M.I., Ballesteros, I., Moraga, A., Nombela, F., Vivancos, J., Hamilton, J.A., Corbí, Á.L., Lizasoain, I., and Moro, M.A. (2013). N2 neutrophils, novel players in brain inflammation after stroke: modulation by the PPARγ agonist rosiglitazone. Stroke *44*, 3498–3508.

Cui, B.-B., Tan, C.-Y., Schorn, C., Tang, H.-H., Liu, Y., and Zhao, Y. (2012). Neutrophil extracellular traps in sterile inflammation: the story after dying? Autoimmunity *45*, 593–596.

Cui, L.N., Coderre, E., and Renaud, L.P. (2001). Glutamate and GABA mediate suprachiasmatic nucleus inputs to spinal-projecting paraventricular neurons. Am J Physiol Regul Integr Comp Physiol *281*, R1283-1289.

D'Abbondanza, M., Martorelli, E.E., Ricci, M.A., De Vuono, S., Migliola, E.N., Godino, C., Corradetti, S., Siepi, D., Paganelli, M.T., Maugeri, N., et al. (2019). Increased plasmatic NETs by-products in patients in severe obesity. Sci Rep *9*, 14678.

Dale, D.C., Boxer, L., and Liles, W.C. (2008). The phagocytes: neutrophils and monocytes. Blood *112*, 935–945.

Dallmann, R., and Weaver, D.R. (2010). Altered body mass regulation in male mPeriod mutant mice on high-fat diet. Chronobiol Int *27*, 1317–1328.

Damiola, F., Le Minh, N., Preitner, N., Kornmann, B., Fleury-Olela, F., and Schibler, U. (2000). Restricted feeding uncouples circadian oscillators in peripheral tissues from the central pacemaker in the suprachiasmatic nucleus. Genes Dev *14*, 2950–2961.

Dancey, J.T., Deubelbeiss, K.A., Harker, L.A., and Finch, C.A. (1976). Neutrophil kinetics in man. J Clin Invest *58*, 705–715.

Dandona, P., Weinstock, R., Thusu, K., Abdel-Rahman, E., Aljada, A., and Wadden, T. (1998). Tumor necrosis factor-alpha in sera of obese patients: fall with weight loss. J Clin Endocrinol Metab *83*, 2907–2910.

Dardente, H., Fortier, E.E., Martineau, V., and Cermakian, N. (2007). Cryptochromes impair phosphorylation of transcriptional activators in the clock: a general mechanism for circadian repression. Biochem. J. *402*, 525–536.

Das, H., Kumar, A., Lin, Z., Patino, W.D., Hwang, P.M., Feinberg, M.W., Majumder, P.K., and Jain, M.K. (2006). Kruppel-like factor 2 (KLF2) regulates proinflammatory activation of monocytes. Proc Natl Acad Sci U S A *103*, 6653–6658.

De Filippo, K., Henderson, R.B., Laschinger, M., and Hogg, N. (2008). Neutrophil chemokines KC and macrophage-inflammatory protein-2 are newly synthesized by tissue macrophages using distinct TLR signaling pathways. J Immunol *180*, 4308–4315.

De Souza, C.T., Araujo, E.P., Bordin, S., Ashimine, R., Zollner, R.L., Boschero, A.C., Saad, M.J.A., and Velloso, L.A. (2005). Consumption of a fat-rich diet activates a proinflammatory response and induces insulin resistance in the hypothalamus. Endocrinology *146*, 4192–4199.

DeBruyne, J.P., Weaver, D.R., and Reppert, S.M. (2007). CLOCK and NPAS2 have overlapping roles in the suprachiasmatic circadian clock. Nat. Neurosci. *10*, 543–545.

Depner, C.M., Stothard, E.R., and Wright, K.P. (2014). Metabolic consequences of sleep and circadian disorders. Curr Diab Rep *14*, 507.

Douglass, J.D., Dorfman, M.D., Fasnacht, R., Shaffer, L.D., and Thaler, J.P. (2017). Astrocyte IKKβ/NF-κB signaling is required for diet-induced obesity and hypothalamic inflammation. Mol Metab *6*, 366–373.

Dresch, C., Najean, Y., and Beauchet, J. (1971). In vitro 51Cr and 32P-DFP labeling of granulocytes in man. J Nucl Med *12*, 774–784.

Druzd, D., Matveeva, O., Ince, L., Harrison, U., He, W., Schmal, C., Herzel, H., Tsang, A.H., Kawakami, N., Leliavski, A., et al. (2017). Lymphocyte Circadian Clocks Control Lymph Node Trafficking and Adaptive Immune Responses. Immunity *46*, 120–132.

Duan, Y., Zeng, L., Zheng, C., Song, B., Li, F., Kong, X., and Xu, K. (2018). Inflammatory Links Between High Fat Diets and Diseases. Front Immunol *9*, 2649.

Dunn, W.B., Hardin, J.H., and Spicer, S.S. (1968). Ultrastructural localization of myeloperoxidase in human neutrophil and rabbit heterophil and eosinophil leukocytes. Blood *32*, 935–944.

Eastman, C.I., Mistlberger, R.E., and Rechtschaffen, A. (1984). Suprachiasmatic nuclei lesions eliminate circadian temperature and sleep rhythms in the rat. Physiol. Behav. *32*, 357–368.

Eastman, C.I., Suh, C., Tomaka, V.A., and Crowley, S.J. (2015). Circadian rhythm phase shifts and endogenous free-running circadian period differ between African-Americans and European-Americans. Sci Rep *5*, 8381.

Ebihara, S., Marks, T., Hudson, D.J., and Menaker, M. (1986). Genetic control of melatonin synthesis in the pineal gland of the mouse. Science *231*, 491–493.

Eckel-Mahan, K., and Sassone-Corsi, P. (2015). Phenotyping Circadian Rhythms in Mice. Curr Protoc Mouse Biol *5*, 271–281.

Elgazar-Carmon, V., Rudich, A., Hadad, N., and Levy, R. (2008). Neutrophils transiently infiltrate intra-abdominal fat early in the course of high-fat feeding. J. Lipid Res. *49*, 1894–1903.

Ella, K., Csépányi-Kömi, R., and Káldi, K. (2016). Circadian regulation of human peripheral neutrophils. Brain Behav. Immun. *57*, 209–221.

Ella, K., Mócsai, A., and Káldi, K. (2018). Circadian regulation of neutrophils: Control by a cell-autonomous clock or systemic factors? Eur. J. Clin. Invest. e12965.

Engin, A. (2017). Circadian Rhythms in Diet-Induced Obesity. Adv Exp Med Biol *960*, 19–52.

al-Essa, L.Y., Niwa, M., Kohno, K., Nozaki, M., and Tsurumi, K. (1995). Heterogeneity of circulating and exudated polymorphonuclear leukocytes in superoxide-generating response to cyclic AMP and cyclic AMP-elevating agents. Investigation of the underlying mechanism. Biochem Pharmacol *49*, 315–322.

Evrard, M., Kwok, I.W.H., Chong, S.Z., Teng, K.W.W., Becht, E., Chen, J., Sieow, J.L., Penny, H.L., Ching, G.C., Devi, S., et al. (2018). Developmental Analysis of Bone Marrow Neutrophils Reveals Populations Specialized in Expansion, Trafficking, and Effector Functions. Immunity *48*, 364-379.e8.

Fadok, V.A., Bratton, D.L., Konowal, A., Freed, P.W., Westcott, J.Y., and Henson, P.M. (1998). Macrophages that have ingested apoptotic cells in vitro inhibit proinflammatory cytokine production through autocrine/paracrine mechanisms involving TGF-beta, PGE2, and PAF. J Clin Invest *101*, 890–898.

Fain, J.N., Madan, A.K., Hiler, M.L., Cheema, P., and Bahouth, S.W. (2004). Comparison of the release of adipokines by adipose tissue, adipose tissue matrix, and adipocytes from visceral and subcutaneous abdominal adipose tissues of obese humans. Endocrinology *145*, 2273–2282.

Fang, H., and Judd, R.L. (2018). Adiponectin Regulation and Function. Compr Physiol *8*, 1031–1063.

Fatima, N., and Rana, S. (2020). Metabolic implications of circadian disruption. Pflugers Arch *472*, 513–526.

Feil, S., Valtcheva, N., and Feil, R. (2009). Inducible Cre mice. Methods Mol Biol *530*, 343–363.

Fine, N., Barzilay, O., Sun, C., Wellappuli, N., Tanwir, F., Chadwick, J.W., Oveisi, M., Tasevski, N., Prescott, D., Gargan, M., et al. (2019). Primed PMNs in healthy mouse and human circulation are first responders during acute inflammation. Blood Adv *3*, 1622–1637.

la Fleur, S.E., Kalsbeek, A., Wortel, J., and Buijs, R.M. (2000). Polysynaptic neural pathways between the hypothalamus, including the suprachiasmatic nucleus, and the liver. Brain Res *871*, 50–56.

Fonken, L.K., Frank, M.G., Kitt, M.M., Barrientos, R.M., Watkins, L.R., and Maier, S.F. (2015). Microglia inflammatory responses are controlled by an intrinsic circadian clock. Brain Behav Immun *45*, 171–179.

Fridlender, Z.G., Sun, J., Kim, S., Kapoor, V., Cheng, G., Ling, L., Worthen, G.S., and Albelda, S.M. (2009). Polarization of Tumor-Associated Neutrophil Phenotype by TGF-β: “N1” versus “N2” TAN. Cancer Cell *16*, 183–194.

Fried, S.K., Bunkin, D.A., and Greenberg, A.S. (1998). Omental and subcutaneous adipose tissues of obese subjects release interleukin-6: depot difference and regulation by glucocorticoid. J Clin Endocrinol Metab *83*, 847–850.

Garaulet, M., Gómez-Abellán, P., Alburquerque-Béjar, J.J., Lee, Y.-C., Ordovás, J.M., and Scheer, F. a. J.L. (2013). Timing of food intake predicts weight loss effectiveness. Int J Obes (Lond) *37*, 604–611.

Gau, D., Lemberger, T., von Gall, C., Kretz, O., Le Minh, N., Gass, P., Schmid, W., Schibler, U., Korf, H.W., and Schütz, G. (2002). Phosphorylation of CREB Ser142 regulates light-induced phase shifts of the circadian clock. Neuron *34*, 245–253.

Gealekman, O., Guseva, N., Hartigan, C., Apotheker, S., Gorgoglione, M., Gurav, K., Tran, K.-V., Straubhaar, J., Nicoloro, S., Czech, M.P., et al. (2011). Depot-specific differences and insufficient subcutaneous adipose tissue angiogenesis in human obesity. Circulation *123*, 186–194.

Gekakis, N., Staknis, D., Nguyen, H.B., Davis, F.C., Wilsbacher, L.D., King, D.P., Takahashi, J.S., and Weitz, C.J. (1998). Role of the CLOCK protein in the mammalian circadian mechanism. Science *280*, 1564–1569.

Gibbs, J.E., Blaikley, J., Beesley, S., Matthews, L., Simpson, K.D., Boyce, S.H., Farrow, S.N., Else, K.J., Singh, D., Ray, D.W., et al. (2012). The nuclear receptor REV-ERBα mediates circadian regulation of innate immunity through selective regulation of inflammatory cytokines. Proc Natl Acad Sci U S A *109*, 582–587.

Ginty, D.D., Kornhauser, J.M., Thompson, M.A., Bading, H., Mayo, K.E., Takahashi, J.S., and Greenberg, M.E. (1993). Regulation of CREB phosphorylation in the suprachiasmatic nucleus by light and a circadian clock. Science *260*, 238–241.

Goossens, G.H., Bizzarri, A., Venteclef, N., Essers, Y., Cleutjens, J.P., Konings, E., Jocken, J.W.E., Cajlakovic, M., Ribitsch, V., Clément, K., et al. (2011). Increased adipose tissue oxygen tension in obese compared with lean men is accompanied by insulin resistance, impaired adipose tissue capillarization, and inflammation. Circulation *124*, 67–76.

Gopalakrishnan, S., and Kannan, N.N. (2020). Only time will tell: the interplay between circadian clock and metabolism. Chronobiol Int 1–19.

Goriki, A., Hatanaka, F., Myung, J., Kim, J.K., Yoritaka, T., Tanoue, S., Abe, T., Kiyonari, H., Fujimoto, K., Kato, Y., et al. (2014). A novel protein, CHRONO, functions as a core component of the mammalian circadian clock. PLoS Biol. *12*, e1001839.

Gray, E., Thomas, T.L., Betmouni, S., Scolding, N., and Love, S. (2007). Elevated Activity and Microglial Expression of Myeloperoxidase in Demyelinated Cerebral Cortex in Multiple Sclerosis. Brain Pathol *18*, 86–95.

Gregor, M.F., and Hotamisligil, G.S. (2011). Inflammatory mechanisms in obesity. Annu Rev Immunol *29*, 415–445.

Griffin, E.A., Staknis, D., and Weitz, C.J. (1999). Light-independent role of CRY1 and CRY2 in the mammalian circadian clock. Science *286*, 768–771.

Grundy, S.M., Brewer, H.B., Cleeman, J.I., Smith, S.C., Lenfant, C., National Heart, Lung, and Blood Institute, and American Heart Association (2004). Definition of metabolic syndrome: report of the National Heart, Lung, and Blood Institute/American Heart Association conference on scientific issues related to definition. Arterioscler Thromb Vasc Biol *24*, e13-18.

Guillaumond, F., Dardente, H., Giguère, V., and Cermakian, N. (2005). Differential control of Bmal1 circadian transcription by REV-ERB and ROR nuclear receptors. J Biol Rhythms *20*, 391–403.

Güler, A.D., Ecker, J.L., Lall, G.S., Haq, S., Altimus, C.M., Liao, H.-W., Barnard, A.R., Cahill, H., Badea, T.C., Zhao, H., et al. (2008). Melanopsin cells are the principal conduits for rod-cone input to non-image-forming vision. Nature *453*, 102–105.

Gupta, S., Knight, A.G., Gupta, S., Keller, J.N., and Bruce-Keller, A.J. (2012). Saturated long-chain fatty acids activate inflammatory signaling in astrocytes. J Neurochem *120*, 1060–1071.

Halberg, N., Khan, T., Trujillo, M.E., Wernstedt-Asterholm, I., Attie, A.D., Sherwani, S., Wang, Z.V., Landskroner-Eiger, S., Dineen, S., Magalang, U.J., et al. (2009). Hypoxia-inducible factor 1alpha induces fibrosis and insulin resistance in white adipose tissue. Mol Cell Biol *29*, 4467–4483.

Hao, H., Allen, D.L., and Hardin, P.E. (1997). A circadian enhancer mediates PER-dependent mRNA cycling in Drosophila melanogaster. Mol Cell Biol *17*, 3687–3693.

Harada, Y., Sakai, M., Kurabayashi, N., Hirota, T., and Fukada, Y. (2005). Ser-557-phosphorylated mCRY2 is degraded upon synergistic phosphorylation by glycogen synthase kinase-3 beta. J Biol Chem *280*, 31714–31721.

van Harmelen, V., Dicker, A., Rydén, M., Hauner, H., Lönnqvist, F., Näslund, E., and Arner, P. (2002). Increased lipolysis and decreased leptin production by human omental as compared with subcutaneous preadipocytes. Diabetes *51*, 2029–2036.

Hasenberg, A., Hasenberg, M., Männ, L., Neumann, F., Borkenstein, L., Stecher, M., Kraus, A., Engel, D.R., Klingberg, A., Seddigh, P., et al. (2015). Catchup: a mouse model for imaging-based tracking and modulation of neutrophil granulocytes. Nat Methods *12*, 445–452.

Hatori, M., Vollmers, C., Zarrinpar, A., DiTacchio, L., Bushong, E.A., Gill, S., Leblanc, M., Chaix, A., Joens, M., Fitzpatrick, J.A.J., et al. (2012). Time-restricted feeding without reducing caloric intake prevents metabolic diseases in mice fed a high-fat diet. Cell Metab *15*, 848–860.

Hattar, S., Liao, H.W., Takao, M., Berson, D.M., and Yau, K.W. (2002). Melanopsin-containing retinal ganglion cells: architecture, projections, and intrinsic photosensitivity. Science *295*, 1065–1070.

He, W., Holtkamp, S., Hergenhan, S.M., Kraus, K., de Juan, A., Weber, J., Bradfield, P., Grenier, J.M.P., Pelletier, J., Druzd, D., et al. (2018). Circadian Expression of Migratory Factors Establishes Lineage-Specific Signatures that Guide the Homing of Leukocyte Subsets to Tissues. Immunity.

Hellmann, J., Zhang, M.J., Tang, Y., Rane, M., Bhatnagar, A., and Spite, M. (2013). Increased Saturated Fatty Acids in Obesity Alter Resolution of Inflammation in Part by Stimulating Prostaglandin Production. The Journal of Immunology *191*, 1383–1392.

Hemmeryckx, B., Himmelreich, U., Hoylaerts, M.F., and Lijnen, H.R. (2011). Impact of clock gene Bmal1 deficiency on nutritionally induced obesity in mice. Obesity (Silver Spring) *19*, 659–661.

Heyde, I., and Oster, H. (2019). Differentiating external zeitgeber impact on peripheral circadian clock resetting. Sci Rep *9*, 20114.

Hidalgo, A., Chilvers, E.R., Summers, C., and Koenderman, L. (2019). The Neutrophil Life Cycle. Trends Immunol.

Hodson, L., Humphreys, S.M., Karpe, F., and Frayn, K.N. (2013). Metabolic signatures of human adipose tissue hypoxia in obesity. Diabetes *62*, 1417–1425.

Hogenesch, J.B., Gu, Y.Z., Jain, S., and Bradfield, C.A. (1998). The basic-helix-loop-helix-PAS orphan MOP3 forms transcriptionally active complexes with circadian and hypoxia factors. Proc Natl Acad Sci U S A *95*, 5474–5479.

Holland, W.L., Bikman, B.T., Wang, L.-P., Yuguang, G., Sargent, K.M., Bulchand, S., Knotts, T.A., Shui, G., Clegg, D.J., Wenk, M.R., et al. (2011). Lipid-induced insulin resistance mediated by the proinflammatory receptor TLR4 requires saturated fatty acid-induced ceramide biosynthesis in mice. J Clin Invest *121*, 1858–1870.

Honma, S., Kawamoto, T., Takagi, Y., Fujimoto, K., Sato, F., Noshiro, M., Kato, Y., and Honma, K. (2002). Dec1 and Dec2 are regulators of the mammalian molecular clock. Nature *419*, 841–844.

van der Horst, G.T., Muijtjens, M., Kobayashi, K., Takano, R., Kanno, S., Takao, M., de Wit, J., Verkerk, A., Eker, A.P., van Leenen, D., et al. (1999). Mammalian Cry1 and Cry2 are essential for maintenance of circadian rhythms. Nature *398*, 627–630.

Hotamisligil, G.S., Shargill, N.S., and Spiegelman, B.M. (1993). Adipose expression of tumor necrosis factor-alpha: direct role in obesity-linked insulin resistance. Science *259*, 87–91.

Hotamisligil, G.S., Arner, P., Caro, J.F., Atkinson, R.L., and Spiegelman, B.M. (1995). Increased adipose tissue expression of tumor necrosis factor-alpha in human obesity and insulin resistance. J Clin Invest *95*, 2409–2415.

Hriscu, M.L. (2005). Modulatory factors of circadian phagocytic activity. Ann. N. Y. Acad. Sci. *1057*, 403–430.

Hriscu, M., Saulea, G., Ostriceanu, S., and Baciu, I. (2002). Circadian phagocytic activity in rats under light-dark and constant light regimens. Rom J Physiol *39–40*, 17–26.

Huang, H., Tohme, S., Al-Khafaji, A.B., Tai, S., Loughran, P., Chen, L., Wang, S., Kim, J., Billiar, T., Wang, Y., et al. (2015). Damage-associated molecular pattern-activated neutrophil extracellular trap exacerbates sterile inflammatory liver injury. Hepatology *62*, 600–614.

Hube, F., Lietz, U., Igel, M., Jensen, P.B., Tornqvist, H., Joost, H.G., and Hauner, H. (1996). Difference in leptin mRNA levels between omental and subcutaneous abdominal adipose tissue from obese humans. Horm Metab Res *28*, 690–693.

Hunter, A.L., Pelekanou, C.E., Barron, N.J., Northeast, R.C., Grudzien, M., Adamson, A.D., Downton, P., Cornfield, T., Cunningham, P.S., Billaud, J.-N., et al. (2021). Adipocyte NR1D1 dictates adipose tissue expansion during obesity. Elife *10*, e63324.

Husse, J., Leliavski, A., Tsang, A.H., Oster, H., and Eichele, G. (2014). The light-dark cycle controls peripheral rhythmicity in mice with a genetically ablated suprachiasmatic nucleus clock. FASEB J. *28*, 4950–4960.

Hwang, I., Jo, K., Shin, K.C., Kim, J.I., Ji, Y., Park, Y.J., Park, J., Jeon, Y.G., Ka, S., Suk, S., et al. (2019). GABA-stimulated adipose-derived stem cells suppress subcutaneous adipose inflammation in obesity. Proc. Natl. Acad. Sci. U.S.A. *116*, 11936–11945.

Jacobi, D., Liu, S., Burkewitz, K., Kory, N., Knudsen, N.H., Alexander, R.K., Unluturk, U., Li, X., Kong, X., Hyde, A.L., et al. (2015). Hepatic Bmal1 Regulates Rhythmic Mitochondrial Dynamics and Promotes Metabolic Fitness. Cell Metab *22*, 709–720.

Jeong, H.-K., Ji, K., Kim, B., Kim, J., Jou, I., and Joe, E. (2010). Inflammatory responses are not sufficient to cause delayed neuronal death in ATP-induced acute brain injury. PLoS One *5*, e13756.

Jeong, H.-K., Ji, K., Min, K., and Joe, E.-H. (2013). Brain Inflammation and Microglia: Facts and Misconceptions. Exp Neurobiol *22*, 59–67.

Jernås, M., Palming, J., Sjöholm, K., Jennische, E., Svensson, P.-A., Gabrielsson, B.G., Levin, M., Sjögren, A., Rudemo, M., Lystig, T.C., et al. (2006). Separation of human adipocytes by size: hypertrophic fat cells display distinct gene expression. FASEB J *20*, 1540–1542.

Ji, K.-A., Yang, M.-S., Jeong, H.-K., Min, K.-J., Kang, S.-H., Jou, I., and Joe, E.-H. (2007). Resident microglia die and infiltrated neutrophils and monocytes become major inflammatory cells in lipopolysaccharide-injected brain. Glia *55*, 1577–1588.

Ji, K.-A., Eu, M.Y., Kang, S.-H., Gwag, B.J., Jou, I., and Joe, E.-H. (2008). Differential neutrophil infiltration contributes to regional differences in brain inflammation in the substantia nigra pars compacta and cortex. Glia *56*, 1039–1047.

Jiao, P., Ma, J., Feng, B., Zhang, H., Diehl, J.A., Chin, Y.E., Yan, W., and Xu, H. (2011). FFA-induced adipocyte inflammation and insulin resistance: involvement of ER stress and IKKβ pathways. Obesity (Silver Spring) *19*, 483–491.

Joe, A.W.B., Yi, L., Even, Y., Vogl, A.W., and Rossi, F.M.V. (2009). Depot-specific differences in adipogenic progenitor abundance and proliferative response to high-fat diet. Stem Cells *27*, 2563–2570.

Johnson, C.H., Golden, S.S., Ishiura, M., and Kondo, T. (1996). Circadian clocks in prokaryotes. Mol Microbiol *21*, 5–11.

Jorch, S.K., and Kubes, P. (2017). An emerging role for neutrophil extracellular traps in noninfectious disease. Nature Medicine *23*, 279–287.

Kabon, B., Nagele, A., Reddy, D., Eagon, C., Fleshman, J.W., Sessler, D.I., and Kurz, A. (2004). Obesity decreases perioperative tissue oxygenation. Anesthesiology *100*, 274–280.

Kalsbeek, A., Garidou, M.L., Palm, I.F., Van Der Vliet, J., Simonneaux, V., Pévet, P., and Buijs, R.M. (2000). Melatonin sees the light: blocking GABA-ergic transmission in the paraventricular nucleus induces daytime secretion of melatonin. Eur J Neurosci *12*, 3146–3154.

Kalsbeek, A., Palm, I.F., La Fleur, S.E., Scheer, F. a. J.L., Perreau-Lenz, S., Ruiter, M., Kreier, F., Cailotto, C., and Buijs, R.M. (2006). SCN outputs and the hypothalamic balance of life. J Biol Rhythms *21*, 458–469.

Kawamoto, T., Noshiro, M., Sato, F., Maemura, K., Takeda, N., Nagai, R., Iwata, T., Fujimoto, K., Furukawa, M., Miyazaki, K., et al. (2004). A novel autofeedback loop of Dec1 transcription involved in circadian rhythm regulation. Biochem Biophys Res Commun *313*, 117–124.

Kecklund, G., and Axelsson, J. (2016). Health consequences of shift work and insufficient sleep. BMJ *355*, i5210.

Keesler, G.A., Camacho, F., Guo, Y., Virshup, D., Mondadori, C., and Yao, Z. (2000). Phosphorylation and destabilization of human period I clock protein by human casein kinase I epsilon. Neuroreport *11*, 951–955.

Keller, M., Mazuch, J., Abraham, U., Eom, G.D., Herzog, E.D., Volk, H.-D., Kramer, A., and Maier, B. (2009). A circadian clock in macrophages controls inflammatory immune responses. PNAS *106*, 21407–21412.

Kennaway, D.J., Varcoe, T.J., Voultsios, A., and Boden, M.J. (2013). Global loss of bmal1 expression alters adipose tissue hormones, gene expression and glucose metabolism. PLoS One *8*, e65255.

Kern, P.A., Ranganathan, S., Li, C., Wood, L., and Ranganathan, G. (2001). Adipose tissue tumor necrosis factor and interleukin-6 expression in human obesity and insulin resistance. Am J Physiol Endocrinol Metab *280*, E745-751.

Kernie, S.G., Liebl, D.J., and Parada, L.F. (2000). BDNF regulates eating behavior and locomotor activity in mice. EMBO J *19*, 1290–1300.

Kim, D., Lee, J.E., Jung, Y.J., Lee, A.S., Lee, S., Park, S.K., Kim, S.H., Park, B.-H., Kim, W., and Kang, K.P. (2013). Metformin decreases high-fat diet-induced renal injury by regulating the expression of adipokines and the renal AMP-activated protein kinase/acetyl-CoA carboxylase pathway in mice. Int J Mol Med *32*, 1293–1302.

Kim, H., Kim, M., Im, S.-K., and Fang, S. (2018). Mouse Cre-LoxP system: general principles to determine tissue-specific roles of target genes. Lab Anim Res *34*, 147–159.

Kim, M.-H., Yang, D., Kim, M., Kim, S.-Y., Kim, D., and Kang, S.-J. (2017). A late-lineage murine neutrophil precursor population exhibits dynamic changes during demand-adapted granulopoiesis. Sci Rep *7*, 39804.

Kim, M.-K., Huang, Z.-Y., Hwang, P.-H., Jones, B.A., Sato, N., Hunter, S., Kim-Han, T.-H., Worth, R.G., Indik, Z.K., and Schreiber, A.D. (2003). Fcgamma receptor transmembrane domains: role in cell surface expression, gamma chain interaction, and phagocytosis. Blood *101*, 4479–4484.

Kim, S.-W., Lee, H., Lee, H.-K., Kim, I.-D., and Lee, J.-K. (2019). Neutrophil extracellular trap induced by HMGB1 exacerbates damages in the ischemic brain. Acta Neuropathol Commun *7*, 11.

Kitchen, G.B., Cunningham, P.S., Poolman, T.M., Iqbal, M., Maidstone, R., Baxter, M., Bagnall, J., Begley, N., Saer, B., Hussell, T., et al. (2020). The clock gene Bmal1 inhibits macrophage motility, phagocytosis, and impairs defense against pneumonia. Proc Natl Acad Sci U S A *117*, 1543–1551.

Kleinridders, A., Schenten, D., Könner, A.C., Belgardt, B.F., Mauer, J., Okamura, T., Wunderlich, F.T., Medzhitov, R., and Brüning, J.C. (2009). MyD88 signaling in the CNS is required for development of fatty acid-induced leptin resistance and diet-induced obesity. Cell Metab *10*, 249–259.

Kohsaka, A., Laposky, A.D., Ramsey, K.M., Estrada, C., Joshu, C., Kobayashi, Y., Turek, F.W., and Bass, J. (2007). High-fat diet disrupts behavioral and molecular circadian rhythms in mice. Cell Metab *6*, 414–421.

Kreier, F., Fliers, E., Voshol, P.J., Van Eden, C.G., Havekes, L.M., Kalsbeek, A., Van Heijningen, C.L., Sluiter, A.A., Mettenleiter, T.C., Romijn, J.A., et al. (2002). Selective parasympathetic innervation of subcutaneous and intra-abdominal fat--functional implications. J Clin Invest *110*, 1243–1250.

Kubota, N., Yano, W., Kubota, T., Yamauchi, T., Itoh, S., Kumagai, H., Kozono, H., Takamoto, I., Okamoto, S., Shiuchi, T., et al. (2007). Adiponectin stimulates AMP-activated protein kinase in the hypothalamus and increases food intake. Cell Metab *6*, 55–68.

Kuck, J., Pantke, M., and Flick, U. (2014). Effects of social activation and physical mobilization on sleep in nursing home residents. Geriatr Nurs *35*, 455–461.

Kume, K., Zylka, M.J., Sriram, S., Shearman, L.P., Weaver, D.R., Jin, X., Maywood, E.S., Hastings, M.H., and Reppert, S.M. (1999). mCRY1 and mCRY2 are essential components of the negative limb of the circadian clock feedback loop. Cell *98*, 193–205.

La Cava, A. (2017). Leptin in inflammation and autoimmunity. Cytokine *98*, 51–58.

Lahoz-Beneytez, J., Elemans, M., Zhang, Y., Ahmed, R., Salam, A., Block, M., Niederalt, C., Asquith, B., and Macallan, D. (2016). Human neutrophil kinetics: modeling of stable isotope labeling data supports short blood neutrophil half-lives. Blood *127*, 3431–3438.

Lamia, K.A., Storch, K.-F., and Weitz, C.J. (2008). Physiological significance of a peripheral tissue circadian clock. Proc Natl Acad Sci U S A *105*, 15172–15177.

Lamia, K.A., Sachdeva, U.M., DiTacchio, L., Williams, E.C., Alvarez, J.G., Egan, D.F., Vasquez, D.S., Juguilon, H., Panda, S., Shaw, R.J., et al. (2009). AMPK regulates the circadian clock by cryptochrome phosphorylation and degradation. Science *326*, 437–440.

Landgraf, D., Wang, L.L., Diemer, T., and Welsh, D.K. (2016). NPAS2 Compensates for Loss of CLOCK in Peripheral Circadian Oscillators. PLoS Genet. *12*, e1005882.

Laule, C.F., Odean, E.J., Wing, C.R., Root, K.M., Towner, K.J., Hamm, C.M., Gilbert, J.S., Fleming, S.D., and Regal, J.F. (2019). Role of B1 and B2 lymphocytes in placental ischemia-induced hypertension. Am J Physiol Heart Circ Physiol *317*, H732–H742.

Lawler, H.M., Underkofler, C.M., Kern, P.A., Erickson, C., Bredbeck, B., and Rasouli, N. (2016). Adipose Tissue Hypoxia, Inflammation, and Fibrosis in Obese Insulin-Sensitive and Obese Insulin-Resistant Subjects. J Clin Endocrinol Metab *101*, 1422–1428.

Lawrence, V.J., and Kopelman, P.G. (2004). Medical consequences of obesity. Clin Dermatol *22*, 296–302.

Le Minh, N., Damiola, F., Tronche, F., Schütz, G., and Schibler, U. (2001). Glucocorticoid hormones inhibit food-induced phase-shifting of peripheral circadian oscillators. EMBO J. *20*, 7128–7136.

Lee, B.-C., and Lee, J. (2014). Cellular and molecular players in adipose tissue inflammation in the development of obesity-induced insulin resistance. Biochim Biophys Acta *1842*, 446–462.

Lee, Y.S., and Olefsky, J. (2021). Chronic tissue inflammation and metabolic disease. Genes Dev *35*, 307–328.

Lee, B.-C., Kim, M.-S., Pae, M., Yamamoto, Y., Eberlé, D., Shimada, T., Kamei, N., Park, H.-S., Sasorith, S., Woo, J.R., et al. (2016). Adipose Natural Killer Cells Regulate Adipose Tissue Macrophages to Promote Insulin Resistance in Obesity. Cell Metab *23*, 685–698.

Lee, Y.S., Kim, J.-W., Osborne, O., Oh, D.Y., Sasik, R., Schenk, S., Chen, A., Chung, H., Murphy, A., Watkins, S.M., et al. (2014). Increased adipocyte O2 consumption triggers HIF-1α, causing inflammation and insulin resistance in obesity. Cell *157*, 1339–1352.

Ley, K., Laudanna, C., Cybulsky, M.I., and Nourshargh, S. (2007). Getting to the site of inflammation: the leukocyte adhesion cascade updated. Nat. Rev. Immunol. *7*, 678–689.

Li, B., Matter, E., Hoppert, H., Seeley, R., and Sandoval, D. (2014). Identification of optimal reference genes for RT-qPCR in the rat hypothalamus and intestine for the study of obesity. Int J Obes (Lond) *38*, 192–197.

Li, C., Menoret, A., Farragher, C., Ouyang, Z., Bonin, C., Holvoet, P., Vella, A.T., and Zhou, B. (2019). Single cell transcriptomics based-MacSpectrum reveals novel macrophage activation signatures in diseases. JCI Insight *5*, 126453.

Li, P., Oh, D.Y., Bandyopadhyay, G., Lagakos, W.S., Talukdar, S., Osborn, O., Johnson, A., Chung, H., Maris, M., Ofrecio, J.M., et al. (2015). LTB4 promotes insulin resistance in obese mice by acting on macrophages, hepatocytes and myocytes. Nat Med *21*, 239–247.

Li, S., Zhang, H.-Y., Hu, C.C., Lawrence, F., Gallagher, K.E., Surapaneni, A., Estrem, S.T., Calley, J.N., Varga, G., Dow, E.R., et al. (2008). Assessment of diet-induced obese rats as an obesity model by comparative functional genomics. Obesity (Silver Spring) *16*, 811–818.

Liew, P.X., and Kubes, P. (2019). The Neutrophil's Role During Health and Disease. Physiol Rev *99*, 1223–1248.

Lin, D., Chun, T.-H., and Kang, L. (2016). Adipose extracellular matrix remodelling in obesity and insulin resistance. Biochem Pharmacol *119*, 8–16.

Lin, J., Tang, W., Liu, W., Yu, F., Wu, Y., Fang, X., Zhou, M., Hao, W., and Hu, W. (2020). Decreased B1 and B2 Lymphocytes Are Associated With Mortality in Elderly Patients With Chronic Kidney Diseases. Front Med (Lausanne) *7*, 75.

Linhares-Lacerda, L., Temerozo, J.R., Ribeiro-Alves, M., Azevedo, E.P., Mojoli, A., Nascimento, M.T.C., Silva-Oliveira, G., Savino, W., Foguel, D., Bou-Habib, D.C., et al. (2020). Neutrophil extracellular trap-enriched supernatants carry microRNAs able to modulate TNF-α production by macrophages. Sci Rep *10*, 2715.

Liu, A.C., Tran, H.G., Zhang, E.E., Priest, A.A., Welsh, D.K., and Kay, S.A. (2008). Redundant function of REV-ERBalpha and beta and non-essential role for Bmal1 cycling in transcriptional regulation of intracellular circadian rhythms. PLoS Genet *4*, e1000023.

Liu, Y., Cao, Z.-T., Xu, C.-F., Lu, Z.-D., Luo, Y.-L., and Wang, J. (2018). Optimization of lipid-assisted nanoparticle for disturbing neutrophils-related inflammation. Biomaterials *172*, 92–104.

Livak, K.J., and Schmittgen, T.D. (2001). Analysis of relative gene expression data using real-time quantitative PCR and the 2(-Delta Delta C(T)) Method. Methods *25*, 402–408.

Lopez-Molina, L., Conquet, F., Dubois-Dauphin, M., and Schibler, U. (1997). The DBP gene is expressed according to a circadian rhythm in the suprachiasmatic nucleus and influences circadian behavior. EMBO J *16*, 6762–6771.

Løvås, K., Knudsen, E., Iversen, P.O., and Benestad, H.B. (1996). Sequestration patterns of transfused rat neutrophilic granulocytes under normal and inflammatory conditions. Eur J Haematol *56*, 221–229.

Lowden, A., Moreno, C., Holmbäck, U., Lennernäs, M., and Tucker, P. (2010). Eating and shift work - effects on habits, metabolism and performance. Scand J Work Environ Health *36*, 150–162.

Lui, J.C., Garrison, P., and Baron, J. (2015). Regulation of Body Growth. Curr Opin Pediatr *27*, 502–510.

Lumeng, C.N., Bodzin, J.L., and Saltiel, A.R. (2007a). Obesity induces a phenotypic switch in adipose tissue macrophage polarization. J Clin Invest *117*, 175–184.

Lumeng, C.N., Deyoung, S.M., Bodzin, J.L., and Saltiel, A.R. (2007b). Increased inflammatory properties of adipose tissue macrophages recruited during diet-induced obesity. Diabetes *56*, 16–23.

Machnicki, A.L., White, C.A., Meadows, C.A., McCloud, D., Evans, S., Thomas, D., Hurley, J.D., Crow, D., Chirchir, H., and Serrat, M.A. (2022). Altered IGF-I activity and accelerated bone elongation in growth plates precedes excess weight gain in a mouse model of juvenile obesity. J Appl Physiol (1985).

Manella, G., Sabath, E., Aviram, R., Dandavate, V., Ezagouri, S., Golik, M., Adamovich, Y., and Asher, G. (2021). The liver-clock coordinates rhythmicity of peripheral tissues in response to feeding. Nat Metab.

Marcheva, B., Ramsey, K.M., Peek, C.B., Affinati, A., Maury, E., and Bass, J. (2013). Circadian clocks and metabolism. Handb Exp Pharmacol 127–155.

Martin, C., Burdon, P.C.E., Bridger, G., Gutierrez-Ramos, J.C., Williams, T.J., and Rankin, S.M. (2003). Chemokines acting via CXCR2 and CXCR4 control the release of neutrophils from the bone marrow and their return following senescence. Immunity *19*, 583–593.

Marwick, J.A., Mills, R., Kay, O., Michail, K., Stephen, J., Rossi, A.G., Dransfield, I., and Hirani, N. (2018). Neutrophils induce macrophage anti-inflammatory reprogramming by suppressing NF-κB activation. Cell Death Dis *9*, 665.

Mason, I.C., Qian, J., Adler, G.K., and Scheer, F.A.J.L. (2020). Impact of circadian disruption on glucose metabolism: implications for type 2 diabetes. Diabetologia *63*, 462–472.

McDonald, B., Pittman, K., Menezes, G.B., Hirota, S.A., Slaba, I., Waterhouse, C.C.M., Beck, P.L., Muruve, D.A., and Kubes, P. (2010). Intravascular danger signals guide neutrophils to sites of sterile inflammation. Science *330*, 362–366.

McHill, A.W., and Wright, K.P. (2017). Role of sleep and circadian disruption on energy expenditure and in metabolic predisposition to human obesity and metabolic disease. Obes Rev *18 Suppl 1*, 15–24.

Melchart, D., Martin, P., Hallek, M., Holzmann, M., Jurcic, X., and Wagner, H. (1992). Circadian variation of the phagocytic activity of polymorphonuclear leukocytes and of various other parameters in 13 healthy male adults. Chronobiol. Int. *9*, 35–45.

de Mello, A.H., Costa, A.B., Engel, J.D.G., and Rezin, G.T. (2018). Mitochondrial dysfunction in obesity. Life Sci *192*, 26–32.

Mendoza, J., Pévet, P., and Challet, E. (2008). High-fat feeding alters the clock synchronization to light. J Physiol *586*, 5901–5910.

Meng, Q.-J., Logunova, L., Maywood, E.S., Gallego, M., Lebiecki, J., Brown, T.M., Sládek, M., Semikhodskii, A.S., Glossop, N.R.J., Piggins, H.D., et al. (2008). Setting clock speed in mammals: the CK1 epsilon tau mutation in mice accelerates circadian pacemakers by selectively destabilizing PERIOD proteins. Neuron *58*, 78–88.

Meyer, C.W., Willershäuser, M., Jastroch, M., Rourke, B.C., Fromme, T., Oelkrug, R., Heldmaier, G., and Klingenspor, M. (2010). Adaptive thermogenesis and thermal conductance in wild-type and UCP1-KO mice. Am J Physiol Regul Integr Comp Physiol *299*, R1396-1406.

MGI – Mouse Gene Expression Database, 2021: http://www.informatics.jax.org/gxd#gxd=nomenclature%3DMrp8%26vocabTerm%3D%26annotationId%3D%26locations%3D%26locationUnit%3Dbp%26structure%3D%26structureID%3D%26theilerStage%3D0%26assayType%3DImmunohistochemistry%26assayType%3DIn%20situ%20reporter%20%28knock%20in%29%26assayType%3DRNA%20in%20situ%26assayType%3DNorthern%20blot%26assayType%3DNuclease%20S1%26assayType%3DRNase%20protection%26assayType%3DRT-PCR%26assayType%3DWestern%20blot%26results%3D100%26startIndex%3D0%26sort%3D%26dir%3Dasc%26tab%3Dresultstab, accessed December 16, 2021

Milanski, M., Degasperi, G., Coope, A., Morari, J., Denis, R., Cintra, D.E., Tsukumo, D.M.L., Anhe, G., Amaral, M.E., Takahashi, H.K., et al. (2009). Saturated fatty acids produce an inflammatory response predominantly through the activation of TLR4 signaling in hypothalamus: implications for the pathogenesis of obesity. J Neurosci *29*, 359–370.

Mills, C.D., Kincaid, K., Alt, J.M., Heilman, M.J., and Hill, A.M. (2000). M-1/M-2 macrophages and the Th1/Th2 paradigm. J Immunol *164*, 6166–6173.

Mitsui, S., Yamaguchi, S., Matsuo, T., Ishida, Y., and Okamura, H. (2001). Antagonistic role of E4BP4 and PAR proteins in the circadian oscillatory mechanism. Genes Dev *15*, 995–1006.

Molofsky, A.B., Nussbaum, J.C., Liang, H.-E., Van Dyken, S.J., Cheng, L.E., Mohapatra, A., Chawla, A., and Locksley, R.M. (2013). Innate lymphoid type 2 cells sustain visceral adipose tissue eosinophils and alternatively activated macrophages. J Exp Med *210*, 535–549.

Moore, R.Y., and Eichler, V.B. (1972). Loss of a circadian adrenal corticosterone rhythm following suprachiasmatic lesions in the rat. Brain Res. *42*, 201–206.

Moore, R.Y., and Lenn, N.J. (1972). A retinohypothalamic projection in the rat. Journal of Comparative Neurology *146*, 1–14.

Moraes, J.C., Coope, A., Morari, J., Cintra, D.E., Roman, E.A., Pauli, J.R., Romanatto, T., Carvalheira, J.B., Oliveira, A.L.R., Saad, M.J., et al. (2009). High-fat diet induces apoptosis of hypothalamic neurons. PLoS One *4*, e5045.

Mueller, H., Stadtmann, A., Van Aken, H., Hirsch, E., Wang, D., Ley, K., and Zarbock, A. (2010). Tyrosine kinase Btk regulates E-selectin-mediated integrin activation and neutrophil recruitment by controlling phospholipase C (PLC) gamma2 and PI3Kgamma pathways. Blood *115*, 3118–3127.

Murano, I., Barbatelli, G., Parisani, V., Latini, C., Muzzonigro, G., Castellucci, M., and Cinti, S. (2008). Dead adipocytes, detected as crown-like structures, are prevalent in visceral fat depots of genetically obese mice. J Lipid Res *49*, 1562–1568.

Nakashima, A., Kawamoto, T., Honda, K.K., Ueshima, T., Noshiro, M., Iwata, T., Fujimoto, K., Kubo, H., Honma, S., Yorioka, N., et al. (2008). DEC1 modulates the circadian phase of clock gene expression. Mol Cell Biol *28*, 4080–4092.

Nakatani, Y., Kaneto, H., Kawamori, D., Hatazaki, M., Miyatsuka, T., Matsuoka, T.-A., Kajimoto, Y., Matsuhisa, M., Yamasaki, Y., and Hori, M. (2004). Modulation of the JNK pathway in liver affects insulin resistance status. J Biol Chem *279*, 45803–45809.

Nea, F.M., Kearney, J., Livingstone, M.B.E., Pourshahidi, L.K., and Corish, C.A. (2015). Dietary and lifestyle habits and the associated health risks in shift workers. Nutr Res Rev *28*, 143–166.

Ng, L.G., Ostuni, R., and Hidalgo, A. (2019). Heterogeneity of neutrophils. Nat. Rev. Immunol. *19*, 255–265.

Nguyen, K.D., Fentress, S.J., Qiu, Y., Yun, K., Cox, J.S., and Chawla, A. (2013). Circadian Gene Bmal1 Regulates Diurnal Oscillations of Ly6Chi Inflammatory Monocytes. Science *341*, 1483–1488.

Nishimura, S., Manabe, I., Nagasaki, M., Eto, K., Yamashita, H., Ohsugi, M., Otsu, M., Hara, K., Ueki, K., Sugiura, S., et al. (2009). CD8+ effector T cells contribute to macrophage recruitment and adipose tissue inflammation in obesity. Nat Med *15*, 914–920.

Nussbaum, J.C., Van Dyken, S.J., von Moltke, J., Cheng, L.E., Mohapatra, A., Molofsky, A.B., Thornton, E.E., Krummel, M.F., Chawla, A., Liang, H.-E., et al. (2013). Type 2 innate lymphoid cells control eosinophil homeostasis. Nature *502*, 245–248.

Oh, D.Y., Morinaga, H., Talukdar, S., Bae, E.J., and Olefsky, J.M. (2012). Increased macrophage migration into adipose tissue in obese mice. Diabetes *61*, 346–354.

Orr, J.S., Puglisi, M.J., Ellacott, K.L.J., Lumeng, C.N., Wasserman, D.H., and Hasty, A.H. (2012). Toll-like receptor 4 deficiency promotes the alternative activation of adipose tissue macrophages. Diabetes *61*, 2718–2727.

Orr, Y., Wilson, D.P., Taylor, J.M., Bannon, P.G., Geczy, C., Davenport, M.P., and Kritharides, L. (2007). A kinetic model of bone marrow neutrophil production that characterizes late phenotypic maturation. Am J Physiol Regul Integr Comp Physiol *292*, R1707-1716.

O'Sullivan, T.E., Rapp, M., Fan, X., Weizman, O.-E., Bhardwaj, P., Adams, N.M., Walzer, T., Dannenberg, A.J., and Sun, J.C. (2016). Adipose-Resident Group 1 Innate Lymphoid Cells Promote Obesity-Associated Insulin Resistance. Immunity *45*, 428–441.

Oved, J.H., Paris, A.J., Gollomp, K., Dai, N., Rubey, K., Wang, P., Spruce, L.A., Seeholzer, S.H., Poncz, M., and Worthen, G.S. (2021). Neutrophils promote clearance of nuclear debris following acid-induced lung injury. Blood *137*, 392–397.

Påhlman, L.I., Mörgelin, M., Eckert, J., Johansson, L., Russell, W., Riesbeck, K., Soehnlein, O., Lindbom, L., Norrby-Teglund, A., Schumann, R.R., et al. (2006). Streptococcal M protein: a multipotent and powerful inducer of inflammation. J Immunol *177*, 1221–1228.

Palmisano, B.T., Stafford, J.M., and Pendergast, J.S. (2017). High-Fat Feeding Does Not Disrupt Daily Rhythms in Female Mice because of Protection by Ovarian Hormones. Front Endocrinol (Lausanne) *8*, 44.

Panda, S., Sato, T.K., Castrucci, A.M., Rollag, M.D., DeGrip, W.J., Hogenesch, J.B., Provencio, I., and Kay, S.A. (2002). Melanopsin (Opn4) requirement for normal light-induced circadian phase shifting. Science *298*, 2213–2216.

Papayannopoulos, V. (2018). Neutrophil extracellular traps in immunity and disease. Nat Rev Immunol *18*, 134–147.

Parsons, R., Parsons, R., Garner, N., Oster, H., and Rawashdeh, O. (2020). CircaCompare: a method to estimate and statistically support differences in mesor, amplitude and phase, between circadian rhythms. Bioinformatics *36*, 1208–1212.

Pasarica, M., Sereda, O.R., Redman, L.M., Albarado, D.C., Hymel, D.T., Roan, L.E., Rood, J.C., Burk, D.H., and Smith, S.R. (2009). Reduced adipose tissue oxygenation in human obesity: evidence for rarefaction, macrophage chemotaxis, and inflammation without an angiogenic response. Diabetes *58*, 718–725.

Paschos, G.K., Ibrahim, S., Song, W.-L., Kunieda, T., Grant, G., Reyes, T.M., Bradfield, C.A., Vaughan, C.H., Eiden, M., Masoodi, M., et al. (2012). Obesity in mice with adipocyte-specific deletion of clock component Arntl. Nat Med *18*, 1768–1777.

Passegué, E., Wagner, E.F., and Weissman, I.L. (2004). JunB deficiency leads to a myeloproliferative disorder arising from hematopoietic stem cells. Cell *119*, 431–443.

Patel, H., Kerndt, C.C., and Bhardwaj, A. (2021). Physiology, Respiratory Quotient. In StatPearls, (Treasure Island (FL): StatPearls Publishing)

Patke, A., Young, M.W., and Axelrod, S. (2020). Molecular mechanisms and physiological importance of circadian rhythms. Nat Rev Mol Cell Biol *21*, 67–84.

Pendergast, J.S., Branecky, K.L., Yang, W., Ellacott, K.L.J., Niswender, K.D., and Yamazaki, S. (2013). High-fat diet acutely affects circadian organisation and eating behavior. Eur J Neurosci *37*, 1350–1356.

Perreau-Lenz, S., Kalsbeek, A., Garidou, M.-L., Wortel, J., van der Vliet, J., van Heijningen, C., Simonneaux, V., Pévet, P., and Buijs, R.M. (2003). Suprachiasmatic control of melatonin synthesis in rats: inhibitory and stimulatory mechanisms. Eur J Neurosci *17*, 221–228.

Pflieger, F.J., Hernandez, J., Schweighöfer, H., Herden, C., Rosengarten, B., and Rummel, C. (2018a). The role of neutrophil granulocytes in immune-to-brain communication. Temperature (Austin) *5*, 296–307.

Pflieger, F.J., Hernandez, J., Schweighöfer, H., Herden, C., Rosengarten, B., and Rummel, C. (2018b). The role of neutrophil granulocytes in immune-to-brain communication. Temperature (Austin) *5*, 296–307.

Phillipson, M., Heit, B., Colarusso, P., Liu, L., Ballantyne, C.M., and Kubes, P. (2006). Intraluminal crawling of neutrophils to emigration sites: a molecularly distinct process from adhesion in the recruitment cascade. J Exp Med *203*, 2569–2575.

Phosat, C., Panprathip, P., Chumpathat, N., Prangthip, P., Chantratita, N., Soonthornworasiri, N., Puduang, S., and Kwanbunjan, K. (2017). Elevated C-reactive protein, interleukin 6, tumor necrosis factor alpha and glycemic load associated with type 2 diabetes mellitus in rural Thais: a cross-sectional study. BMC Endocr Disord *17*, 44.

Pillay, J., den Braber, I., Vrisekoop, N., Kwast, L.M., de Boer, R.J., Borghans, J.A.M., Tesselaar, K., and Koenderman, L. (2010). In vivo labeling with 2H2O reveals a human neutrophil lifespan of 5.4 days. Blood *116*, 625–627.

Poon, K., Barson, J.R., Ho, H.T., and Leibowitz, S.F. (2016). Relationship of the Chemokine, CXCL12, to Effects of Dietary Fat on Feeding-Related Behaviors and Hypothalamic Neuropeptide Systems. Frontiers in Behavioral Neuroscience *10*, 51.

Posey, K.A., Clegg, D.J., Printz, R.L., Byun, J., Morton, G.J., Vivekanandan-Giri, A., Pennathur, S., Baskin, D.G., Heinecke, J.W., Woods, S.C., et al. (2009). Hypothalamic proinflammatory lipid accumulation, inflammation, and insulin resistance in rats fed a high-fat diet. Am J Physiol Endocrinol Metab *296*, E1003-1012.

Preitner, N., Damiola, F., Lopez-Molina, L., Zakany, J., Duboule, D., Albrecht, U., and Schibler, U. (2002). The orphan nuclear receptor REV-ERBalpha controls circadian transcription within the positive limb of the mammalian circadian oscillator. Cell *110*, 251–260.

Puellmann, K., Kaminski, W.E., Vogel, M., Nebe, C.T., Schroeder, J., Wolf, H., and Beham, A.W. (2006). A variable immunoreceptor in a subpopulation of human neutrophils. Proc Natl Acad Sci U S A *103*, 14441–14446.

Rada, B. (2019). Neutrophil Extracellular Traps. Methods Mol. Biol. *1982*, 517–528.

Rakshit, K., Hsu, T.W., and Matveyenko, A.V. (2016). Bmal1 is required for beta cell compensatory expansion, survival and metabolic adaptation to diet-induced obesity in mice. Diabetologia *59*, 734–743.

Ralph, M.R., and Menaker, M. (1988). A mutation of the circadian system in golden hamsters. Science *241*, 1225–1227.

Ralph, M.R., Foster, R.G., Davis, F.C., and Menaker, M. (1990). Transplanted suprachiasmatic nucleus determines circadian period. Science *247*, 975–978.

Ramkhelawon, B., Hennessy, E.J., Ménager, M., Ray, T.D., Sheedy, F.J., Hutchison, S., Wanschel, A., Oldebeken, S., Geoffrion, M., Spiro, W., et al. (2014). Netrin-1 promotes adipose tissue macrophage retention and insulin resistance in obesity. Nat Med *20*, 377–384.

Rasmussen, M.S., Lihn, A.S., Pedersen, S.B., Bruun, J.M., Rasmussen, M., and Richelsen, B. (2006). Adiponectin receptors in human adipose tissue: effects of obesity, weight loss, and fat depots. Obesity (Silver Spring) *14*, 28–35.

Ringling, R.E., Gastecki, M.L., Woodford, M.L., Lum-Naihe, K.J., Grant, R.W., Pulakat, L., Vieira-Potter, V.J., and Padilla, J. (2016). Loss of Nlrp3 Does Not Protect Mice from Western Diet-Induced Adipose Tissue Inflammation and Glucose Intolerance. PLoS One *11*, e0161939.

Roseboom, P.H., Namboodiri, M.A., Zimonjic, D.B., Popescu, N.C., Rodriguez, I.R., Gastel, J.A., and Klein, D.C. (1998). Natural melatonin "knockdown" in C57BL/6J mice: rare mechanism truncates serotonin N-acetyltransferase. Brain Res Mol Brain Res *63*, 189–197.

Rouault, C., Pellegrinelli, V., Schilch, R., Cotillard, A., Poitou, C., Tordjman, J., Sell, H., Clément, K., and Lacasa, D. (2013). Roles of chemokine ligand-2 (CXCL2) and neutrophils in influencing endothelial cell function and inflammation of human adipose tissue. Endocrinology *154*, 1069–1079.

Saberi, M., Woods, N.-B., de Luca, C., Schenk, S., Lu, J.C., Bandyopadhyay, G., Verma, I.M., and Olefsky, J.M. (2009). Hematopoietic cell-specific deletion of toll-like receptor 4 ameliorates hepatic and adipose tissue insulin resistance in high-fat-fed mice. Cell Metab *10*, 419–429.

Saini, C., Morf, J., Stratmann, M., Gos, P., and Schibler, U. (2012). Simulated body temperature rhythms reveal the phase-shifting behavior and plasticity of mammalian circadian oscillators. Genes Dev *26*, 567–580.

Salgado-Delgado, R., Angeles-Castellanos, M., Saderi, N., Buijs, R.M., and Escobar, C. (2010). Food intake during the normal activity phase prevents obesity and circadian desynchrony in a rat model of night work. Endocrinology *151*, 1019–1029.

Sasaki, T., Moro, K., Kubota, T., Kubota, N., Kato, T., Ohno, H., Nakae, S., Saito, H., and Koyasu, S. (2019). Innate Lymphoid Cells in the Induction of Obesity. Cell Rep *28*, 202-217.e7.

Sato, T.K., Panda, S., Miraglia, L.J., Reyes, T.M., Rudic, R.D., McNamara, P., Naik, K.A., FitzGerald, G.A., Kay, S.A., and Hogenesch, J.B. (2004). A functional genomics strategy reveals Rora as a component of the mammalian circadian clock. Neuron *43*, 527–537.

Sato, T.K., Yamada, R.G., Ukai, H., Baggs, J.E., Miraglia, L.J., Kobayashi, T.J., Welsh, D.K., Kay, S.A., Ueda, H.R., and Hogenesch, J.B. (2006). Feedback repression is required for mammalian circadian clock function. Nat. Genet. *38*, 312–319.

Satoh, Y., Kawai, H., Kudo, N., Kawashima, Y., and Mitsumoto, A. (2006). Time-restricted feeding entrains daily rhythms of energy metabolism in mice. Am J Physiol Regul Integr Comp Physiol *290*, R1276-1283.

Scheiermann, C., Gibbs, J., Ince, L., and Loudon, A. (2018). Clocking in to immunity. Nat. Rev. Immunol.

Schultz, J., Corlin, R., Oddi, F., Kaminker, K., and Jones, W. (1965). Myeloperoxidase of the leucocyte of normal human blood. 3. Isolation of the peroxidase granule. Arch Biochem Biophys *111*, 73–79.

Schwartz, W.J., and Zimmerman, P. (1990). Circadian timekeeping in BALB/c and C57BL/6 inbred mouse strains. J Neurosci *10*, 3685–3694.

Schweighöfer, H., Rummel, C., Roth, J., and Rosengarten, B. (2016). Modulatory effects of vagal stimulation on neurophysiological parameters and the cellular immune response in the rat brain during systemic inflammation. Intensive Care Med Exp *4*, 19.

Segal, A.W. (2005). How neutrophils kill microbes. Annu. Rev. Immunol. *23*, 197–223.

Sengeløv, H., Kjeldsen, L., and Borregaard, N. (1993). Control of exocytosis in early neutrophil activation. J Immunol *150*, 1535–1543.

Seo, J.B., Riopel, M., Cabrales, P., Huh, J.Y., Bandyopadhyay, G.K., Andreyev, A.Y., Murphy, A.N., Beeman, S.C., Smith, G.I., Klein, S., et al. (2019). Knockdown of Ant2 Reduces Adipocyte Hypoxia And Improves Insulin Resistance in Obesity. Nat Metab *1*, 86–97.

Shi, H., Kokoeva, M.V., Inouye, K., Tzameli, I., Yin, H., and Flier, J.S. (2006). TLR4 links innate immunity and fatty acid-induced insulin resistance. J Clin Invest *116*, 3015–3025.

Shigeyoshi, Y., Taguchi, K., Yamamoto, S., Takekida, S., Yan, L., Tei, H., Moriya, T., Shibata, S., Loros, J.J., Dunlap, J.C., et al. (1997). Light-induced resetting of a mammalian circadian clock is associated with rapid induction of the mPer1 transcript. Cell *91*, 1043–1053.

Shimba, S., Ogawa, T., Hitosugi, S., Ichihashi, Y., Nakadaira, Y., Kobayashi, M., Tezuka, M., Kosuge, Y., Ishige, K., Ito, Y., et al. (2011). Deficient of a clock gene, brain and muscle Arnt-like protein-1 (BMAL1), induces dyslipidemia and ectopic fat formation. PLoS One *6*, e25231.

Shin, D., and Lee, K.-W. (2021). CLOCK Gene Variation Is Associated with the Incidence of Metabolic Syndrome Modulated by Monounsaturated Fatty Acids. J Pers Med *11*.

Shoelson, S.E., Lee, J., and Yuan, M. (2003). Inflammation and the IKK beta/I kappa B/NF-kappa B axis in obesity- and diet-induced insulin resistance. Int J Obes Relat Metab Disord *27 Suppl 3*, S49-52.

Silver, A.C., Arjona, A., Hughes, M.E., Nitabach, M.N., and Fikrig, E. (2012). Circadian expression of clock genes in mouse macrophages, dendritic cells, and B cells. Brain Behav Immun *26*, 407–413.

Simon, S.I., Hu, Y., Vestweber, D., and Smith, C.W. (2000). Neutrophil tethering on E-selectin activates beta 2 integrin binding to ICAM-1 through a mitogen-activated protein kinase signal transduction pathway. J Immunol *164*, 4348–4358.

Singh, R.B., Cornelissen, G., Mojto, V., Fatima, G., Wichansawakun, S., Singh, M., Kartikey, K., Sharma, J.P., Torshin, V.I., Chibisov, S., et al. (2020). Effects of circadian restricted feeding on parameters of metabolic syndrome among healthy subjects. Chronobiol Int *37*, 395–402.

Snodgrass, R.G., Huang, S., Choi, I.-W., Rutledge, J.C., and Hwang, D.H. (2013). Inflammasome-mediated secretion of IL-1β in human monocytes through TLR2 activation; modulation by dietary fatty acids. J Immunol *191*, 4337–4347.

Soehnlein, O., Zernecke, A., Eriksson, E.E., Rothfuchs, A.G., Pham, C.T., Herwald, H., Bidzhekov, K., Rottenberg, M.E., Weber, C., and Lindbom, L. (2008). Neutrophil secretion products pave the way for inflammatory monocytes. Blood *112*, 1461–1471.

Stackowicz, J., Jönsson, F., and Reber, L.L. (2020). Mouse Models and Tools for the in vivo Study of Neutrophils. Front Immunol *10*, 3130.

Stefanovic-Racic, M., Yang, X., Turner, M.S., Mantell, B.S., Stolz, D.B., Sumpter, T.L., Sipula, I.J., Dedousis, N., Scott, D.K., Morel, P.A., et al. (2012). Dendritic cells promote macrophage infiltration and comprise a substantial proportion of obesity-associated increases in CD11c+ cells in adipose tissue and liver. Diabetes *61*, 2330–2339.

StemCell Technologies 2021. Frequencies and Percentages of Mouse Immune Cell Types: https://www.stemcell.com/media/files/wallchart/WA10011-Frequencies_Percentages_Mouse_Immune_Cell_Types.pdf, accessed December 29, 2021

Stephan, F.K., and Zucker, I. (1972). Circadian rhythms in drinking behavior and locomotor activity of rats are eliminated by hypothalamic lesions. Proc Natl Acad Sci U S A *69*, 1583–1586.

Stetler, C., Dickerson, S.S., and Miller, G.E. (2004). Uncoupling of social zeitgebers and diurnal cortisol secretion in clinical depression. Psychoneuroendocrinology *29*, 1250–1259.

Stienstra, R., van Diepen, J.A., Tack, C.J., Zaki, M.H., van de Veerdonk, F.L., Perera, D., Neale, G.A., Hooiveld, G.J., Hijmans, A., Vroegrijk, I., et al. (2011). Inflammasome is a central player in the induction of obesity and insulin resistance. Proc Natl Acad Sci U S A *108*, 15324–15329.

Stokkan, K.A., Yamazaki, S., Tei, H., Sakaki, Y., and Menaker, M. (2001). Entrainment of the circadian clock in the liver by feeding. Science *291*, 490–493.

Storch, K.-F., Paz, C., Signorovitch, J., Raviola, E., Pawlyk, B., Li, T., and Weitz, C.J. (2007). Intrinsic circadian clock of the mammalian retina: importance for retinal processing of visual information. Cell *130*, 730–741.

Sudo, M., Sasahara, K., Moriya, T., Akiyama, M., Hamada, T., and Shibata, S. (2003). Constant light housing attenuates circadian rhythms of mPer2 mRNA and mPER2 protein expression in the suprachiasmatic nucleus of mice. Neuroscience *121*, 493–499.

Sun, K., Kusminski, C.M., and Scherer, P.E. (2011). Adipose tissue remodeling and obesity. J Clin Invest *121*, 2094–2101.

Sweet, D.R., Vasudevan, N.T., Fan, L., Booth, C.E., Keerthy, K.S., Liao, X., Vinayachandran, V., Takami, Y., Tugal, D., Sharma, N., et al. (2020). Myeloid Krüppel-like factor 2 is a critical regulator of metabolic inflammation. Nat Commun *11*, 5872.

Tak, T., Tesselaar, K., Pillay, J., Borghans, J.A.M., and Koenderman, L. (2013). What's your age again? Determination of human neutrophil half-lives revisited. Journal of Leukocyte Biology *94*, 595–601.

Takano, T., Azuma, N., Satoh, M., Toda, A., Hashida, Y., Satoh, R., and Hohdatsu, T. (2009). Neutrophil survival factors (TNF-alpha, GM-CSF, and G-CSF) produced by macrophages in cats infected with feline infectious peritonitis virus contribute to the pathogenesis of granulomatous lesions. Arch Virol *154*, 775–781.

Takeda, Y., Jothi, R., Birault, V., and Jetten, A.M. (2012). RORγ directly regulates the circadian expression of clock genes and downstream targets in vivo. Nucleic Acids Res *40*, 8519–8535.

Talukdar, S., Oh, D.Y., Bandyopadhyay, G., Li, D., Xu, J., McNelis, J., Lu, M., Li, P., Yan, Q., Zhu, Y., et al. (2012). Neutrophils mediate insulin resistance in mice fed a high-fat diet through secreted elastase. Nat. Med. *18*, 1407–1412.

Tam, T.H., Chan, K.L., Boroumand, P., Liu, Z., Brozinick, J.T., Bui, H.H., Roth, K., Wakefield, C.B., Penuela, S., Bilan, P.J., et al. (2020). Nucleotides released from palmitate-activated murine macrophages attract neutrophils. J. Biol. Chem.

Tan, B.H., Meinken, C., Bastian, M., Bruns, H., Legaspi, A., Ochoa, M.T., Krutzik, S.R., Bloom, B.R., Ganz, T., Modlin, R.L., et al. (2006). Macrophages acquire neutrophil granules for antimicrobial activity against intracellular pathogens. J Immunol *177*, 1864–1871.

Tao, C., Holland, W.L., Wang, Q.A., Shao, M., Jia, L., Sun, K., Lin, X., Kuo, Y.-C., Johnson, J.A., Gordillo, R., et al. (2017). Short-Term Versus Long-Term Effects of Adipocyte Toll-Like Receptor 4 Activation on Insulin Resistance in Male Mice. Endocrinology *158*, 1260–1270.

Thaler, J.P., Yi, C.-X., Schur, E.A., Guyenet, S.J., Hwang, B.H., Dietrich, M.O., Zhao, X., Sarruf, D.A., Izgur, V., Maravilla, K.R., et al. (2012). Obesity is associated with hypothalamic injury in rodents and humans. J Clin Invest *122*, 153–162.

Torquati, L., Mielke, G.I., Brown, W.J., and Kolbe-Alexander, T. (2018). Shift work and the risk of cardiovascular disease. A systematic review and meta-analysis including dose-response relationship. Scand J Work Environ Health *44*, 229–238.

Travnickova-Bendova, Z., Cermakian, N., Reppert, S.M., and Sassone-Corsi, P. (2002). Bimodal regulation of mPeriod promoters by CREB-dependent signaling and CLOCK/BMAL1 activity. Proc Natl Acad Sci U S A *99*, 7728–7733.

Trim, W., Turner, J.E., and Thompson, D. (2018). Parallels in Immunometabolic Adipose Tissue Dysfunction with Ageing and Obesity. Front Immunol *9*, 169.

Triqueneaux, G., Thenot, S., Kakizawa, T., Antoch, M.P., Safi, R., Takahashi, J.S., Delaunay, F., and Laudet, V. (2004). The orphan receptor Rev-erbalpha gene is a target of the circadian clock pacemaker. J Mol Endocrinol *33*, 585–608.

Tsuhako, R., Yoshida, H., Sugita, C., and Kurokawa, M. (2020). Naringenin suppresses neutrophil infiltration into adipose tissue in high-fat diet-induced obese mice. J Nat Med *74*, 229–237.

Turek, F.W., Joshu, C., Kohsaka, A., Lin, E., Ivanova, G., McDearmon, E., Laposky, A., Losee-Olson, S., Easton, A., Jensen, D.R., et al. (2005). Obesity and metabolic syndrome in circadian Clock mutant mice. Science *308*, 1043–1045.

Uderhardt, S., Martins, A.J., Tsang, J.S., Lämmermann, T., and Germain, R.N. (2019). Resident Macrophages Cloak Tissue Microlesions to Prevent Neutrophil-Driven Inflammatory Damage. Cell *177*, 541-555.e17.

Ueda, H.R., Hayashi, S., Chen, W., Sano, M., Machida, M., Shigeyoshi, Y., Iino, M., and Hashimoto, S. (2005). System-level identification of transcriptional circuits underlying mammalian circadian clocks. Nat Genet *37*, 187–192.

Valassi, E., Scacchi, M., and Cavagnini, F. (2008). Neuroendocrine control of food intake. Nutr Metab Cardiovasc Dis *18*, 158–168.

Valdearcos, M., Robblee, M.M., Benjamin, D.I., Nomura, D.K., Xu, A.W., and Koliwad, S.K. (2014). Microglia dictate the impact of saturated fat consumption on hypothalamic inflammation and neuronal function. Cell Rep *9*, 2124–2138.

Valentinuzzi, V.S., Scarbrough, K., Takahashi, J.S., and Turek, F.W. (1997). Effects of aging on the circadian rhythm of wheel-running activity in C57BL/6 mice. American Journal of Physiology-Regulatory, Integrative and Comparative Physiology *273*, R1957–R1964.

Vandanmagsar, B., Youm, Y.-H., Ravussin, A., Galgani, J.E., Stadler, K., Mynatt, R.L., Ravussin, E., Stephens, J.M., and Dixit, V.D. (2011). The NLRP3 inflammasome instigates obesity-induced inflammation and insulin resistance. Nat Med *17*, 179–188.

Varol, C., Zvibel, I., Spektor, L., Mantelmacher, F.D., Vugman, M., Thurm, T., Khatib, M., Elmaliah, E., Halpern, Z., and Fishman, S. (2014). Long-acting glucose-dependent insulinotropic polypeptide ameliorates obesity-induced adipose tissue inflammation. J Immunol *193*, 4002–4009.

Vetter, C., Dashti, H.S., Lane, J.M., Anderson, S.G., Schernhammer, E.S., Rutter, M.K., Saxena, R., and Scheer, F.A.J.L. (2018). Night Shift Work, Genetic Risk, and Type 2 Diabetes in the UK Biobank. Diabetes Care *41*, 762–769.

Vitaterna, M.H., King, D.P., Chang, A.M., Kornhauser, J.M., Lowrey, P.L., McDonald, J.D., Dove, W.F., Pinto, L.H., Turek, F.W., and Takahashi, J.S. (1994). Mutagenesis and mapping of a mouse gene, Clock, essential for circadian behavior. Science *264*, 719–725.

Wada, T., Ichihashi, Y., Suzuki, E., Kosuge, Y., Ishige, K., Uchiyama, T., Makishima, M., Nakao, R., Oishi, K., and Shimba, S. (2018). Deletion of Bmal1 Prevents Diet-Induced Ectopic Fat Accumulation by Controlling Oxidative Capacity in the Skeletal Muscle. Int J Mol Sci *19*, E2813.

Wanders, D., Graff, E.C., White, B.D., and Judd, R.L. (2013). Niacin increases adiponectin and decreases adipose tissue inflammation in high fat diet-fed mice. PLoS One *8*, e71285.

Wang, H., Wang, Q., Venugopal, J., Wang, J., Kleiman, K., Guo, C., and Eitzman, D.T. (2018). Obesity-induced Endothelial Dysfunction is Prevented by Neutrophil Extracellular Trap Inhibition. Sci Rep *8*, 4881.

Wang, J.B., Patterson, R.E., Ang, A., Emond, J.A., Shetty, N., and Arab, L. (2014a). Timing of energy intake during the day is associated with the risk of obesity in adults. J Hum Nutr Diet *27 Suppl 2*, 255–262.

Wang, Q., Xie, Z., Zhang, W., Zhou, J., Wu, Y., Zhang, M., Zhu, H., and Zou, M.-H. (2014b). Myeloperoxidase deletion prevents high-fat diet-induced obesity and insulin resistance. Diabetes *63*, 4172–4185.

Wang, X., Wang, Y., Antony, V., Sun, H., and Liang, G. (2020). Metabolism-Associated Molecular Patterns (MAMPs). Trends Endocrinol. Metab.

Wang, X.-L., Kooijman, S., Gao, Y., Tzeplaeff, L., Cosquer, B., Milanova, I., Wolff, S.E.C., Korpel, N., Champy, M.-F., Petit-Demoulière, B., et al. (2021). Microglia-specific knock-down of Bmal1 improves memory and protects mice from high fat diet-induced obesity. Mol Psychiatry.

Wang, X.-S., Armstrong, M.E.G., Cairns, B.J., Key, T.J., and Travis, R.C. (2011). Shift work and chronic disease: the epidemiological evidence. Occup Med (Lond) *61*, 78–89.

Wang, Z., Wu, Y., Li, L., and Su, X.-D. (2013). Intermolecular recognition revealed by the complex structure of human CLOCK-BMAL1 basic helix-loop-helix domains with E-box DNA. Cell Res *23*, 213–224.

WHO (2021). Obesity and Overweight. https://www.who.int/news-room/fact-sheets/detail/obesity-and-overweight. Accessed August 20, 2021

Wolff, G., and Esser, K.A. (2012). Scheduled exercise phase shifts the circadian clock in skeletal muscle. Med Sci Sports Exerc *44*, 1663–1670.

Wong, C.K., Botta, A., Pither, J., Dai, C., Gibson, W.T., and Ghosh, S. (2015). A high-fat diet rich in corn oil reduces spontaneous locomotor activity and induces insulin resistance in mice. J Nutr Biochem *26*, 319–326.

Woon, P.Y., Kaisaki, P.J., Bragança, J., Bihoreau, M.-T., Levy, J.C., Farrall, M., and Gauguier, D. (2007). Aryl hydrocarbon receptor nuclear translocator-like (BMAL1) is associated with susceptibility to hypertension and type 2 diabetes. Proc Natl Acad Sci U S A *104*, 14412–14417.

Wu, D., Molofsky, A.B., Liang, H.-E., Ricardo-Gonzalez, R.R., Jouihan, H.A., Bando, J.K., Chawla, A., and Locksley, R.M. (2011a). Eosinophils sustain adipose alternatively activated macrophages associated with glucose homeostasis. Science *332*, 243–247.

Wu, S., Aguilar, A.L., Ostrow, V., and De Luca, F. (2011b). Insulin resistance secondary to a high-fat diet stimulates longitudinal bone growth and growth plate chondrogenesis in mice. Endocrinology *152*, 468–475.

Xi, L., Xiao, C., Bandsma, R.H.J., Naples, M., Adeli, K., and Lewis, G.F. (2011). C-reactive protein impairs hepatic insulin sensitivity and insulin signaling in rats: role of mitogen-activated protein kinases. Hepatology *53*, 127–135.

Xie, X., Kukino, A., Calcagno, H.E., Berman, A.M., Garner, J.P., and Butler, M.P. (2020). Natural food intake patterns have little synchronizing effect on peripheral circadian clocks. BMC Biol *18*, 160.

Xiong, X., Lin, Y., Lee, J., Paul, A., Yechoor, V., Figueiro, M., and Ma, K. (2021). Chronic circadian shift leads to adipose tissue inflammation and fibrosis. Mol Cell Endocrinol *521*, 111110.

Xu, H., Gustafson, C.L., Sammons, P.J., Khan, S.K., Parsley, N.C., Ramanathan, C., Lee, H.-W., Liu, A.C., and Partch, C.L. (2015). Cryptochrome 1 regulates the circadian clock through dynamic interactions with the BMAL1 C terminus. Nat Struct Mol Biol *22*, 476–484.

Yago, T., Shao, B., Miner, J.J., Yao, L., Klopocki, A.G., Maeda, K., Coggeshall, K.M., and McEver, R.P. (2010). E-selectin engages PSGL-1 and CD44 through a common signaling pathway to induce integrin alphaLbeta2-mediated slow leukocyte rolling. Blood *116*, 485–494.

Yamaguchi, S., Mitsui, S., Yan, L., Yagita, K., Miyake, S., and Okamura, H. (2000). Role of DBP in the circadian oscillatory mechanism. Mol Cell Biol *20*, 4773–4781.

Yang, H., Graham, L.C., Reagan, A.M., Grabowska, W.A., Schott, W.H., and Howell, G.R. (2019). Transcriptome profiling of brain myeloid cells revealed activation of Itgal, Trem1, and Spp1 in western diet-induced obesity. J Neuroinflammation *16*, 169.

Yang, S., Liu, A., Weidenhammer, A., Cooksey, R.C., McClain, D., Kim, M.K., Aguilera, G., Abel, E.D., and Chung, J.H. (2009). The role of mPer2 clock gene in glucocorticoid and feeding rhythms. Endocrinology *150*, 2153–2160.

Ye, J., Gao, Z., Yin, J., and He, Q. (2007). Hypoxia is a potential risk factor for chronic inflammation and adiponectin reduction in adipose tissue of ob/ob and dietary obese mice. Am J Physiol Endocrinol Metab *293*, E1118-1128.

Ye, R., Selby, C.P., Chiou, Y.-Y., Ozkan-Dagliyan, I., Gaddameedhi, S., and Sancar, A. (2014). Dual modes of CLOCK:BMAL1 inhibition mediated by Cryptochrome and Period proteins in the mammalian circadian clock. Genes Dev *28*, 1989–1998.

Ying, W., Wollam, J., Ofrecio, J.M., Bandyopadhyay, G., El Ouarrat, D., Lee, Y.S., Oh, D.Y., Li, P., Osborn, O., and Olefsky, J.M. (2017). Adipose tissue B2 cells promote insulin resistance through leukotriene LTB4/LTB4R1 signaling. J Clin Invest *127*, 1019–1030.

Yoshitane, H., Asano, Y., Sagami, A., Sakai, S., Suzuki, Y., Okamura, H., Iwasaki, W., Ozaki, H., and Fukada, Y. (2019). Functional D-box sequences reset the circadian clock and drive mRNA rhythms. Commun Biol *2*, 300.

Yu, F., Wang, Z., Zhang, T., Chen, X., Xu, H., Wang, F., Guo, L., Chen, M., Liu, K., and Wu, B. (2021). Deficiency of intestinal Bmal1 prevents obesity induced by high-fat feeding. Nat Commun *12*, 5323.

Zatterale, F., Longo, M., Naderi, J., Raciti, G.A., Desiderio, A., Miele, C., and Beguinot, F. (2019). Chronic Adipose Tissue Inflammation Linking Obesity to Insulin Resistance and Type 2 Diabetes. Front Physiol *10*, 1607.

Zhang, D., Chen, G., Manwani, D., Mortha, A., Xu, C., Faith, J.J., Burk, R.D., Kunisaki, Y., Jang, J.-E., Scheiermann, C., et al. (2015). Neutrophil ageing is regulated by the microbiome. Nature *525*, 528–532.

Zhang, R., Lahens, N.F., Ballance, H.I., Hughes, M.E., and Hogenesch, J.B. (2014). A circadian gene expression atlas in mammals: Implications for biology and medicine. PNAS *111*, 16219–16224.

Zheng, B., Albrecht, U., Kaasik, K., Sage, M., Lu, W., Vaishnav, S., Li, Q., Sun, Z.S., Eichele, G., Bradley, A., et al. (2001). Nonredundant roles of the mPer1 and mPer2 genes in the mammalian circadian clock. Cell *105*, 683–694.

Zheng, C., Yang, Q., Cao, J., Xie, N., Liu, K., Shou, P., Qian, F., Wang, Y., and Shi, Y. (2016). Local proliferation initiates macrophage accumulation in adipose tissue during obesity. Cell Death Dis *7*, e2167.

Zhong, L.-X., Li, X.-N., Yang, G.-Y., Zhang, X., Li, W.-X., Zhang, Q.-Q., Pan, H.-X., Zhang, H.-H., Zhou, M.-Y., Wang, Y.-D., et al. (2019). Circadian misalignment alters insulin sensitivity during the light phase and shifts glucose tolerance rhythms in female mice. PLoS One *14*, e0225813.

Supplements

```r
# Install the packages
install.packages("circacompare")

# Make the package accessible
library (circacompare)

# Set working directory to the folder where files can be found
setwd("path")

# Load your data
x <- read.table("eWAT long-term for rhythms.txt",
                header = TRUE, sep ="\t" )

# Execute CircaCompare
# Make sure that the names in "" below correspond to
# column headings of your dataset
# Repeat this for each gene or condition.
Neutrophils <- circacompare(x, col_time = "time", col_group = "genotype",
                            col_outcome = "Neutros", period = 24,
                            alpha_threshold = 0.05, timeout_n = 100000)

# To create a table with the results, use the following function:
capture.output(Neutrophils, file="results eWAT long-term Neutrophils.txt")
```

Supplemental Figure S1: R code that was used to analyze datasets for circadian rhythmicity using CircaCompare. Lines that start with a hashtag contain explanations. First, the package was installed and activated. Next, a data table was loaded and given a name (here: x). The table needed to contain at least three columns, one with information on time, one with information on the group (here: genotype), and one containing the outcome (for example, percentage of a given cell population) and it needed to be saved as tab-delimited text file. With this, the CircaCompare function could be executed. It yielded information on rhythmicity of the two groups. If both groups were rhythmic, the parameters mesor, amplitude and phase were analyzed and directly compared between groups.

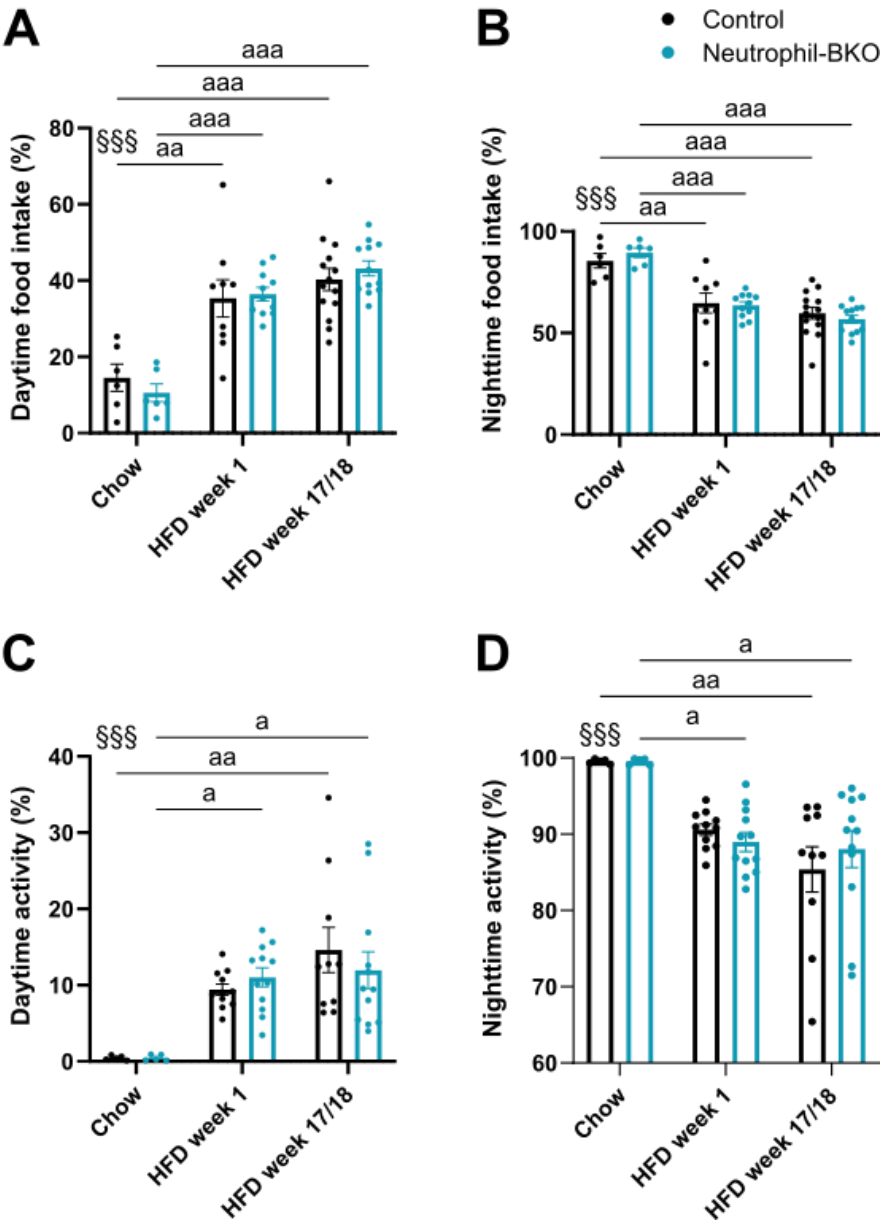

Supplemental Figure S2: Food intake and locomotor activity across different dietary conditions. **A, B:** Relative daytime (A) and nighttime (B) food intake across different dietary conditions. Relate to Figure 7 E and Figure 11 B, C. n = 6/9-14 per condition. **C, D:** Relative daytime (C) and nighttime (D) activity across different dietary conditions. Relate to Figure 7 C and Figure 12 C, D. n = 5/10-12 per condition. §§§ $p < 0.01$ effect of diet type (two-way ANOVA). a $p < 0.05$, aa $p < 0.01$, aaa $p < 0.001$ (Bonferroni post-test). For a clearer presentation, significant differences of post-tests were only plotted for comparisons of equal genotypes or equal dietary condition. Data are presented as means ± SEMs.

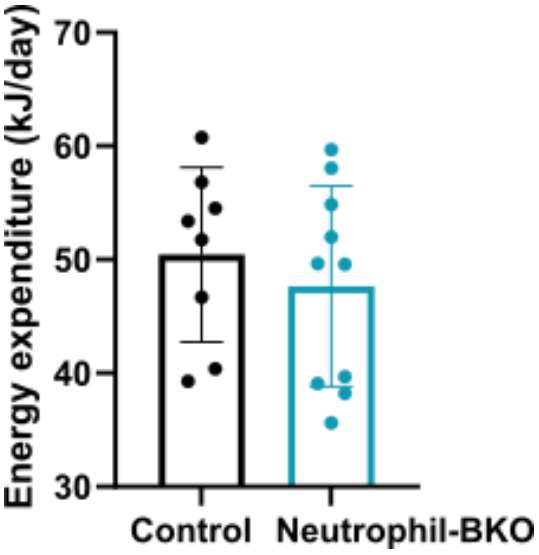

Supplemental Figure S3: Energy expenditure per day during long-term HFD feeding. Relates to Figure 12 E. n = 8/10 per genotype. Data are presented as means ± SEMs.

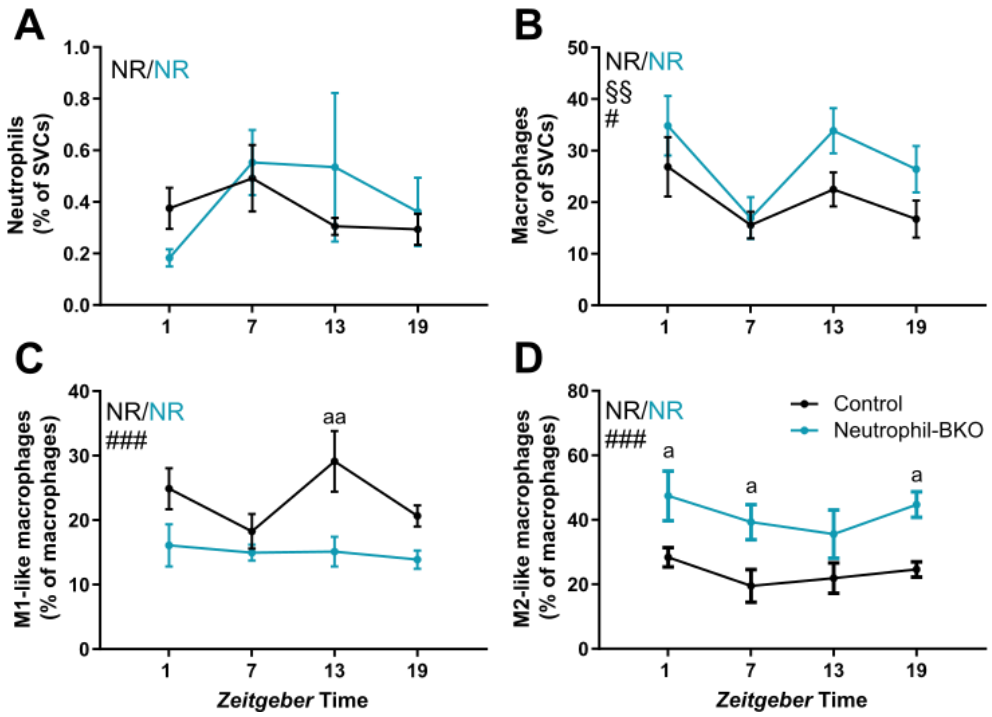

Supplemental Figure S4: Immune cell populations in eWAT after long-term HFD feeding. A: Neutrophils as percentage of SVCs. Relates to Figure 13 B. **B:** Macrophages as percentage of SVCs. Relates to Figure 14 A. **C:** M1-like macrophages and **D:** M2-like macrophages across the 24-hour cycle. Relate to Figure 14 B. n = 7/8 per condition. §§ $p < 0.01$ time effect, # $p < 0.05$ and ### $p < 0.001$ genotype effect (two-way ANOVA). aa $p < 0.01$ (Bonferroni post-test). R: rhythmic ($p < 0.05$), NR: non-rhythmic (CircaCompare). Data are presented as means ± SEMs.

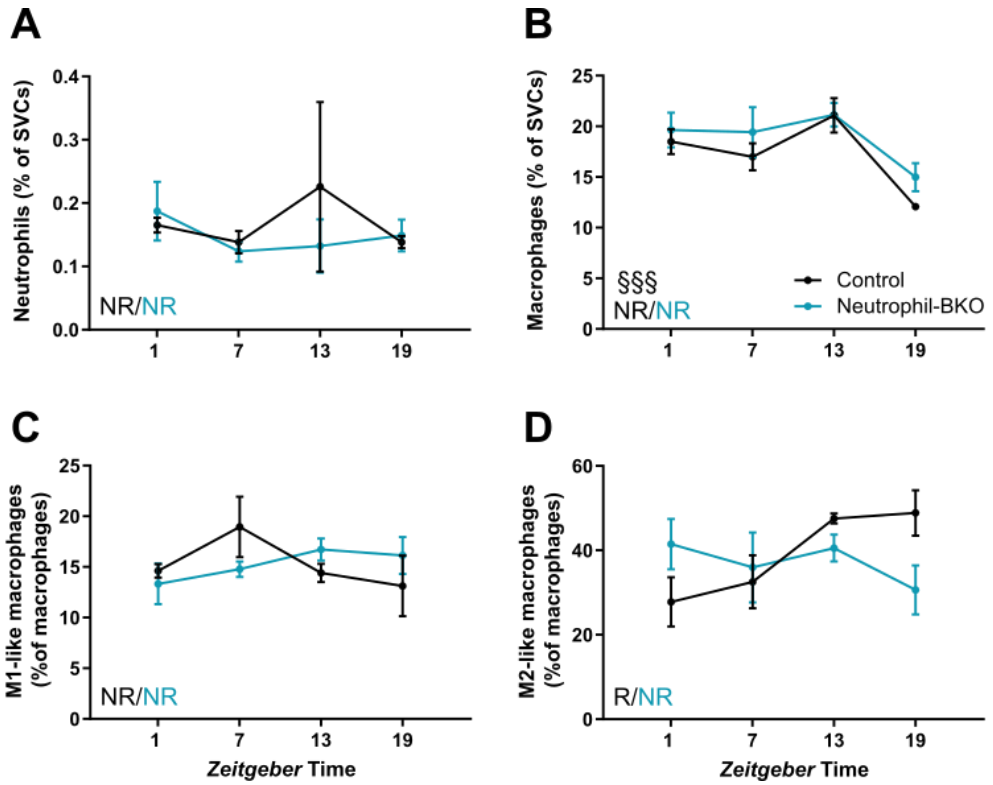

Supplemental Figure S5: Immune cell populations after short-term HFD feeding. A: Neutrophils in scWAT as percentage SVCs. Relates to Figure 16 B. **B:** Macrophages in scWAT as percentage of SVCs. Relates to Figure 17 A. **C:** M1-like macrophages and **D:** M2-like macrophages in eWAT across the 24-hour cycle. Relate to Figure 17 C. n = 3-5 per condition. §§§ $p < 0.001$ time effect (two-way ANOVA). R: rhythmic ($p < 0.05$), NR: non-rhythmic (CircaCompare). Data are presented as means ± SEMs.

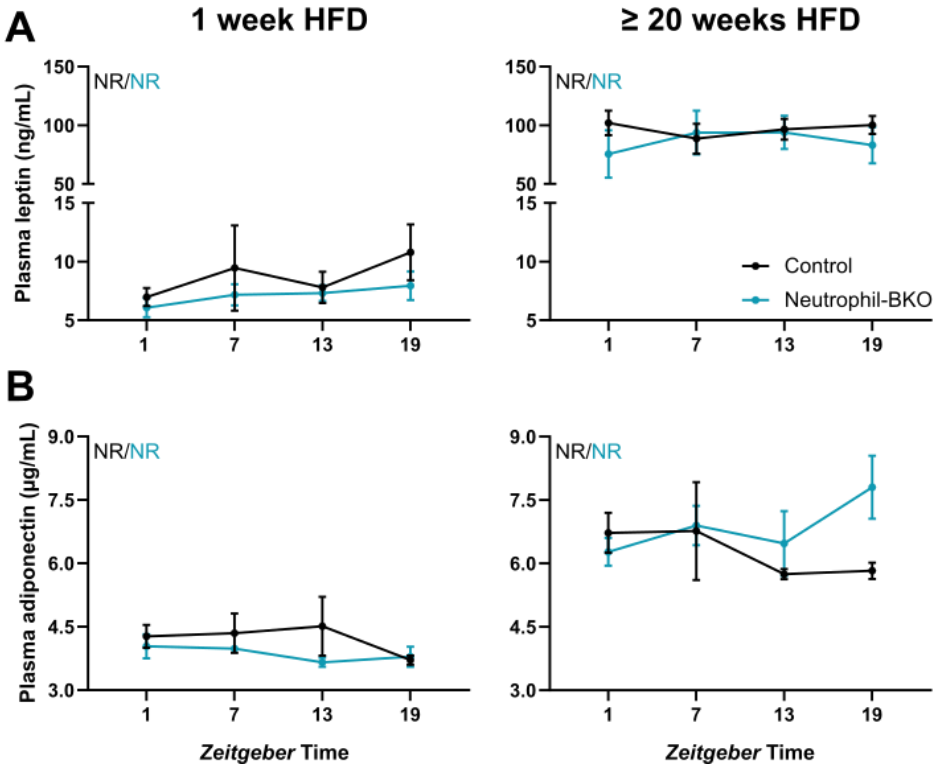

Supplemental Figure S6: Plasma adipokine levels across the 24-hour cycle. Plasma levels of leptin (**A**) and adiponectin (**B**) were detected after short-term HFD feeding (left panels) or long-term HFD feeding (right panels). Relates to Figure 18. n = 3-5 per condition. R: rhythmic ($p < 0.05$), NR: non-rhythmic (CircaCompare). Data are presented as means ± SEMs.

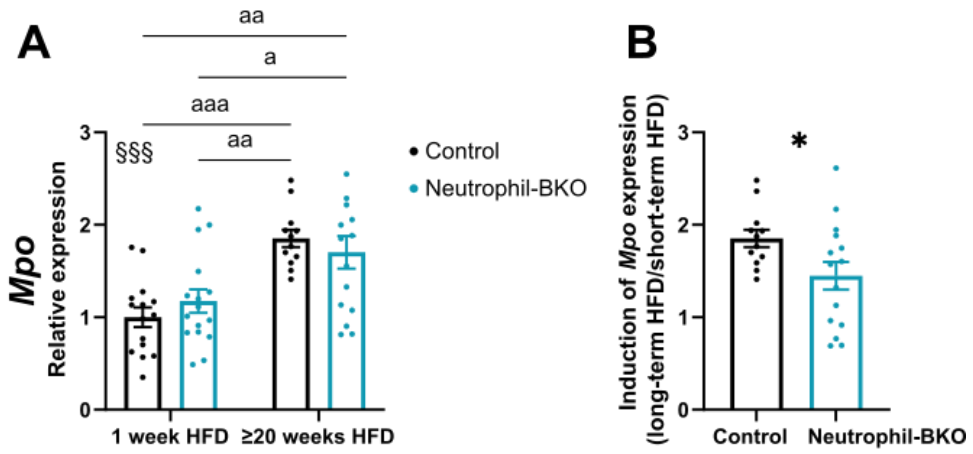

Supplemental Figure S7: *Mpo* mRNA expression after short-term (1 week) and long-term (≥20 weeks) HFD feeding. A: *Mpo* mRNA expression was normalized to the Control group that received HFD for 1 week. n = 12/15/16 per condition. **B:** Fold induction of *Mpo* mRNA expression after long-term HFD relative to the genotype-matched short-term HFD group. n = 12/15 per genotype. Relate to Figure 20 C. §§§ $p < 0.001$ effect of HFD duration (two-way ANOVA). a $p < 0.05$, aa $p < 0.01$, aaa $p < 0.001$ (Bonferroni post-test). * $p < 0.05$ (unpaired t-test). Data are presented as means ± SEMs.

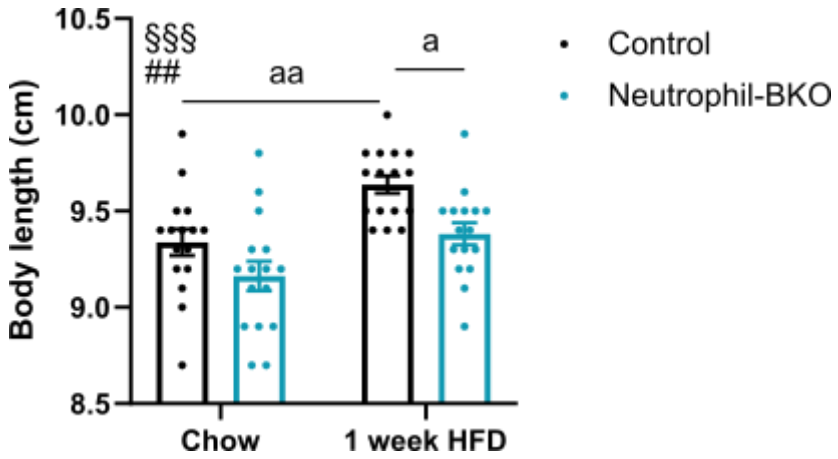

Supplemental Figure S8: Body length of animal cohorts fed normal chow or HFD for one week. Body length was measured at the age of 5-6 weeks. n = 16 per condition. §§§ $p < 0.001$ diet effect, ## $p < 0.01$ genotype effect (two-way ANOVA). a $p < 0.05$, aa $p < 0.01$ (Bonferroni post-test). Data are presented as means ± SEMs.

Supplemental Table S1: P-values for differences of rhythmic parameters between genotypes. P-values were generated by CircaCompare analysis if conditions were considered rhythmic for both genotypes. Differences were considered statistically significant when $p < 0.05$ (marked by asterix).

Condition	Relates to figure	P-value mesor	P-value amplitude	P-value phase
24-h chow intake	7 E	1.0000	0.1718	0.3060
24-h HFD intake early	11 B	1.0000	0.3718	0.0870
24-h HFD intake late	11 C	1.0000	0.0357 *	0.4228
Neutrophils eWAT short-term HFD	16 B	0.0813	0.7825	0.5103
Macrophages scWAT short-term HFD	17 A	0.9170	0.3817	0.8238
Agrp expression short-term HFD	19 C	0.1693	0.3467	0.1940
Npy expression short-term HFD	19 D	0.3292	0.1538	0.0619

Acknowledgements

“In the universe, there are things that are known, and things that are unknown, and in between, there are doors.”

William Blake

Meine große Freude daran, einige dieser Türen aufzuspüren und ein Stück zu verschieben, war maßgeblich geprägt von vielen lieben Menschen, bei denen ich mich hier bedanken möchte. This is the section to say thank you to all the people who accompanied and shaped my discoveries of some of these doors and who helped pushing them to increase the side of things that are known.

An erster Stelle steht dabei Henrik Oster. Ich bin riesig beeindruckt von deiner Art als Chef mit der genau richtigen Mischung aus Laufenlassen und Nachfragen in der Betreuung. Trotz stetig wachsender Mitarbeiterzahl hast du dir ein offenes Ohr und eine offene Tür bewahrt, sodass ich immer die Unterstützung erfahren habe, die ich gebraucht habe. Ich habe großartige, gefühlt fast grenzenlose Möglichkeiten genossen, meine eigenen Ideen zu entwickeln und umzusetzen. Besonders dankbar bin ich dir auch für dein Verständnis in Zeiten mit hohen familiären Anforderungen. Gerade dann war es unheimlich entlastend, dein Vertrauen in meine Arbeit zu spüren und ohne Bürokratie oder Druck von deiner Seite meine Aufgaben sortieren zu können. Außerdem war es spannend, deine Entwicklung vom Leiter der Arbeitsgruppe Chronophysiologie hin zum Institutsdirektor miterleben zu dürfen.

Bedanken möchte mich auch bei meiner Zweitgutachterin, Henriette Kirchner, für die spontane Bereitschaft, diese Aufgabe zu übernehmen. Es hat sich immer gut angefühlt, eine erfolgreiche Wissenschaftlerin in der Nähe zu wissen, die Familie hat. Zu merken, dass ich mit bestimmten Herausforderungen nicht alleine bin, hat es leichter gemacht, diese zu meistern.

Für die Vereinbarung von Familie und Wissenschaft war auch die Unterstützung der Christiane Nüsslein-Volhard-Stiftung eine große Hilfe und Bereicherung. Ich finde es einen wunderbar pragmatischen Ansatz, junge Wissenschaftlerinnen finanziell zu entlasten und untereinander zu vernetzen und bin dankbar dafür, diese Förderung genossen zu haben.

Ein weiterer großer Dank geht nach Berlin an Achim Kramer und Bert Maier. Ihr habt meine Begeisterung für die Chronobiologie geweckt und wachsen lassen und mich darin bestärkt, eine Promotion anzufangen. Ich erinnere mich auch gern an so manche Jogging-Runde am Bundeskanzleramt entlang und an die berüchtigten Grill-Events auf dem Balkon.

Während meiner Doktorarbeit habe ich wunderbare technische Unterstützung erhalten. Zuallererst gilt mein Dank dabei Prof. Christian Sadik für das unkomplizierte Bereitstellen von *Mpr8-Cre*-Mäusen, mit denen ich die Zucht meiner Linie starten konnte. Ebenso unkompliziert war das Nutzen des Hämatologie-Gerätes bei Prof. Gabriela Riemekasten, vielen Dank dafür. Beim Team der GTH möchte ich mich für das Versorgen der Tiere und für die Unterstützung in allen anderen Anliegen bedanken. Eine spannende und für mein Projekt zentrale Herausforderung war für mich das Erlernen der FACS-Technik. Ludmila, deine Expertise, deine Geduld und deine Genauigkeit waren dabei unschätzbar wertvoll und ich bin dir sehr dankbar, dass du all dein Wissen mit mir geteilt hast. Ohne das würde ich

wahrscheinlich immer noch an der Autofluoreszenz der Fettgewebs-Zellen verzweifeln. Weiterhin möchte ich mich bei Tillman Vollbrandt bedanken. Du warst der perfekte Ansprechpartner für alle Fragen rund um die CanaCore und deine fröhliche Art hat wunderbar gute Laune gemacht. Dir und Sven Geisler gemeinsam danke für das Sorten meiner Neutrophil-Proben. Zuletzt an dieser Stelle ein spezieller Dank an Sarah für die praktische Unterstützung und die guten Ideen, die du beigesteuert hast. Was für ein Glücksfall, dass du mit deinem immunologischen Background zu uns gestoßen bist, als es bei mir gerade in die heiße Phase ging. Und irgendwie gingen die Inkubationszeiten auch immer viel schneller rum, wenn ich mich dabei mit dir unterhalten konnte.

I am proud and thankful that my work was embedded in the outstanding community of people at the Institute of Neurobiology. The spirit and the atmosphere are unmatched, and I can't imagine a better place to work. I enjoyed all the critical and fruitful discussions, the willingness to help each other even at inconvenient times of the day (or night), spontaneous chats, lunch and coffee breaks, and the social events. The supportive environment was extremely valuable during tough times, especially during the corona restrictions. It was fantastic to experience how we can all act together for the sake of the community.

Isa und Kimberly, es war eine Freude mit euch das Büro zu teilen! Wir haben wirklich Freud, Leid (und Schokolade) geteilt, sodass das Leid kleiner und die Freude größer wurde (die Schokolade leider nicht mehr…). Isa, wie schön, dass unser gemeinsamer Start nie zu einem Wettlauf geführt hat (den du klar gewonnen hättest...) und wie schön, dass du mich gleich zu Beginn in die Spieleabende integriert hast. Dank dir auch, dass du es immer wieder auf dich genommen hast, Gruppenveranstaltungen zu organisieren und dabei möglichst alle happy zu machen. Und natürlich für die unkomplizierte praktische Unterstützung bei so manchen Experimenten. Das gilt genauso auch dir, Kimberly. Unsere Experimente haben sich ja zum Teil unglaublich gut ergänzt und allein der methodische Austausch mit dir war daher sehr wertvoll für mich. Es hat mich aber auch ungemein beeindruckt (manchmal fast beängstigt), wie du für mich mitgedacht hast – danke!

Ankita, it was a pleasure when you joined our office. Thank you for your positive energy and the coffees that we shared. Lieben Dank an Xenia für die tiefen Gespräche und den Austausch über die Wissenschaft und darüber hinaus. Das war eine tolle Bereicherung! Mariana and Violetta, your are both brilliant sparring partners. Thank you for all the positive feedback and your faith in my scientific skills, that was a great boost of self-confidence for me. Faheem, it was very sweet to share so many homemade pastries with us, thanks a lot! Leo, thank you for your interest in my project and your captivating motivation. Iwona, I like to remember your birthday party that made me discover a new and very nice spot of Lübeck! What a pity that Corona reduced the opportunities for such events during the last months.

Ein großer Dank gilt auch dir, Nadine, für all die Nerven, die du den Instituts-Bestellungen widmest. Was für eine Erleichterung und ein toller Verdienst von dir, dass das in den allermeisten Fällen so reibungslos geklappt hat. Und wenn nicht, dann hast du alle Hebel in Bewegung gesetzt, um den dringend benötigten Antikörper, die fehlenden Pipettenspitzen oder was auch immer ranzukriegen. Danke! Dorothea, danke für deine Fürsorglichkeit und Empathie als gute Seele des Instituts. Cookie, ich danke dir für die vielen hilfreichen Tipps beim Einstieg in Mausexperimente. Isa, auch du hast unermüdlich viel Energie und Ideen ins Organisieren von Gruppenevents gesteckt. Dank dir bin ich in den Genuss von Swingolf und Bogenschießen gekommen. Die Rückenkrauler und die Kaffeepausen waren immer eine wunderbare Abwechslung. Jana, ich glaube ich habe erst von dir gelernt, was Sarkasmus ist. Die Erinnerung an deinen genervt-amüsierten Gesichtsausdruck dabei lässt mich heute

noch schmunzeln. Danke dir für dein Mitgefühl beim MPV-bedingten Totalverlust meiner Mauskolonie. Deine Umarmung in dem Moment hat mir zwar das Ausmaß der Katastrophe stärker bewusst gemacht, war aber gleichzeitig der beste Trost. Anne, auch wenn sich mein Projekt von den ursprünglich geplanten OPs weg entwickelt hat, war es eine Bereicherung mit dir zusammen die Einrichtung zu planen und loszulegen. Danke dir auch für die Disneyabende, die vielen Gespräche und die Spaziergänge. Dank dir kenne ich den Stadtpark jetzt seeehr ausgiebig!

Tina und Angelika, meine MolMeds aus Göttinger Zeiten, ich danke euch fürs Mitfiebern und eure mentale Unterstützung. Tina, ich hoffe, dass wir noch viele Wanderungen zusammen bestreiten. Danke, dass du so treu den Kontakt hältst und nie böse bist, dass ich nicht so gut darin bin. Angelika, danke für die immer neuen Anreize zum Laufen und dafür, dass ich jederzeit bei dir klingeln kann.

Martin und Ralf, ihr wart die besten Mitbewohner überhaupt. Unsere Events haben einen festen Platz in meinen Jahres-Wunschlisten. Bei Kohte, Lagerfeuer und Kräuterschnaps in eurer Gesellschaft kann ich einfach wunderbar abschalten.

Zum Abschalten zwischendurch hat auch unser Segelboot beigetragen. Ein besonderer Dank daher an Manuka. Du gutmütige alte Lady hast uns immer sicher ans nächste Ufer oder die nächste Ankerbucht gebracht und uns viele Dummheiten und Anfängerfehler verziehen. Die Urlaube mit dir waren gerade in der Zeit der Doktorarbeit unglaublich wertvoll!

Zuletzt möchte ich mich bei meiner Familie bedanken. Mama und Papa, eure Liebe und eure bedingungslose Unterstützung haben das Fundament gelegt, dass ich meinen Weg gehen und mich entfalten konnte. Danke ist dafür eigentlich ein viel zu kleines Wort.

Emil, danke dass du in unser Leben gekommen bist und mir so viele Momente des Mutterstolzes, des Staunens und der Freude schenkst. Von dir konnte ich mir abgucken, im Moment zu sein. Eine wunderbare Strategie, um Tiefschläge zu verkraften und nach vorne zu schauen.

Mirco, dein Rückhalt, deine Unterstützung und dein Vertrauen in mich und unsere Beziehung haben mich durch die letzten Jahre getragen. Ob Legerwall vor Heiligenhafen, Land unter im Zelt, schlaflose Eltern-Nächte oder eben die Höhen und Tiefen einer Doktorarbeit, wir schaffen das. Ich bin unendlich dankbar für unseren gemeinsamen Weg - von dir weht mich kein Sturm mehr fort!